



# thrustMIT - Project Rayquaza

## Team 48 Project Technical Report to the 2022 Spaceport America Cup

Aneesh Salian<sup>1</sup>, Aryaman Srivastav<sup>2</sup>, Advait Bongu<sup>3</sup>, Aditya Vamsi Kumbhari<sup>4</sup>, Anshul Agrawal<sup>5</sup>, Samanway Chakraborty<sup>6</sup>, Siddharth Sudhakar<sup>7</sup>, Vignesh R.<sup>8</sup>, Prajwal Jayaraman<sup>9</sup>, Prishita Rathore<sup>10</sup>, Prakhar Swarnakar<sup>11</sup>,

Abhyudaya Singh, Jeslyn Biju, Khushal Agarwal, Nathan Karl Tauro

*Manipal Institute of Technology, Manipal Academy of Higher Education, Manipal, Karnataka (576104), India*

thrustMIT's fourth attempt at the Spaceport America Cup features Rayquaza, a rocket designed to reach an apogee of 10,000 feet with a functioning non-deployable payload, and completely recoverable by a reefed parachute. Powered by Cesaroni's Commercial-Off-The-Shelf solid-propellant Pro98 M3400-P, the rocket shall be carrying a payload investigating the effects of launch vehicle vibrations on Carbon Fibre Reinforced Polymer. The flight computer combines a Commercial-Off-The-Shelf system and a Student Researched And Developed system. The apogee detection system is one unique characteristic of the launch vehicle. The rocket features a carbon fibre composite fuselage and Aluminium 6063 bulkheads, centring rings, stringers, fins and thrust plate for added structural strength. The team was conceived in early 2016 to nurture rocketry as a hobby in India, and by competing at the Spaceport America Cup, the team will get a platform to share its knowledge and learn from fellow students from all around the world.

<sup>1</sup>Project Manager; Team Leader, Aerodynamics Head

<sup>2</sup>Deputy Project Manager; Mechanical Head, Propulsions Head

<sup>3</sup>Safety Operations Lead

<sup>4</sup>Launch Operations Lead

<sup>5</sup>Recovery Operations Lead; Payload and Research Head - Mechanical

<sup>6</sup>Team Manager

<sup>7</sup>Avionics Head, Computation Head

<sup>8</sup>Controls Head

<sup>9</sup>Structures Head

<sup>10</sup>Payload and Research Head - Avionics

<sup>11</sup>Management Head

## Nomenclature

*ABS* Acrylonitrile butadiene styrene

*ADC* Analog-to-Digital Converter

*AGL* Above Ground Level

*CAD* Computer Aided Design

*CFD* Computational Fluid Dynamics

*CFRP* Carbon Fibre Reinforced Polymer

*CNC* Computer Numerical Control

*CNT* Carbon nanotube

*COTS* Commercial-Off-The-Shelf

*CSV* Comma Separated Values

*FPS* Frames per Second

*FPV* First Person View

*GPIO* General-Purpose Input/Output

*GPS* Global Positioning System

*GSM* Grams per Square Meter

*GUI* Graphical User Interface

*I2C* Inter Integrated Circuits

*IMU* Inertial Measurement Unit

*LiPo* Lithium-ion Polymer Battery

*LoS* Line of Sight

*MDF* Medium Density Fibreboard

*MP* Mega Pixel

*PCB* Printed Circuit Board

*PDB* Power Distribution Board

*PLA* Polylactic acid

*RF* Radio Frequency

*SD* Secure Digital

*SDK* Software Development Kit

*SPI* Serial Peripheral Interface

*SRAD* Student Researched And Developed

*TIG* Tungsten Insert Gas

*WEDM* Wire Electrical Discharge Machining

$WPC$	Wood Plastic Composite	
$v_f$	Flutter Velocity of Fin	$\text{m s}^{-1}$ ( $\text{ft s}^{-1}$ )
$a$	Speed of Sound	$\text{m s}^{-1}$ ( $\text{ft s}^{-1}$ )
$G$	Modulus of Rigidity of Fin material	$\text{MPa}$ ( $\text{psi}$ )
$AR$	Aspect Ratio of the Fins	
$t$	Thickness of Fin	$\text{mm}$ ( $\text{in}$ )
$P_a$	Ambient/Atmospheric Pressure	$\text{MPa}$ ( $\text{psi}$ )
$\lambda$	Taper Ratio of the Fins	
$c$	Chord Length of Fin	$\text{mm}$ ( $\text{in}$ )
$F$	Force Desired for Ejection	$\text{N}$ ( $\text{lbf}$ )
$A$	Piston Face Area	$\text{mm}^2$ ( $\text{in}^2$ )
$\delta$	Charge Density	$\text{kg m}^{-3}$ ( $\text{lb ft}^{-3}$ )
$\Delta$	Loading Density	$\text{kg m}^{-3}$ ( $\text{lb ft}^{-3}$ )
$F_e$	Effective Force	$\text{J kg}^{-1}$ ( $\text{ft lbf lb}^{-1}$ )
$m$	Consumed Mass Fraction	
$C$	Original Charge Mass	$\text{kg}$ ( $\text{lb}$ )
$V$	Chamber Volume	$\text{m}^3$ ( $\text{ft}^3$ )
$R$	Universal Gas Constant	$\text{J mol}^{-1} \text{K}^{-1}$ ( $\text{ft lbf lb}^{-1}$ )
$T$	Flame Temperature	$\text{K}$ ( $^{\circ}\text{R}$ )
$M$	Molar Mass	$\text{kg mol}^{-1}$ ( $\text{lb mol}^{-1}$ )
$D_o$	Nominal Diameter of Parachute	$\text{m}$ ( $\text{in}$ )
$C_d$	Coefficient of Drag	
$L$	Suspension Line Length	$\text{m}$ ( $\text{in}$ )
$D$	Canopy Diameter	$\text{m}$ ( $\text{in}$ )
$b$	Canopy Height of Open Parachute	$\text{m}$ ( $\text{in}$ )
$r_b$	Base Radius of Open Parachute	$\text{m}$ ( $\text{in}$ )

## I. Introduction

thrustMIT was established in February 2016 by a group of seven engineering freshmen at Manipal Institute of Technology in Karnataka, India, to promote rocketry as a hobby in India and compete in the Intercollegiate Rocket Engineering Competition against rocketry teams from around the world. In 2022, the team comprises 35 students and has made progress in leaps and bounds. The team structure for the 2022 season is as follows:

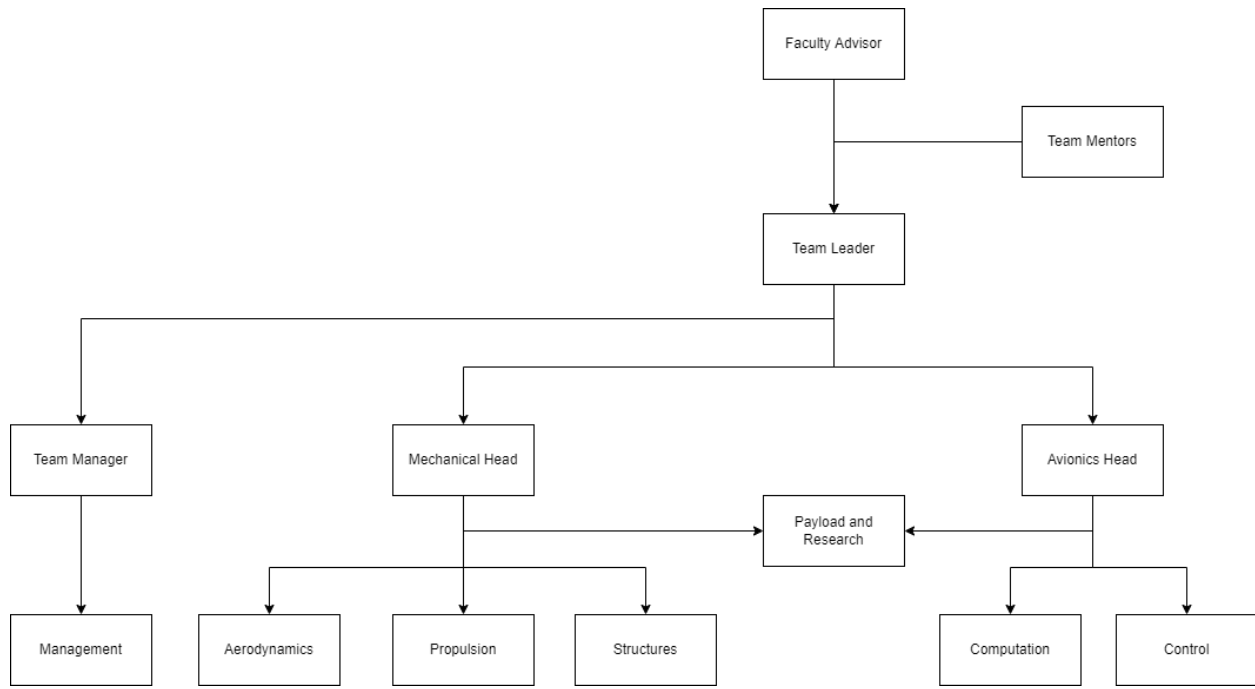


**Figure 1 Team Structure**

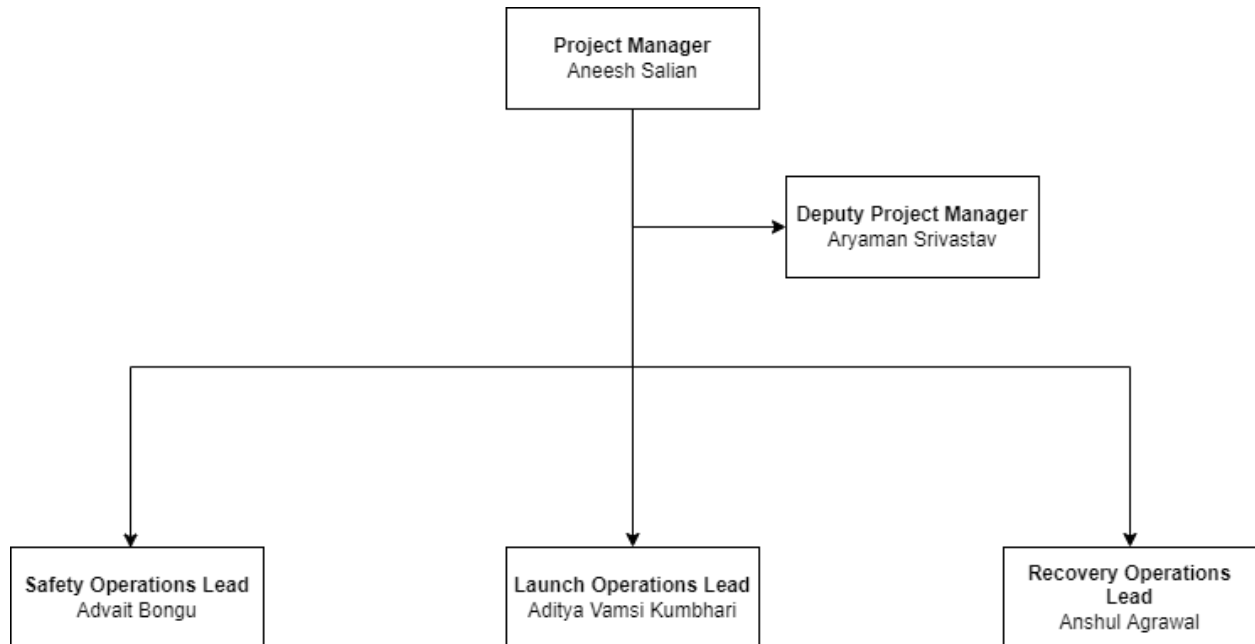


**Figure 2 Student Team Leadership**

thrustMIT is funded by the university, Manipal Academy of Higher Education, and its sponsors provided financial, product, and service support.

thrustMIT is divided into three major subsystems; Mechanical, Avionics and Management, with Mechanical being

further split into three divisions and Avionics into two. The Payload and Research subsystem of the teams falls in the juncture between the Mechanical and Avionics subsystems owing to its multidisciplinary structure and requirements. The Team Lead heads the team, with the Team Manager handling all finance and logistics of the team. The Lead and Manager together form the core of the team leadership and handle the team's progress, plan of action and manage all requirements from the university and the competition authorities.

This year the team is competing in the 10k feet COTS category with our rocket "Project Rayquaza". Named after the King of Dragons, Rayquaza is the successor to "Phoenix", the team's entry to the 2021 Virtual Spaceport America Cup. Having bagged the 7<sup>th</sup> place in the 10k feet COTS category last year, after battling the COVID-19 pandemic, the team aims to soar higher than ever before and achieve the much elusive 10k feet apogee. With a well-established carbon fibre structure, the team implemented many innovations such as a leading-edge extension fins, a composites-based payload, and an energy-efficient flight computer.

## II. System Architecture Overview

The rocket body is made of 3 modular body tubes with an outer diameter of 15 cm (5.906 in), a total length of 2.76 m (108.66 in) and a pad mass of 29.7 kg (65.48 lb). The body tubes are manufactured from carbon fibre composites to keep them lightweight while providing enough structural strength to withstand loads acting on the rocket during its flight. Five layers of carbon fibre fabric of thickness 0.33 mm (0.013 in) each, were laid up to achieve a total thickness of 2 mm (0.079 in). The rocket consists of 5 major components:

- The Nosecone – The top-most part of the rocket that improves the rocket's aerodynamic profile.
- The Recovery Bay – Houses the parachute that helps in the safe recovery of the rocket.
- The Mid Bay – The rocket's payload, flight computer and data loggers are located in this bay. This bay also houses a flight camera and its supporting electronics.
- The Motor Bay – Provides a support structure and framework for the rocket motor. It also contains the support structure for fin attachment.
- The Fins – Improves the stability of the rocket by modifying the rocket's aerodynamic profile.

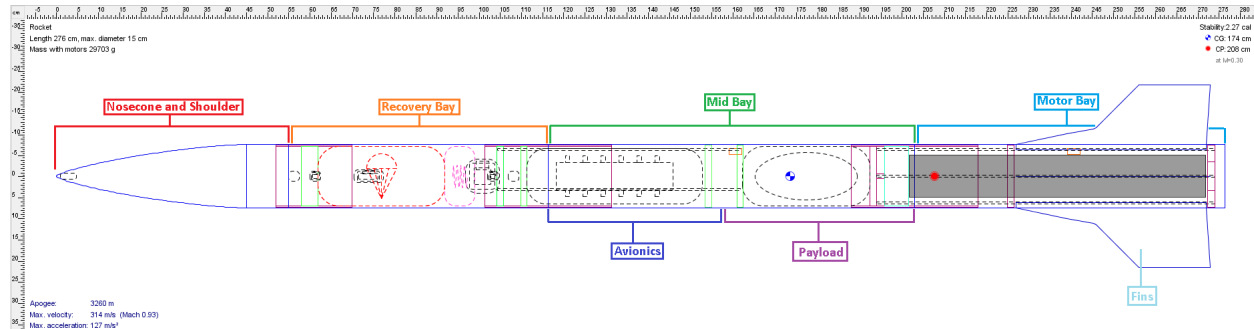


**Figure 3 Schematic of Rayquaza as viewed on OpenRocket**

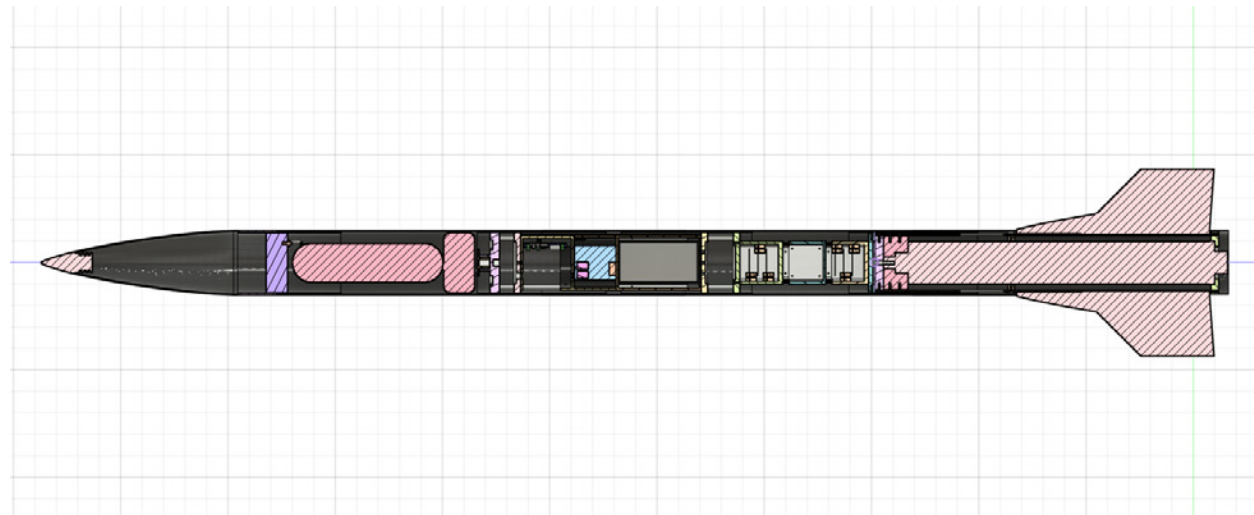


**Figure 4 Section View of Rayquaza (100 mm grid with 5 subdivisions for scale)**

## A. Aerostructures

The aerodynamics and structures team for Project Rayquaza designed the rocket keeping in mind the safety and stability of the flight, along with the given target of achieving an apogee of 10,000 ft. The team used a variety of software to design, simulate and analyse the stability of the rocket and to ensure that all its components remain intact throughout the flight.

The following softwares were used for the design and simulation of the rocket:

- OpenRocket v15.03 - Open-source software for the 2D design plan of the rocket. This software was also used to get flight simulation results and obtain a geometrical understanding of the design.
- Fusion360 V.2.0.12888 - 3D CAD modelling software used to model the entire rocket.
- SolidWorks 2020 SP5 - Design, modelling and analysis of the Nosecone and parachute.
- ANSYS 2022 R1 - The Static Structural module was used to obtain the Stress Analysis results using the Finite Element Method for various components of the rocket. The FLUENT module was used to simulate the flow around the rocket and to calculate the aerodynamic forces on it during flight using the Finite Volume Method. The Explicit Dynamics module was used to obtain impact loading results for the fins. The Modal Analysis module was used to obtain the natural frequencies and vibrational characteristics of the payload.
- RASAero II - This software was used for obtaining accurate flight simulation data in the compressible regime
- MATLAB R2020b - The team's Six Degree of Freedom Simulator code, as well as the script to generate the parachute gore profiles, were written on MATLAB.

**Table 1 Fasteners used in Rayquaza**

Fastener Dimension	Reference Standard	Fastener Material	Comments
#2-56	-	Nylon	Shear pins
M3 × 0.5	DIN 912	A2 Steel (AISI 304)	Used in the CubeSat only
M4 × 0.7	DIN 7991	A2 Steel (AISI 304)	Used in the CubeSat only; Countersunk Head
ST4.8	DIN 7981C	A2 Steel (AISI 304)	Self Tapping Screws
M5 × 0.8	DIN 7380	A2 Steel (AISI 304)	Round Head
M6 × 1.0	DIN 912	A2 Steel (AISI 304)	Used in the CubeSat only
3/8"-16	ANSI/ASME	A2 Steel (AISI 304)	Used for Motor Head attachment
UNC	B1.1		

The structure of the rocket is detailed as follows:

### 1. Nosecone

The primary purpose of the Nosecone is to reduce the form drag of the rocket by displacing the air as the rocket moves through it. Since the maximum speed of our rocket is  $317.7 \text{ m s}^{-1}$  ( $1042.32 \text{ ft s}^{-1}$ ), which is within the transonic regime, it was decided to utilize a Von Kármán Nosecone profile as it is best suited for the subsonic and transonic flight regimes due to its low drag coefficient. The Nosecone has a fineness ratio of 3 : 1 and is fabricated using CFRP to keep it lightweight and rigid enough to counter the dynamic pressure at the front.

The Nosecone base is extended by 10 cm (3.94 in). This extended portion has a 15 cm (5.906 in) long shoulder formed integral with it to facilitate attachment to the recovery bay. A Nosecone bulkhead made of WPC, with a U-bolt bolt fixed in it, is attached at the base to serve as an attachment point for the shock chords.

The Nosecone is split into two parts for ease of manufacturing. The Nosecone tip is made using Aluminium 6063 in a CNC machine. This was done as the small diameter near the tip of the Nosecone would be difficult to layup accurately by hand.

The mould for the Nosecone layup was made by stacking up MDF and gluing them together using a special wood-working adhesive. The stack-up was then machined to the exact dimensions and shape using a CNC Router and sanded with high-grit sandpaper to achieve a uniform finish. The mould was manufactured in 2 halves to simplify the layup process.



**Figure 5 Split-Pattern Female Coupler Mould**

Once the mould was completed, it was prepared for the layup with three coats of release wax followed by a tac layer of epoxy. The Nosecone and shoulder were then laid up together with five layers of CFRP on each half. The halves were then allowed to cure for 3 hours until they achieved their gel-time. Following completion of the gel time, excess CFRP was trimmed, and the two halves were joined using five layers of CFRP strips on either side of the Nosecone seam. The completed layup was then sanded down to remove any blemishes and coated with wood varnish to achieve a uniform finish.

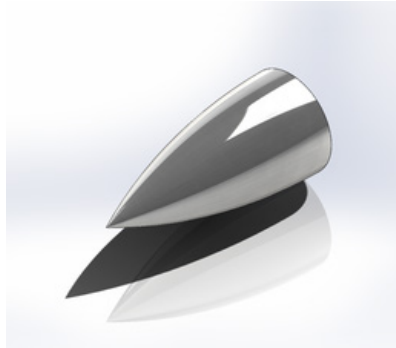


**Figure 6 Isometric View of the Von Kármán Nosecone**



**Figure 7 Isometric View of Nosecone with nose tip**



**Figure 8 Sectional View of Nosecone with nose tip**

## 2. Body Tubes

Body tubes form the main framework of the rocket and house all internal components such as the recovery, the payload, the avionics, and the motor. Over the past two years, the team has developed, tested, and improved on its own in-house composite manufacturing setup for CFRP and chose to continue with the same for this year's Spaceport America Cup project.

The mould was made from high-grade, locally sourced Acacia wood and turned to the rocket's inner diameter on a

wood-working lathe. The mould was then sanded using high-grit sandpaper to make it ideal for a layup. The mould was then prepared for the layup by applying a layer of boric acid powder, followed by carefully wrapping a layer of plastic. This was done to facilitate easy demoulding of the layup and a smooth finish on the inner surface. After placing all five layers of CFRP, the layup was covered with a layer of peel-ply fabric to help get rid of any excess epoxy. After 24 hours of curing time, the layup was sanded and sprayed uniformly with a wood varnish to get a smooth surface. The tubes were further sanded after the varnish set to remove any surface irregularities and get an exceptional aerodynamic finish.

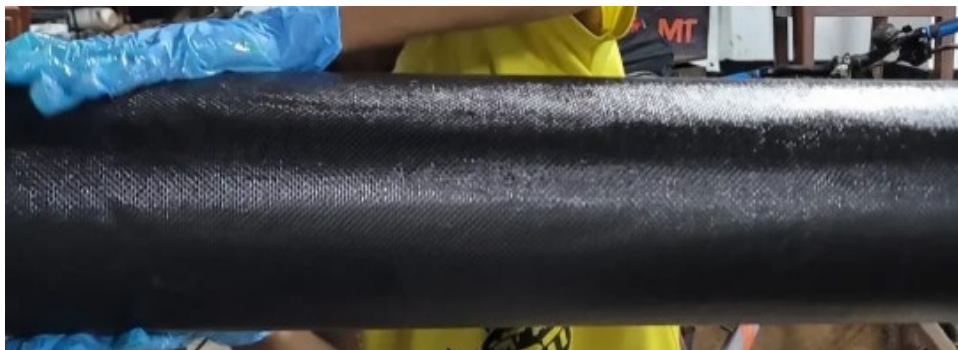


**Figure 9 Carbon Fibre Hand Layup**

Project Rayquaza consists of 3 body tubes – the Recovery bay, housing the recovery hardware; the Mid bay, housing the payload and avionics; and the Motor bay that houses the motor. The Payload and Avionics bay were combined to simplify the assembly process and reduce the overall weight of the rocket.



**Figure 10 Completed Body Tube**

### *3. Couplers*

The mould for couplers was made by the same method followed for the Nosecone mould, using a stack-up of MDF that was machined to the required dimensions. The couplers were laid-up in an internal mould by hand layup, followed by curing for 24 hours. The internal mould ensured an accurate outer diameter for the coupler, ensuring a precise fit inside the body tubes. The couplers were made using five layers of CFRP and are 30 cm (11.81 in) in length. Project

Rayquaza houses two couplers; one to join the Recovery and Mid bays and one to join the Mid and Motor bays.



**Figure 11 Split-Pattern Female Coupler Mould**

#### 4. Fins

Fins ensure flight stability by ensuring the centre of pressure is below the centre of gravity during the ascent, providing a corrective moment about the centre of gravity. Hence, the rocket's orientation will be corrected by aerodynamic forces if wind gusts perturb it. The team chose a four-fin trapezoidal fin set with the root of the leading edge extended to increase the aerodynamic efficiency and get the required stability. The leading edge root extensions alter the airflow over the fins at non-zero angles of attack to provide a better lift to drag ratio. The shape profile of the extended part was based on the works done by [1]. The basic dimensions of the fins are shown in Table 2 and Figure 12. The fins have a rectangular cross-section with 3 mm (0.12 in) thickness. The minimum stability caliber of the rocket at the launch rod clearance is 1.6 and goes up to 3.39 during ascent.

**Table 2 Fin Dimensions**

Shape	Trapezoidal with leading edge	
Material	Aluminium 6063	
Root Chord	450 mm	(17.72 in)
Tip Chord	170 mm	(6.69 in)
Semi-Span	140 mm	(5.51 in)
Thickness	3 mm	(0.12 in)

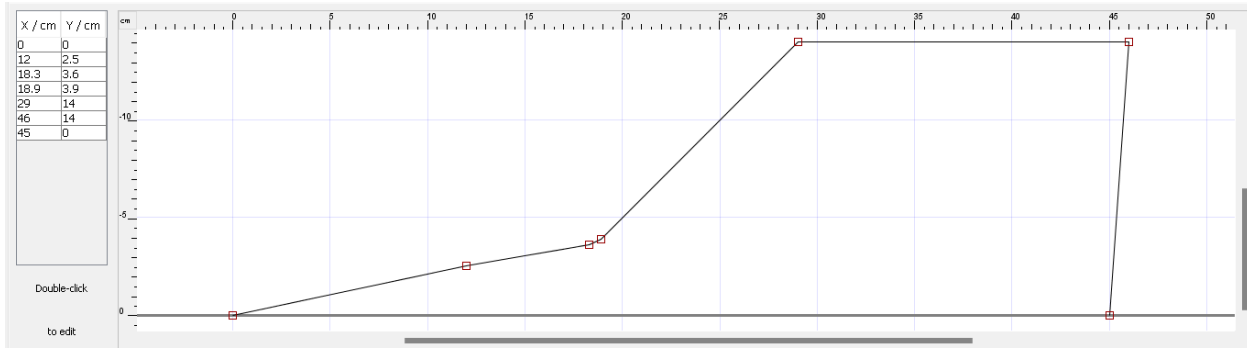


**Figure 12 Fin Profile**

Another critical phenomenon considered while designing the fins is fin flutter. Fin flutter is an aeroelastic phenomenon that arises at high speeds, where an amplification feedback loop is formed due to the physical properties of the fins. This leads to increased oscillation and eventual failure of the fins. The flutter velocity of the fins is calculated using the following equation:

$$v_f = a \cdot \sqrt{\frac{2 \cdot G (AR + 2) t^3}{1.337 \cdot P (\lambda + 1) (c \cdot AR)^3}}$$

On performing the calculations, the flutter velocity was found to be  $395.33 \text{ m s}^{-1}$  ( $1297 \text{ ft s}^{-1}$ ), well above the maximum speed of the rocket.

The team considered multiple materials and mechanisms for mounting the fins onto the rocket. Mechanisms like a composite fin can and CFRP fins were explored but ultimately dismissed because of lack of a reliable method to ensure dimensional accuracy and aerodynamic finish. The team therefore finalised on using aluminium fins along with a stringer-based attachment mechanism.

The fins are made of Aluminium 6063 and cut to the desired geometry using a WEDM machine. The fins have 12 mm (0.47 in) fin tab to facilitate attachment. The fin itself is TIG welded into a slot made in the stringer. A seam weld was used to ensure structural integrity under extreme aerodynamic and impact loading conditions. Aluminium 4043 was utilized as the filler material. The stringer is fastened into the centring ring using one M5 bolt and snug-fit into a slot in the retainer. The attachment is designed so that the fins can be mounted accurately from the outside of the framework after assembly. The fin attachment is designed to keep the fin flutter to a minimum and to ensure the fin does not fail under aerodynamic forces experienced during flight and impact loads at ground hit.

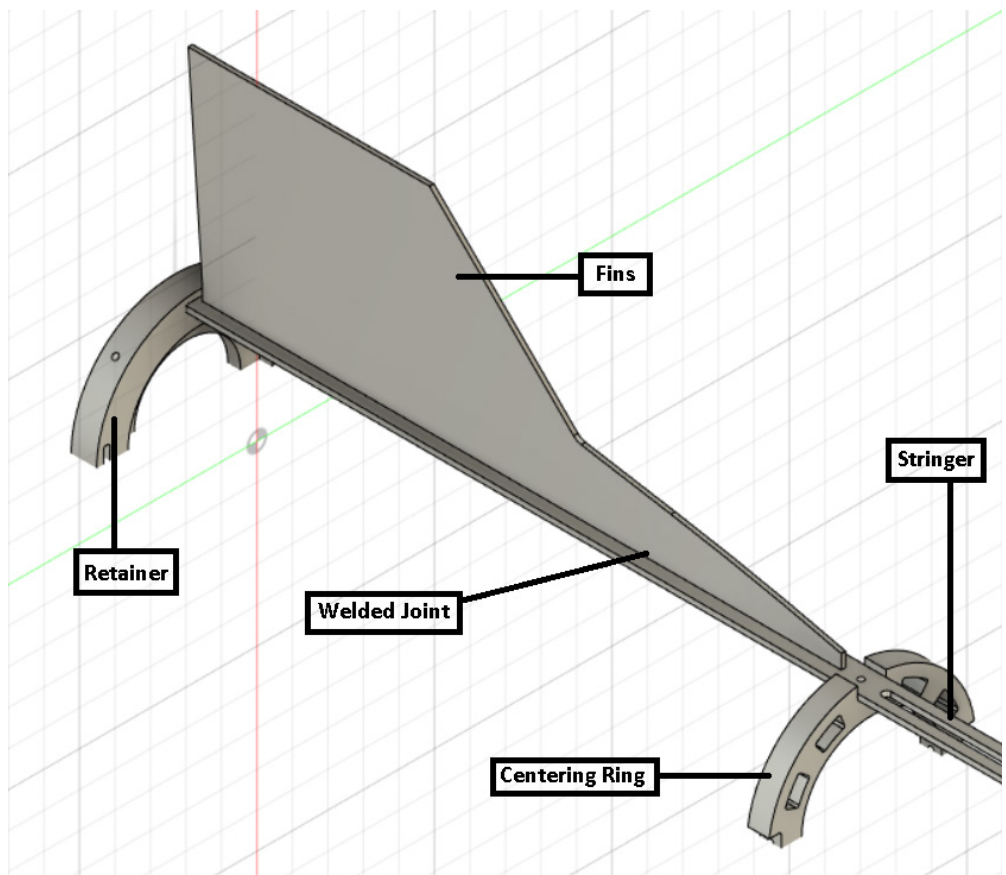
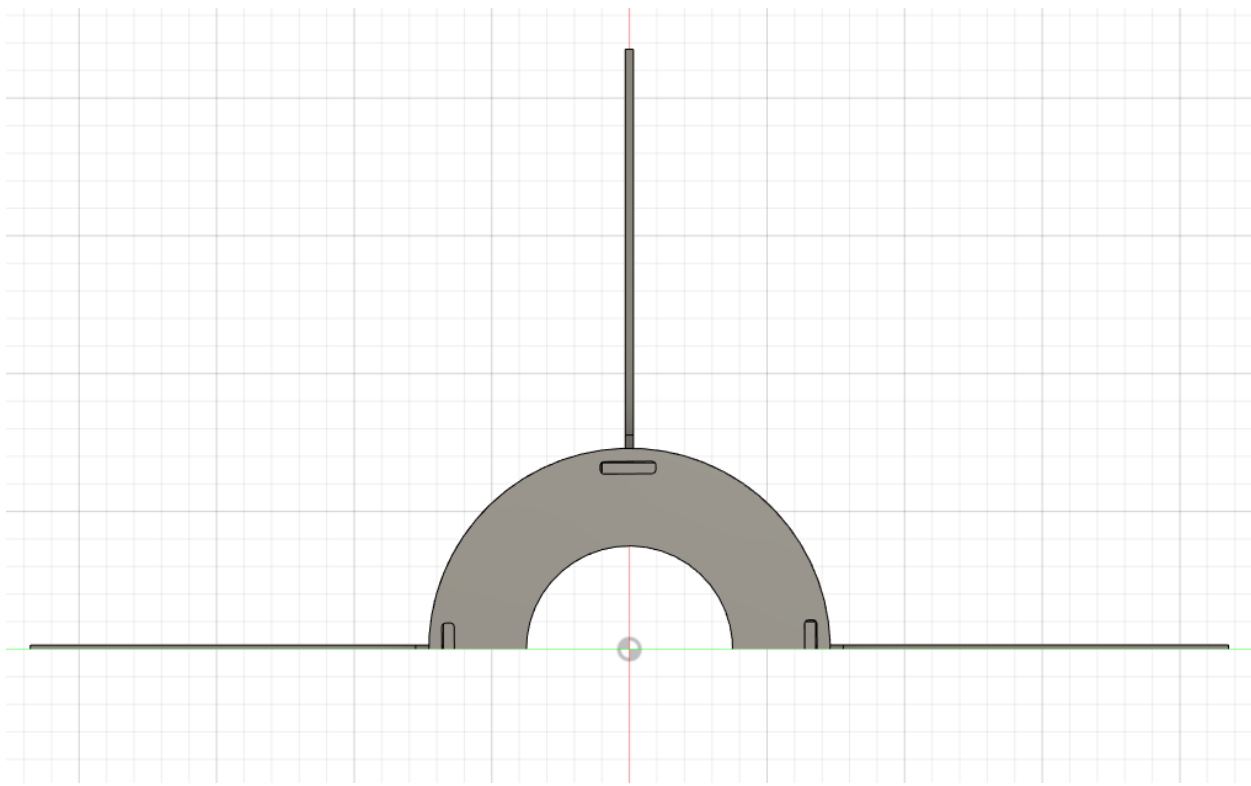
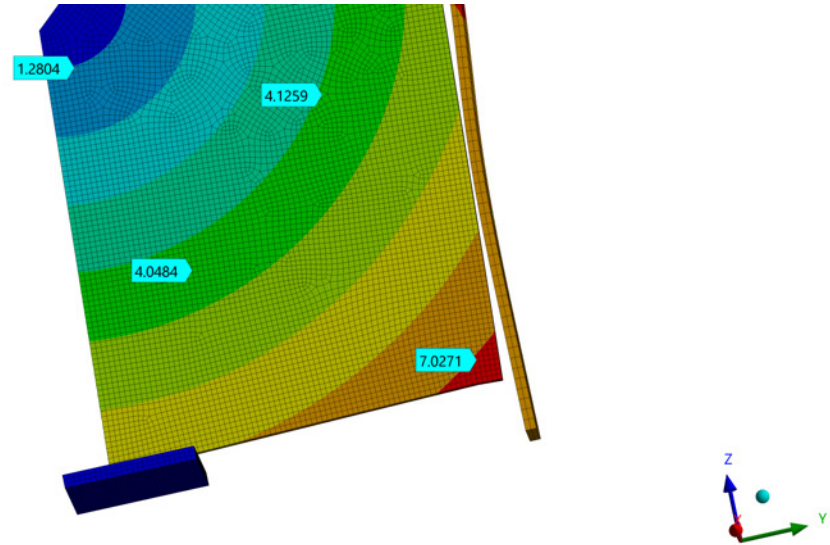


Figure 13 Top View of the fin attachment (10 mm grid with 5 subdivisions for scale)



**Figure 14 Rear View of the Fin Attachment System (10 mm grid with 5 subdivisions for scale)**

An Explicit Dynamics simulation was performed on the fins and their attachment mechanism to test the forces experienced by the setup during severe impact events and under high forces. A impact velocity of  $12 \text{ m s}^{-1}$  ( $39.37 \text{ ft s}^{-1}$ ) was taken keeping in mind a safety factor of 1.5. A breaking stress criteria for the seam weld was added in the simulation settings to ensure accurate results that take into account the weld efficiency and strength. A deformation of 7 mm (0.28 in) was obtained on the fin without the retainer support and reduced to 5.7 mm (0.22 in) and maximum stress of 96 MPa (13 924 psi) was observed on the fin attachment structure at the point where the stringer connects to the centring ring. A thorough analysis of the results shows minimal damage to the attachment mechanism. It should be noted that these results are for extreme loading conditions, with the analysis performed on a simplified model. The presence of other components will improve the structural stability of the fin and the attachment structure. Therefore, we concluded that these fins and their attachment mechanism could withstand any sudden impacts and the aerodynamic forces they experience in flight.



**Figure 15 Fin Deformation on Impact (without the Retainer Support) in mm**

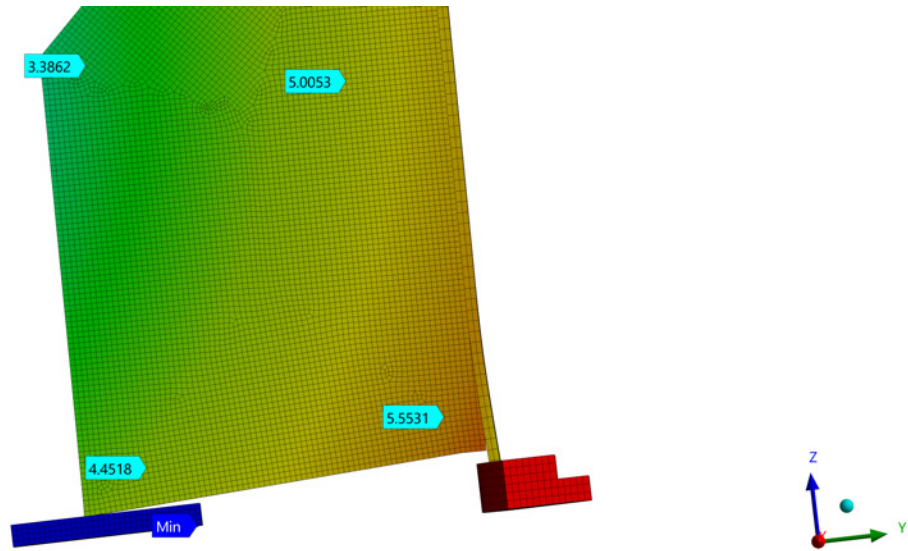


**Figure 16 Fin Deformation on Impact (with the Retainer Support) in mm**

### 5. Aerodynamic Design Simulations

The team started with OpenRocket for preliminary simulations and to design the rocket's internal structure. OpenRocket also allowed for the selection of a suitable motor to get the required apogee and launch rod exit velocity. The masses and centre of gravity of the rocket components were overridden by the values found in CAD as the design progressed. Throughout the design iterations, along with OpenRocket, the same rocket design was concomitantly

made on RASAero II software due to its superiority over OpenRocket in aerodynamic modelling. It allowed further optimization of the rocket in terms of the weight distribution and locating the centre of gravity of the rocket, as well as in the design of the fins. As the design progressed, multiple simulations were performed at worst- and best-case wind conditions, which are expected at launch site based on past year's weather reports, to determine the wind tolerance limit within which all stability criteria were met.

After reassuring a stable and safe flight of the rocket, at the final design stage, an in-house developed simulator code, built on MATLAB, was used to simulate the rocket's flight. This was done to get a more accurate apogee prediction as both the above-mentioned software would not accurately model the effects of the vortices generated by the leading edge extensions.

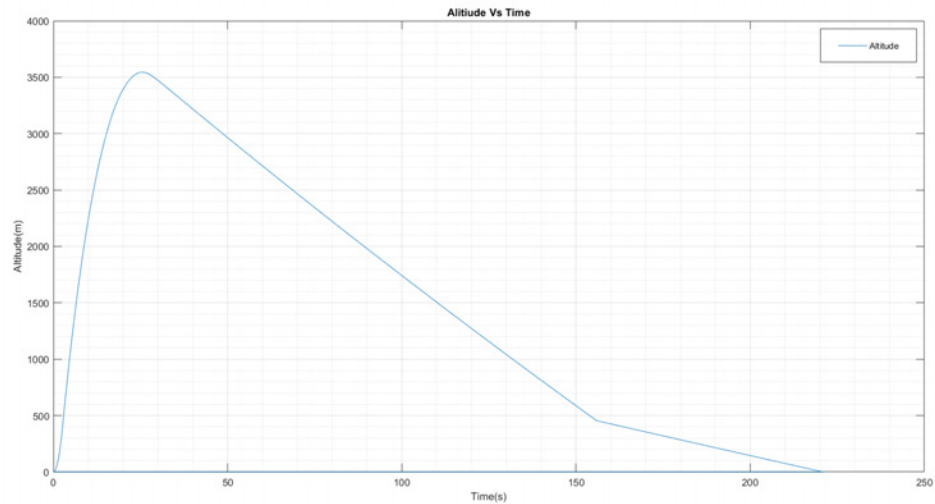


**Figure 17 Altitude vs Time**

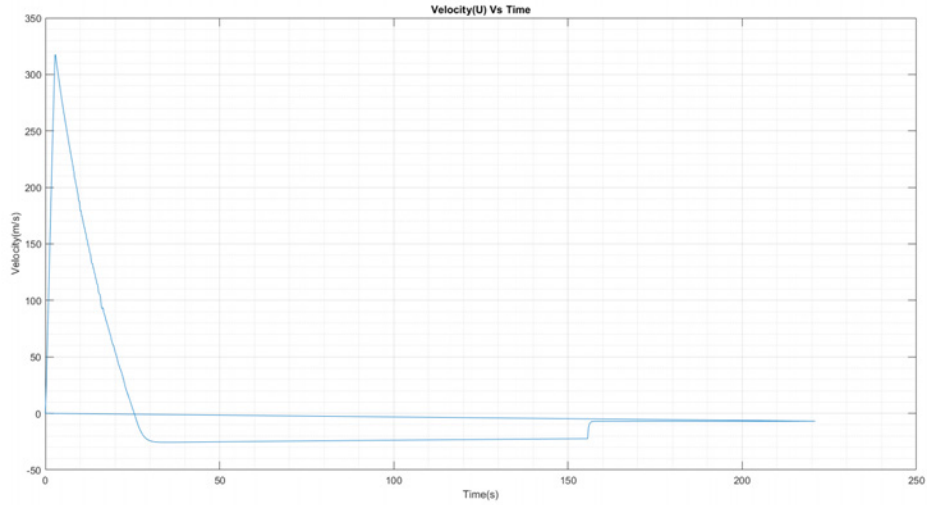


**Figure 18 Velocity vs Time**

CFD simulations were performed on the entire rocket at different Mach numbers and angles of attack to generate an aerodynamic data set consisting of aerodynamic force coefficients and the centre of pressure of the rocket. This data set, along with the motor thrust time curves and rocket's weight and centre of gravity, found from CAD, were fed into the code. The apogee predicted by this code is selected as the final predicted apogee of the rocket.

Details regarding the working and validation of the simulator code are given in Appendix H.

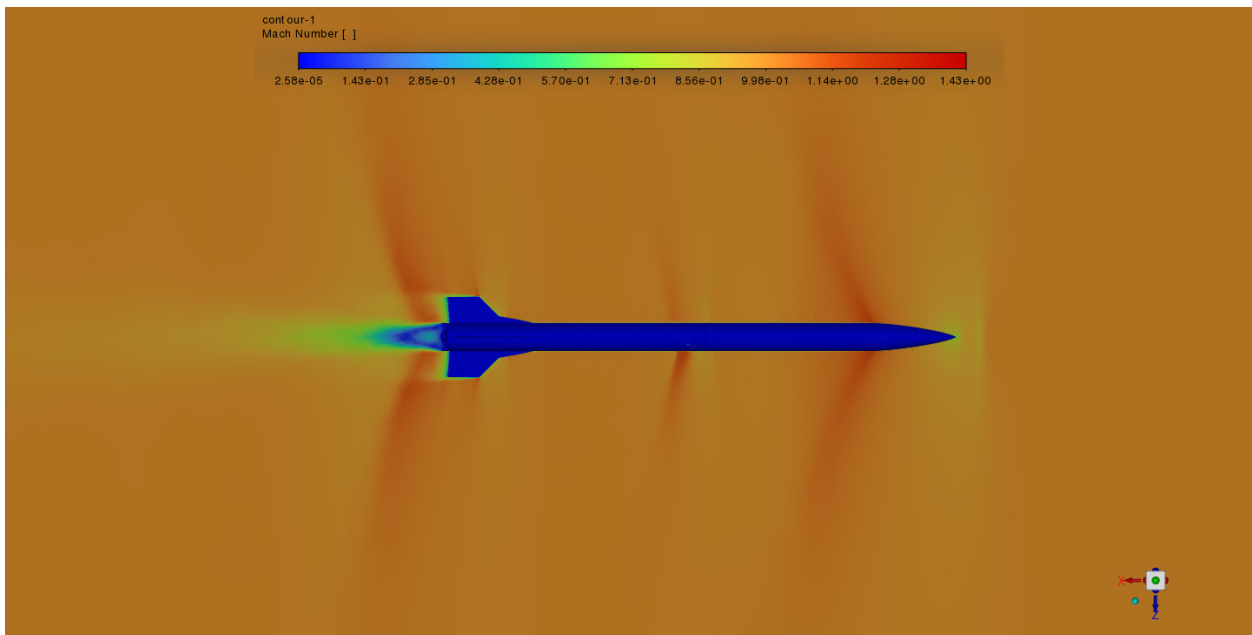


**Figure 19 Mach Contour**

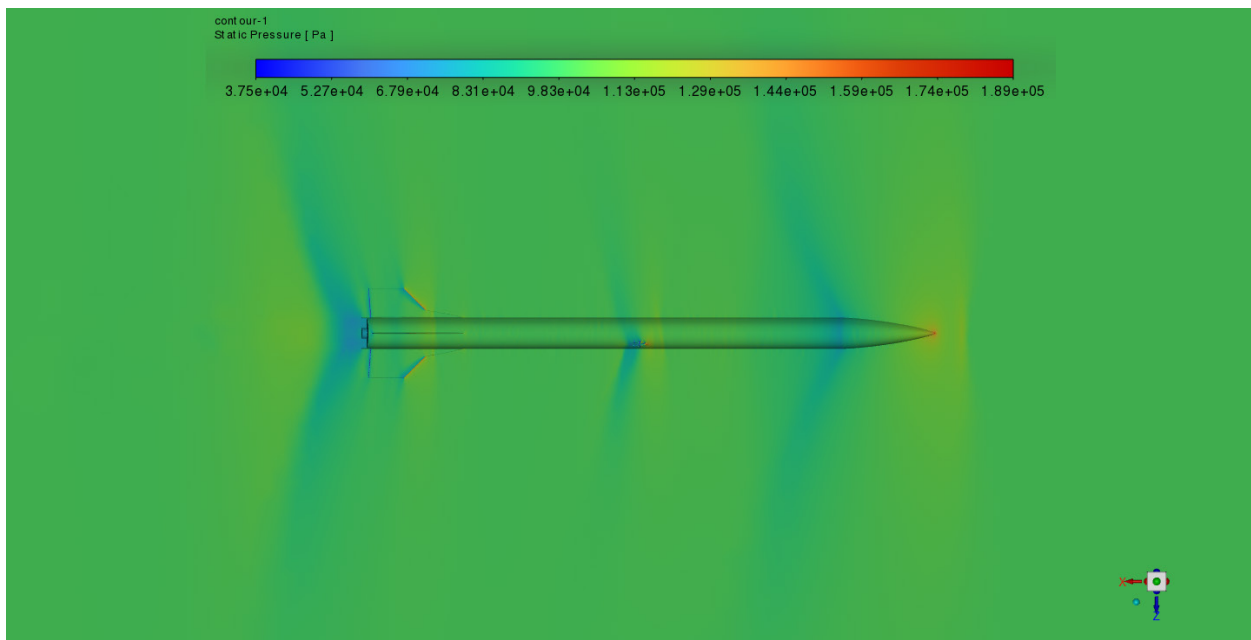


**Figure 20 Pressure Contour**

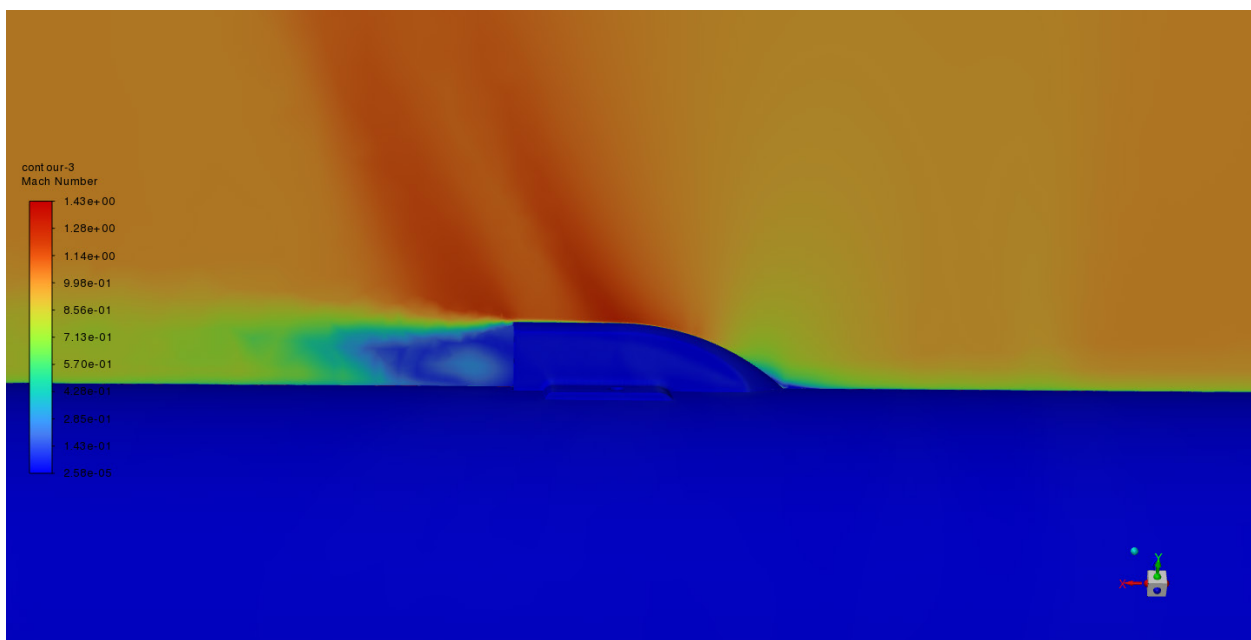


**Figure 21 Mach Contour - Camera Module**

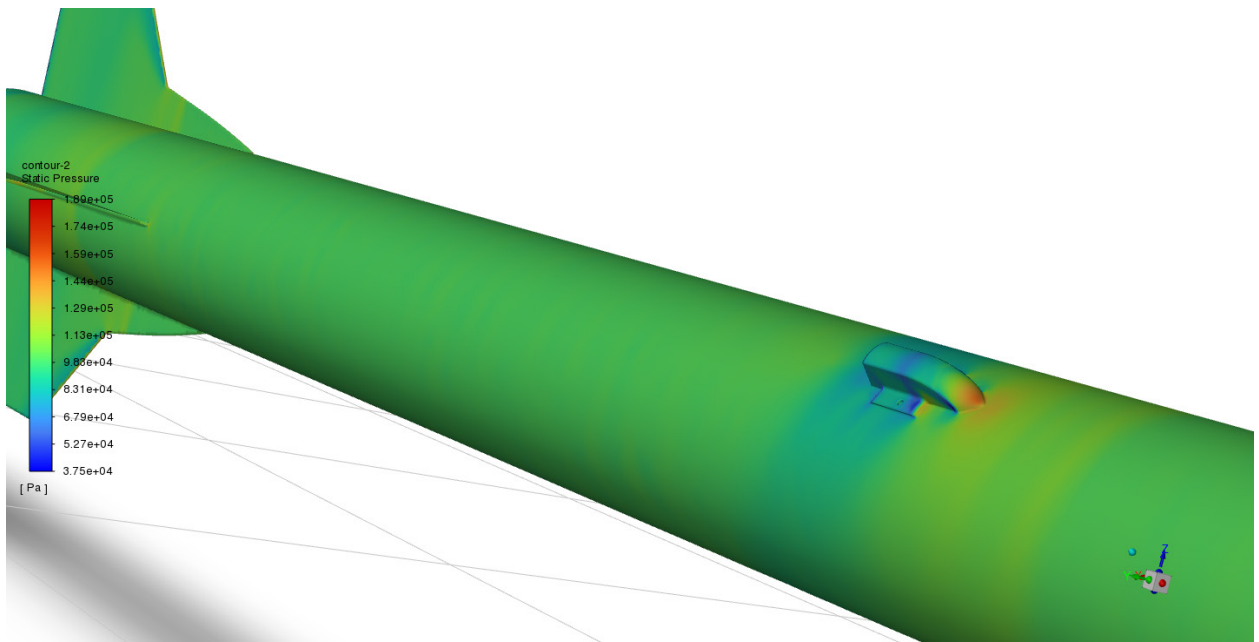


**Figure 22 Pressure Contour - Camera Module**

#### 6. Rail Buttons

Two airfoil type rail buttons made of Ultra High Molecular Weight Polyethylene, a tough, abrasion, and wear-resistant plastic, are installed into the rocket. One button is mounted to the stringer for the avionics bay, and the other to the centring ring in the motor bay. This is done keeping in mind the position of the rocket's centre of gravity as the launch buttons must bear the weight of the entire rocket while on the launch pad. The launch buttons were fixed to the components using a 1/4"-20 UNC bolt.



**Figure 23 Rail Button**

## B. Propulsion

### 1. Motor Details

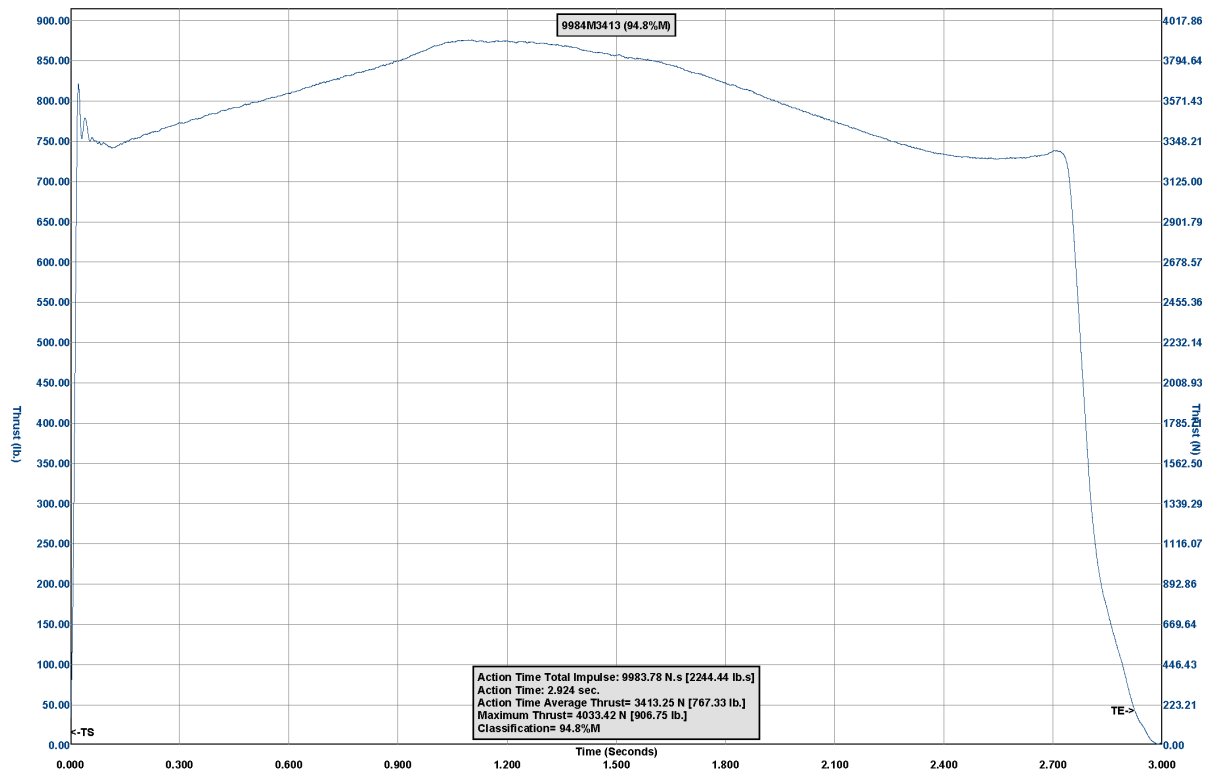
Rayquaza uses a COTS motor. The motor selection was an iterative process involving the satisfaction of various criteria such as launch requirements, maximum flight velocity and achieving the apogee constraints. The motor that was ultimately selected was a Cesaroni Technology Pro98 9994M3400-P. The M3400-P is an M class reusable 98 mm (3.86 in) motor. The performance characteristics of the motor are shown in Table 3. The certification thrust-time curve of the motor is shown in Fig. 24.

The motor comprises a 4-segment cored grain manufactured with a proprietary Ammonium Perchlorate Composite Propellant. The grains are liner bonded via the application of a manufacturer-recommended adhesive.

**Table 3 Performance Characteristics of Pro98 M3400-P**

Total Impulse	9994.5 N s (2246.85 lbs)
Specific Impulse	228.92 s
Average Thrust	3421.1 N (769.09 lb)
Maximum Thrust	3983 N (895.41 lb)
Burn Time	2.92 s

Ignition of the motor is carried out by the proprietary pyrogen igniter supplied with the motor – ProFire. Two ignitors shall be installed in the motor to ensure reliable ignition and reduce the risk of a hangfire. The ESRA provided ignition system will be used for initiating ignition. At lift-off, the thrust-to-weight ratio of the rocket will be 11.97.



Tue 10-Nov-2009  
11:21 AM

Page 1 of 1

**Figure 24 Pro98 9994M3400-P Thrust-Time Curve**

## 2. Bay Design

The Motor Bay consists of the primary motor bay fuselage measuring 735 mm (28.94 in) in length and one coupler of 300 mm (11.81 in) connecting the Motor Bay to the Payload Bay.

The interior of the motor bay was designed keeping in mind the thrust and vibrational forces along with the thermal loads that will be experienced in flight. A thrust plate of 20 mm (0.79 in) thickness made of Aluminium 6063 attaches to the motor with a 3/8" bolt.

The thrust plate is attached to the fuselage and stringer via eight M5 bolts at 45° to each other. The thrust plate is a load-bearing component and must withstand the entire thrust of the motor throughout the burn time.

The thrust force is transferred to the thrust plate through the damper, which acts as a female clamp to the motor-head and helps dampen out some of the vibrations produced by the motor during the burn. The thickness of the damper is 57 mm (2.24 in) and is placed below the thrust plate. It is attached to the motor by the 3/8" bolt used to attach the motor and the thrust plate. The damper itself is attached to the fuselage by two sets of four M5 bolts 90° to each other.

There are four stringers attached to the thrust plate. The stringers run axially through the motor bay to provide stability and rigidity to the entire assembly. All four stringers are attached to the thrust plate via M5 bolts. The set of four stringers are attached to the damper by eight M5 bolts.

One centring ring of 15 mm (0.59 in) thickness made of Aluminium 6063 is used to keep the motor centred along the rocket axis. It is attached to the fuselage by four M5 bolts 90° to each other. The centring ring is also designed to accommodate the fin attachment system. The stringers are attached via M5 bolts to the centring ring.

An Aluminium 6063 retainer of thickness 18 mm (0.71 in) is placed at the bottom of the motor to hold the motor's weight after burnout in case the thrust plate bolt fails. This retainer is placed within the motor bay and is attached to the fuselage using four M5 bolts.

Each component of the motor bay underwent topology optimization to achieve minimum component mass for maximum structural strength while ensuring ease of manufacturability. Material selection for all the components was influenced by in-flight loading conditions and research and development of the team's future SRAD propulsion systems.

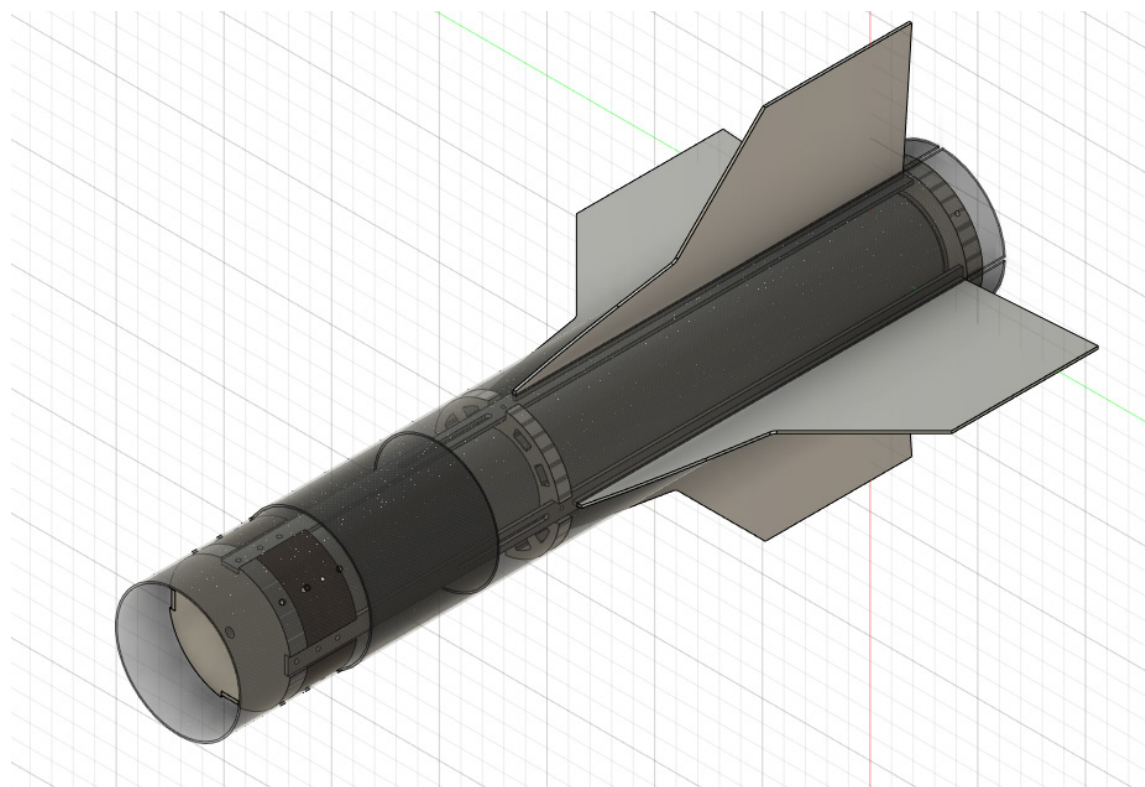


**Figure 25 Motor Bay (50 mm grid with 5 subdivisions for scale)**

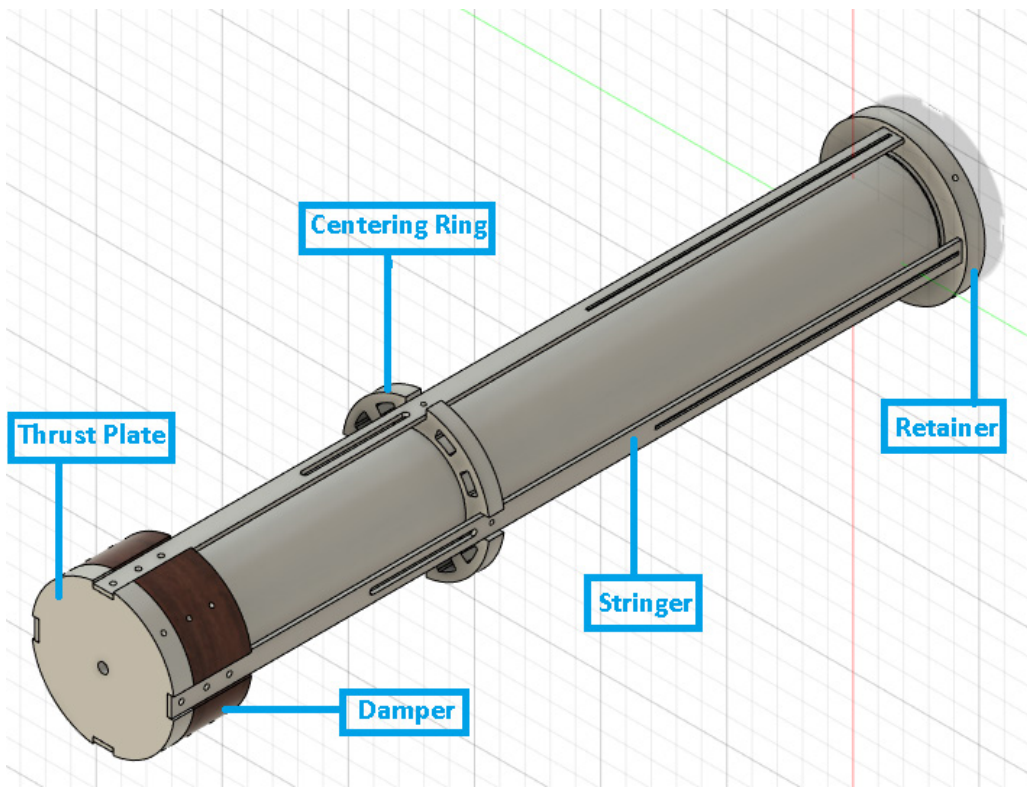


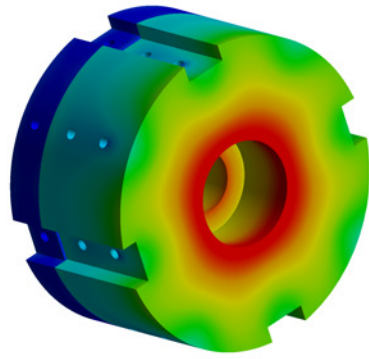
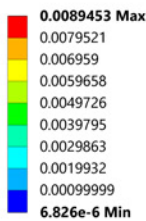
**Figure 26 Internal support structure for the motor bay (50 mm grid with 5 subdivisions for scale)**

The structural integrity of the motor bay and all its supporting components is of paramount importance to the rocket's success and its mission. Hence, a variety of simulations were run on the individual components of the motor bay to test their strength and stability under worst-case conditions.

The damper and the thrust plate were tested for shock absorption and stability. The thrust force of 6000 N (1348.85 lbf) including a factor of safety of 1.5, was applied to the lower surfaces of the damper and thrust plate, along with constraints at the edges of the bolt holes to simulate the connection between the fuselage and thrust plate/damper.

A maximum deformation of 0.008 mm (0.00031 in) at the point of application of direct thrust force was found, which is negligible, along with a maximum stress of 38.131 MPa (5530 psi) at the bolt holes that hold the components in place. This low stress can be explained by the high compressive strength of WPC, which enables it to absorb most of the load.

A: Static Structural  
 Total Deformation  
 Type: Total Deformation  
 Unit: mm  
 Time: 1  
 10-05-2022 22:51



0.00 50.00 100.00 (mm)  
 25.00 75.00

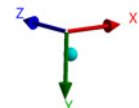
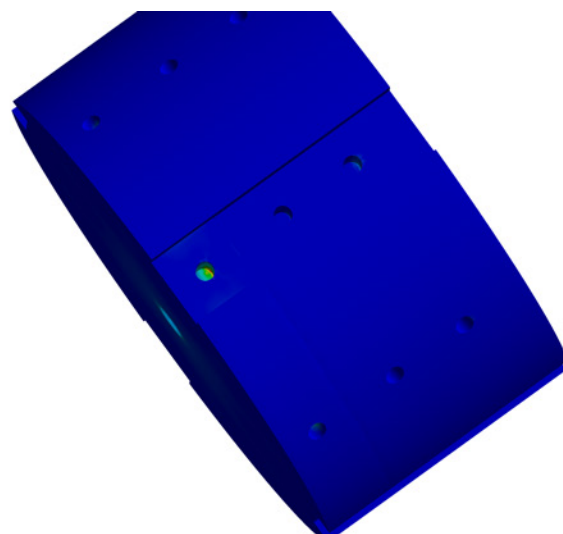
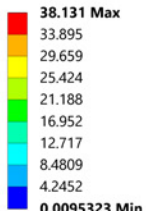


**Figure 27** Deformation results for the Damper and Thrust Plate

A: Static Structural  
 Equivalent Stress  
 Type: Equivalent (von-Mises) Stress  
 Unit: MPa  
 Time: 1  
 10-05-2022 22:51



0.00 50.00 100.00 (mm)  
 25.00 75.00

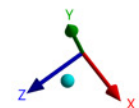


**Figure 28** Von-Mises stress results for the Damper and Thrust Plate

A separate simulation was performed to test the stability of the centring ring being used in the motor bay. This was done to see the effect of the shear forces the motor would have on the rings.

The centring rings were subjected to an approximate shearing thrust force exerted by the motor of 3000 N (674.43 lbf) and constrained at the edges of the bolt holes to simulate the connection between the fuselage and centring rings using bolts.

It was observed that the centring rings underwent a deformation of  $0.005\text{ mm}$  ( $2.0 \times 10^{-4}\text{ in}$ ) along the inner surface of the ring, with the deformation localized to the region in between the shape optimization slots with a maximum stress of  $71.132\text{ MPa}$  ( $10316\text{ psi}$ ) near bolt hole edges. These values are well within the acceptable limits. In actual practice, the stress expected to be experienced by the centring rings will be significantly lower due to lower loading conditions and reinforcement by other components attached to the rings. Therefore, it was concluded that the centring rings are safe for use in-flight.

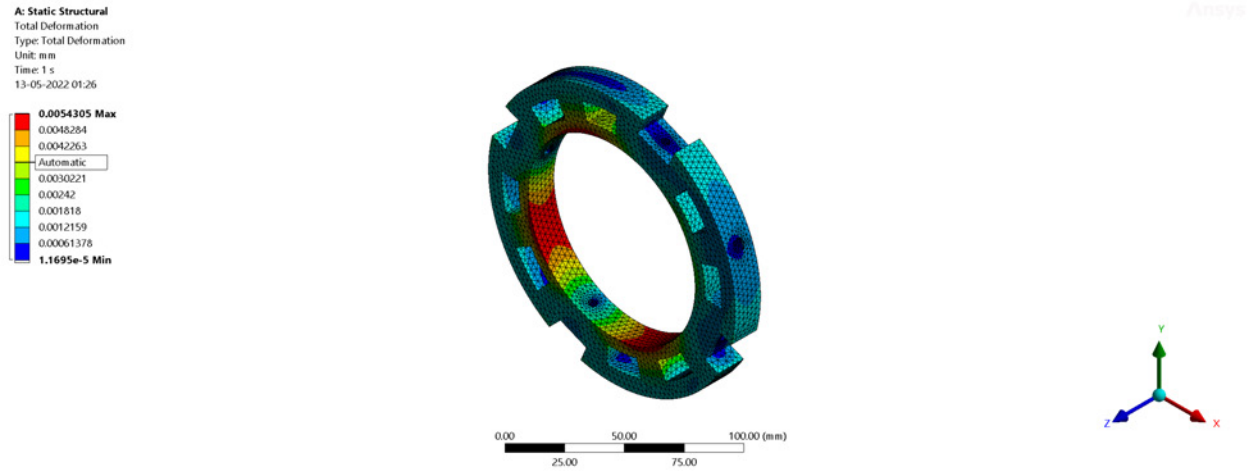


**Figure 29** Deformation results for the Centering Ring

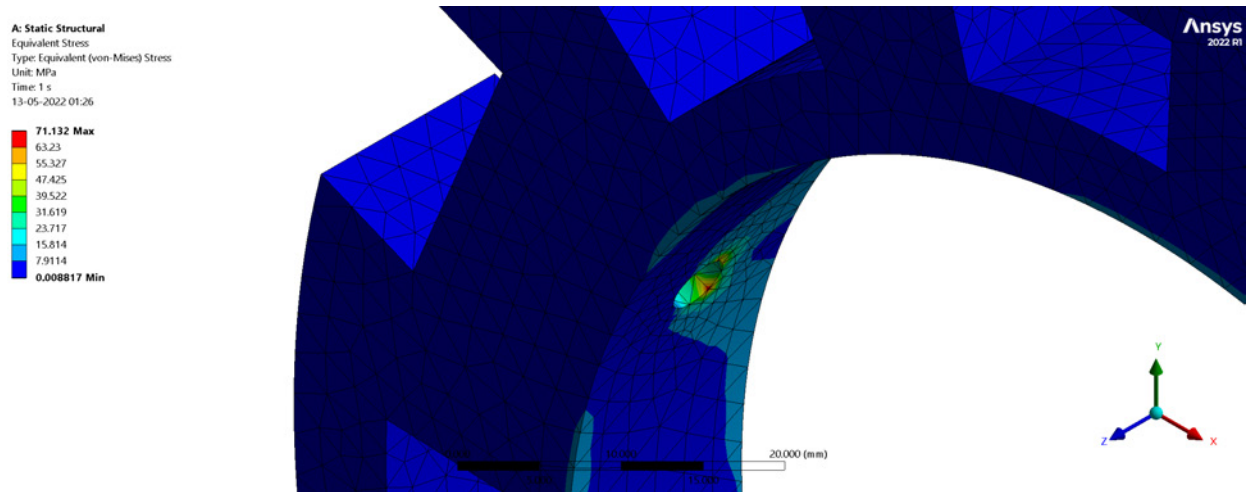


**Figure 30** Von-Mises stress results for the Centering Ring

A simulation was performed to test the strength of the retainer being used at the bottom of the rocket. This simulation was necessary to determine the ability of the retainer to hold the motor in place in case of failure of the bolt holding the motor in place.

The retainer was subjected to a downward weight of the motor of  $2400\text{ N}$  ( $539.54\text{ lbf}$ ) and constrained at the edges of

the bolt holes to capture the attachment of the retainer to the body tube using bolts.

The retainer underwent a deformation of 0.003 mm ( $1.2 \times 10^{-4}$  in) along with a maximum stress of 20.661 MPa (2997 psi).

In actual practice, the stress expected to be experienced by the retainer will be significantly lower due to lower loading conditions and reinforcement by other components attached to it.

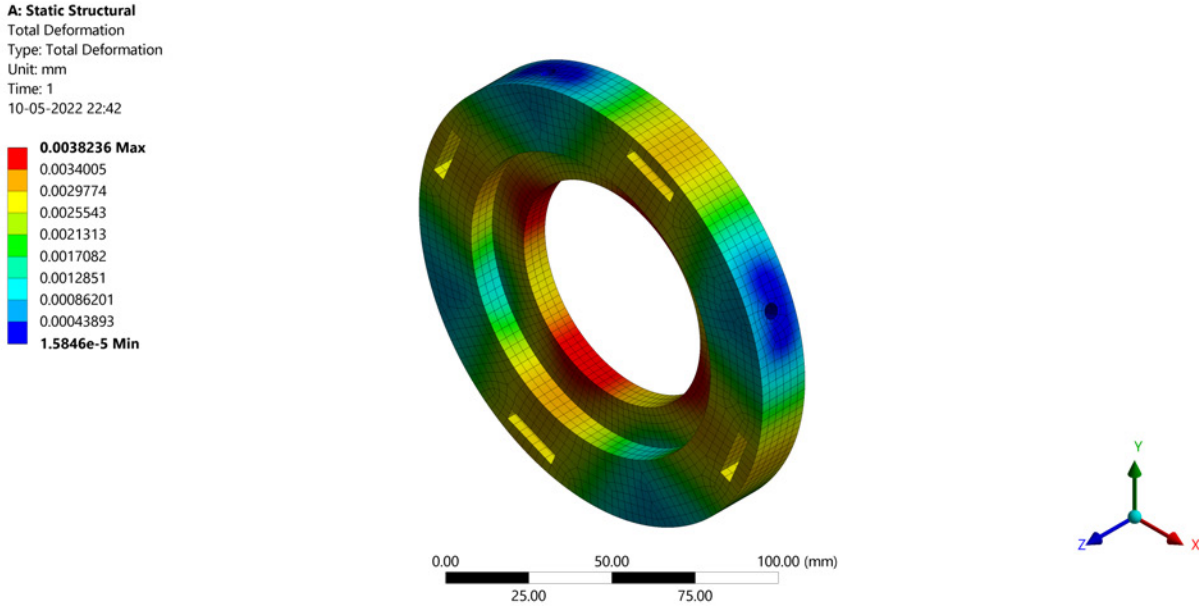


Figure 31 Deformation results for the Retainer

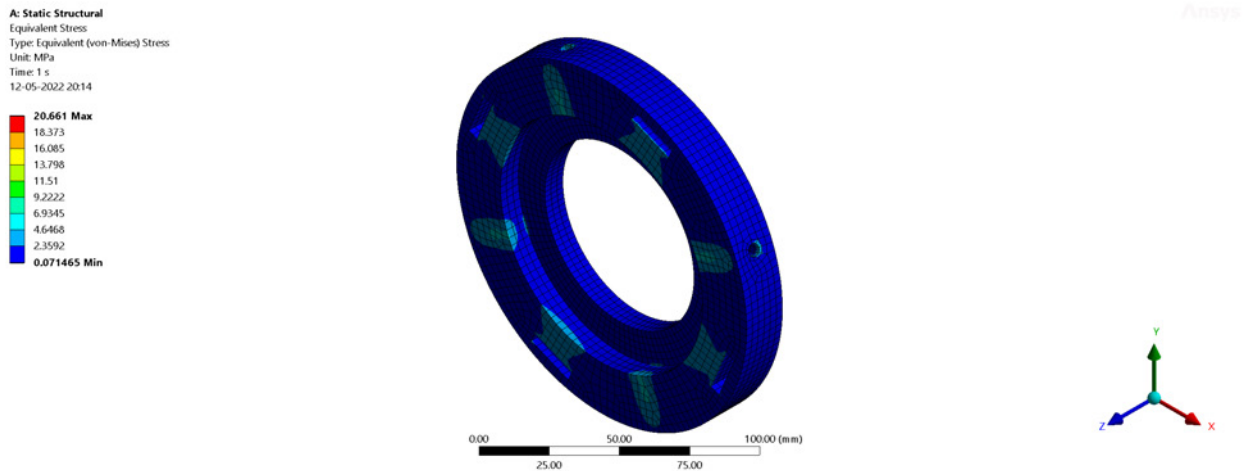


Figure 32 Von-Mises stress results for the Retainer

### C. Recovery

The rocket will be recovered by a single parachute acting as both the drogue parachute (in reefed condition) and main parachute (in a dis-reefed condition).

The parachute is folded and packed inside a Kevlar blanket to protect the parachute from the high-temperature gases released by the ejection mechanism. The Recovery bay is located immediately below the Nosecone. The Nosecone is attached to the fuselage by four #2-56 Nylon shear pins. At the bottom end of the bay, a piston-cylinder arrangement is used to deploy the parachute. The cylinder is made integral on the 15 mm (0.59 in) thick Aluminium 6063 bulkhead separating the Recovery and the Mid bays. A piston head is fitted into the cylinder. The piston consists of a solid disk with a cylindrical extrusion, with the piston and cylinder designed and manufactured to have a clearance fit between them to facilitate ease of assembly.

An electric match constructed from multiple 24 AWG Nichrome bridgewires passes from the other end of the bulkhead through two holes drilled 20 mm (0.79 in) apart, into the cylinder section. The recovery mechanism is triggered when the flight computer detects that the rocket has reached apogee. The electric match ignites the ejection charge, building up pressure in the cylinder until it is high enough to push out the piston and the parachute placed on top of the piston. The parachute pushes onto a 50 mm (1.97 in) WPC bulkhead. This bulkhead is attached to the shoulder of the Nosecone using phenolic resin. This sequence of events produces enough force to break the shear pins and push the Nosecone away, releasing the parachute from the rocket body.

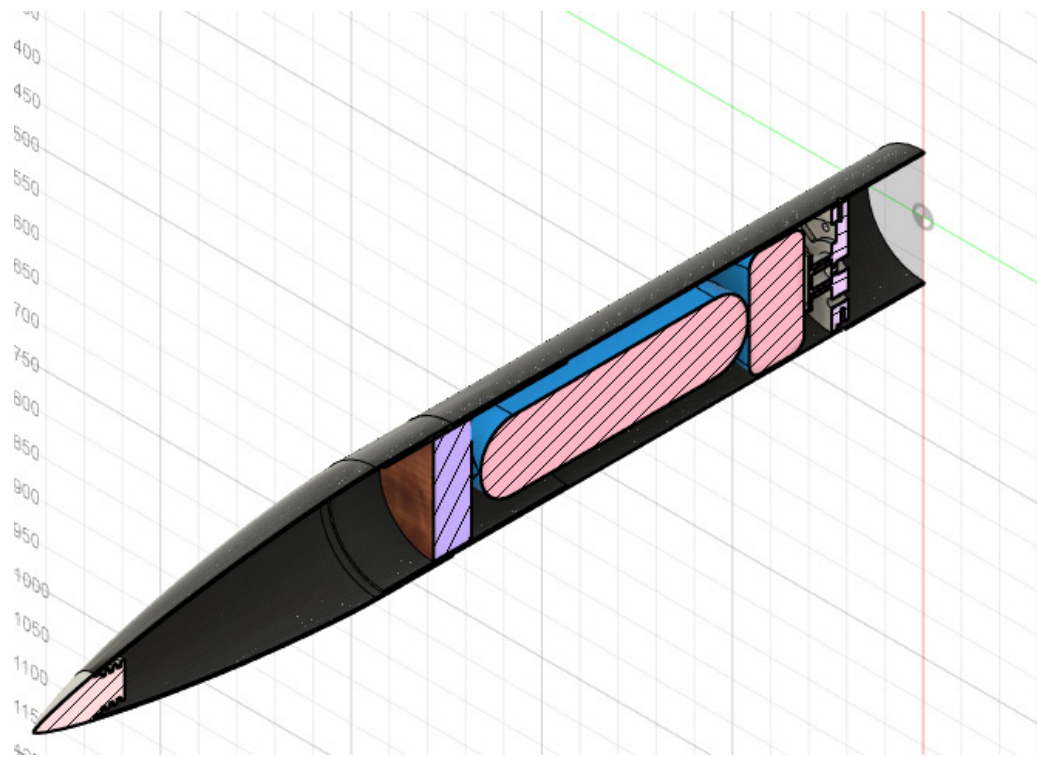


**Figure 33 Cross-section of the Recovery bay and Nosecone (20 mm grid with 5 subdivisions for scale)**

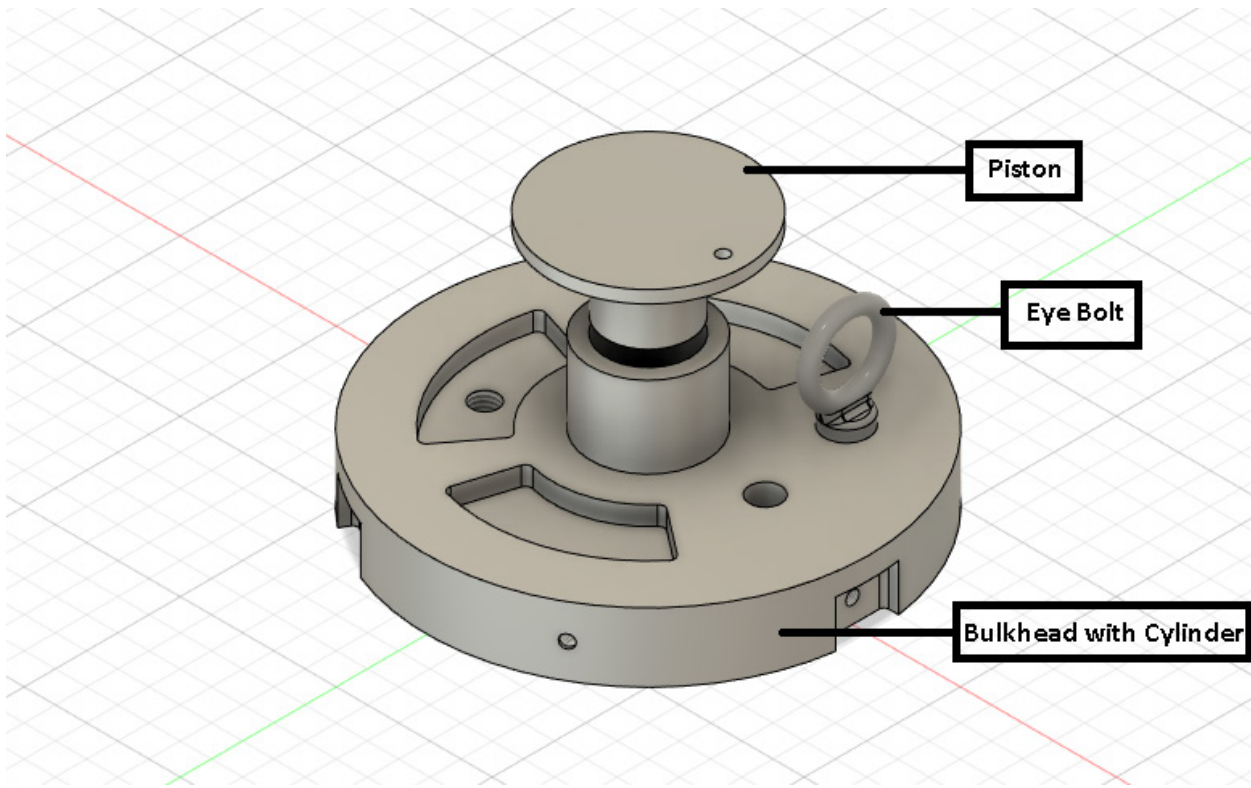


**Figure 34 Ejection Mechanism mounted on the recovery bulkhead (10 mm grid with 5 subdivisions for scale)**

The recovery bulkhead was tested to check for failure upon the force generated by the ignition of the ejection charge. The bulkhead was constrained at the four bolt edges to simulate the bolted connections between the bulkhead and the recovery fuselage. The simulations results yielded a deformation of 0.003 mm ( $1.2 \times 10^{-4}$  in) along with a maximum stress of 16.88 MPa (2448 psi). The maximum deformation was observed directly at the base of the ejection cylinder and a uniform outward reducing trend of deformation, indicative of the impact caused by the pressurising of the ejection system and eventual deployment of the parachute. High-stress concentration was observed at the edges of the bolt holes connecting the bulkhead to the body tube. The location of the stress is attributed to the load that the bolts will face upon the impact of the ignition of the ejection system.

Overall, these stress and deformation values and their distribution pattern were deemed acceptable and safe for use within the rocket.

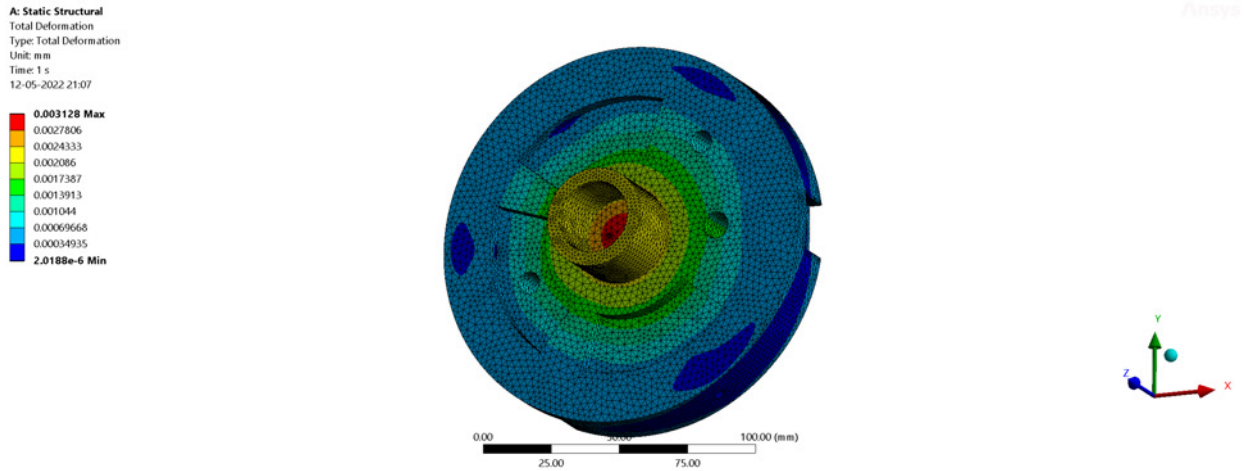


**Figure 35 Deformation results for the recovery bulkhead**

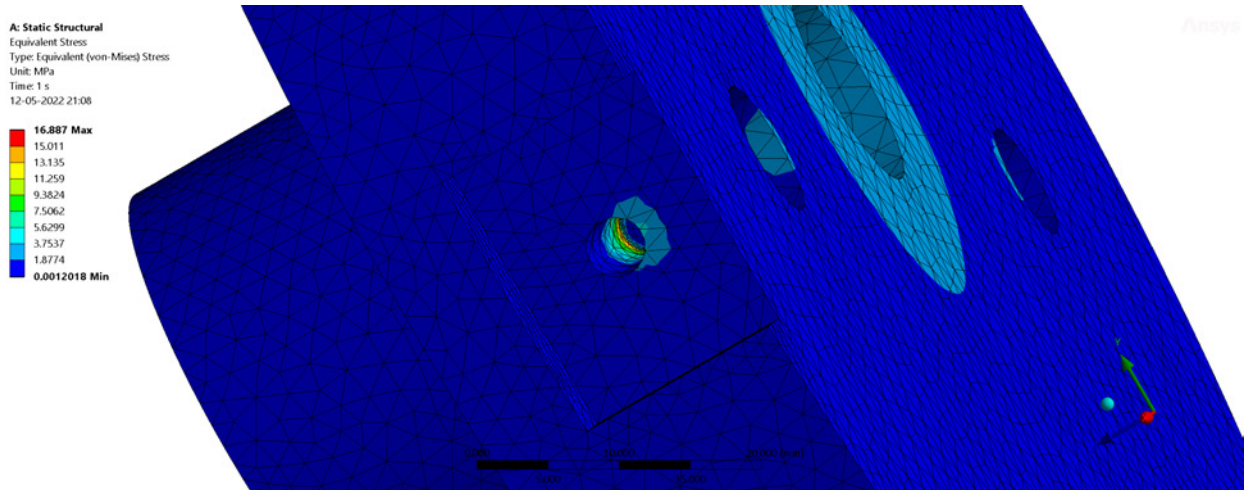


**Figure 36 Von-Mises Stress results for the recovery bulkhead**

The structure of the rocket recovery system is described in detail as follows:

### 1. Deployment mechanism

Parachute deployment denotes the sequence of events that begins with the opening of a parachute compartment or parachute pack attached to the body to be recovered. Deployment continues with the extraction of the parachute until the canopy and suspension lines are stretched behind the body, and the parachute canopy is ready to start the inflation process. This deployment is associated with a mass shock (snatch force) created due to sudden deceleration of rocket due to inflation of canopy. The parachute is reefed and deployed near the apogee by the flight computer. A maximum time delay of 2 s is given between the rocket attaining apogee and the parachute's deployment to allow the canopy to inflate.

## 2. Deployment Charge

The charge used in the deployment mechanism is commercial 4F grade black powder. The powder is filled into the cylinder and the piston then snugly fitted. When the flight computer initiates deployment, the Nichrome bridgewire ignites the ejection charge and generates enough pressure within the cylinder-piston setup to blow off the Nosecone and eject the parachute.

For determining the amount of ejection charge required, the following equation based on the ideal gas model is used (Equation 26, [2]):

$$\frac{F}{A} = P_a + \frac{\delta \Delta F_e m}{\delta - \Delta}$$

where

$$\Delta = \frac{C}{V}$$

$$\lambda = \frac{RT}{M}$$

For commercial 4F grade ejection charge, the charge density  $\delta$  is  $3780 \text{ kg m}^{-3}$  ( $236 \text{ lb ft}^{-3}$ ) and the effective force  $F_e$  is  $299 \text{ kJ kg}^{-1}$  ( $1 \times 10^5 \text{ ft lbf lb}^{-1}$ ). Experimental testing of the recovery mechanism showed a total charge mass of 3 g (0.11 oz) resulted in reliable ejection of the parachute. This corresponds to a consumed charge mass  $m$  of 25 %, accounting for the transient losses, losses due to incomplete combustion of the mixture and losses due to non-adiabatic combustion/non-adiabatic expansion of the combustion gasses. To provide redundancy, an additional fail-safe charge of 4 g (0.14 oz) is utilised.

## 3. Parachute Design

The Nominal Diameter  $D_o$  of the parachute can be calculated from the total canopy surface area, including the area of the vent and all other openings. For the descent, the recommended canopy shapes are flat circular and hemispherical.

TYPE	CONSTRUCTED SHAPE		$\frac{D_c}{D_o}$	$\frac{D_p}{D_o}$	DRAG COEF $C_{D_o}$ RANGE	OPENING FORCE COEF $C_X$ (INF MASS)	AVERAGE ANGLE OF OSCILLATION, DEGREES	GENERAL APPLICATION
	PLAN	PROFILE						
FLAT CIRCULAR		— —	1.00	0.67 TO 0.70	0.75 TO 0.80	~1.7	:10 TO :40	DESCENT, OBSOLETE
CONICAL		0.93 TO 0.95	0.70	0.75 TO 0.90	~1.8	:10 TO :30	DESCENT, $M < 0.5$	
BICONICAL		0.90 TO 0.95	0.70	0.75 TO 0.92	~1.8	:10 TO :30	DESCENT, $M < 0.5$	
TRICONICAL POLYCONICAL		0.90 TO 0.95	0.70	0.80 TO 0.96	~1.8	:10 TO :20	DESCENT, $M < 0.5$	
EXTENDED SKIRT 10% FLAT		0.86	0.66 TO 0.70	0.78 TO 0.87	~1.4	:10 TO :15	DESCENT, $M < 0.5$	
EXTENDED SKIRT 14.3% FULL		0.81 TO 0.85	0.66 TO 0.70	0.75 TO 0.90	~1.4	:10 TO :15	DESCENT, $M < 0.5$	
HEMISPERICAL		0.71	0.66	0.62 TO 0.77	-1.6	:10 TO :15	DESCENT, $M < 0.5$ , OBSOLETE	

Figure 37 Types of parachute canopies

The recovery system in our rocket is a single parachute dual sequence deployment. To accomplish this objective, we use a ten-gore skirt reefed elliptical canopy parachute of projected diameter 3600 mm (141.73 in) where the ratio of height to radius is 0.707. The rocket will achieve an ultimate terminal velocity of  $8.1 \text{ m s}^{-1}$  ( $26.57 \text{ ft s}^{-1}$ ).

A parachute with an elliptical canopy has essentially the same  $C_d$  as a hemispherical parachute or a parasheet of the same deployed diameter. However, it uses less material in the assembled parachute than the hemispherical or parasheet type and, as a result, should be lighter than the parasheet type of equivalent diameter.

To form a parachute that deploys as a semi-ellipsoid, we take the desired three-dimensional semi-ellipsoidal shape and divide it into several two-dimensional panels, called gores. Each gore is individually cut to a specific shape so that when re-assembled, it will form a semi-ellipsoid upon deployment.

This particular parachute comprises ten gores individually cut from the fabric material and sewn together to form the canopy. The shape of the gores was calculated and generated using MATLAB to achieve a height to radius ratio of 0.707. The MATLAB code used has been attached to the end of this report as Appendix K.

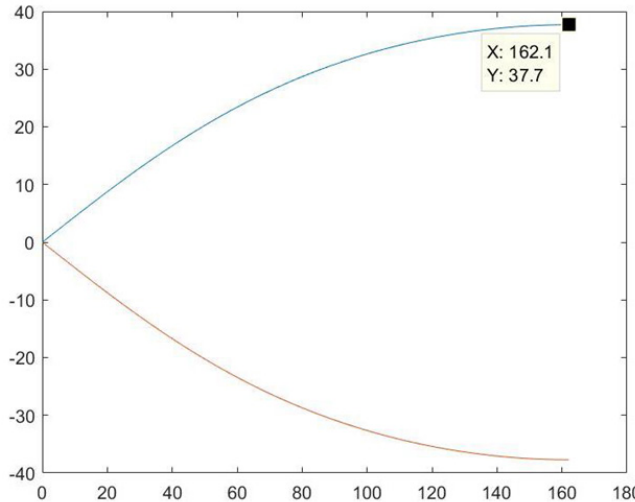


**Figure 38 Gore pattern plot**

The above pattern was traced out on the fabric and hemmed along the curved edges and bottom edges. Ten such patterns were produced. The panels were then joined using seam binding. Four such lengths of seam binding, long enough to span the entire arc length of the canopy, were used.

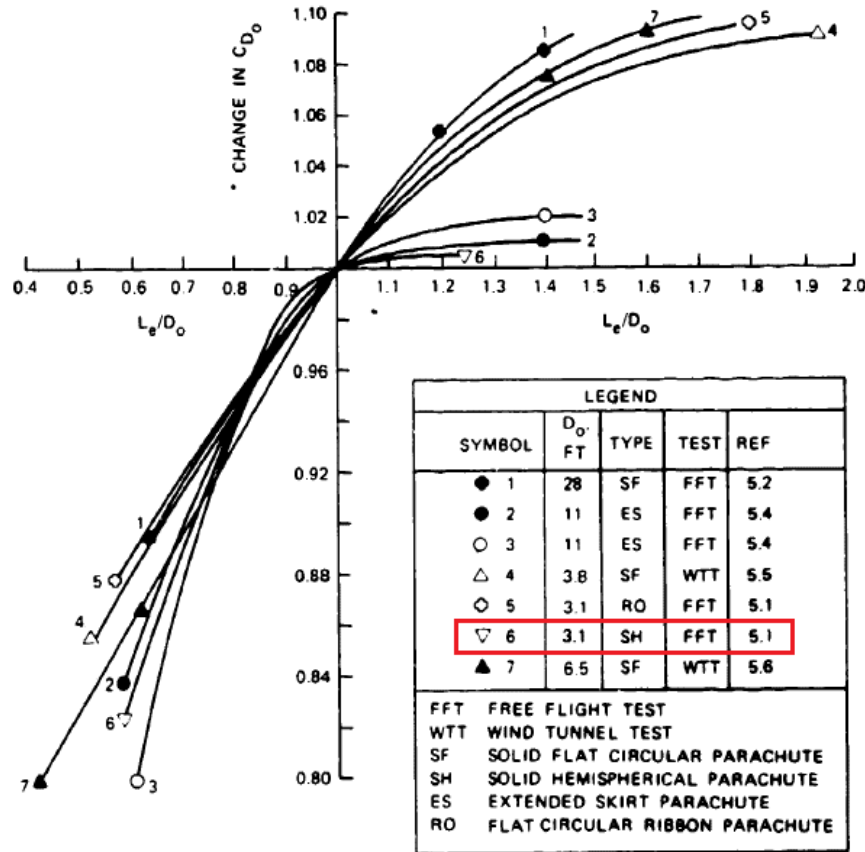


**Figure 39 Variation of  $C_d$  with  $\frac{L}{D}$**

The drag coefficient increases with an increase in the suspension-line ratio  $\frac{L}{D}$ . The slopes of the curves for the area and projected diameter growth indicate that using suspension-line ratios larger than 1.1 may increase drag. The calculations indicate that line-length ratios above 1.5 may be detrimental because of the associated weight increase of the long lines. The canopy dimensions stated above the length of the suspension lines are 2880 mm (113.39 in) (taking line ratio  $\frac{L}{D}$  as 1.2).

Four ellipsoidal parachutes with different  $\frac{b}{r_b}$  ratios are analysed under the same physical conditions of pressure, velocity, and temperature. The inlet velocity is taken as  $20 \text{ m s}^{-1}$  ( $65.62 \text{ ft s}^{-1}$ ) in the positive Y-direction at 1 atm (14.70 psi) and 293.2 K (68.09 °F).

CFD simulations in SolidWorks were performed to decide an efficient canopy shape of our parachute. The following are the pressure contours on the surface of the canopies:

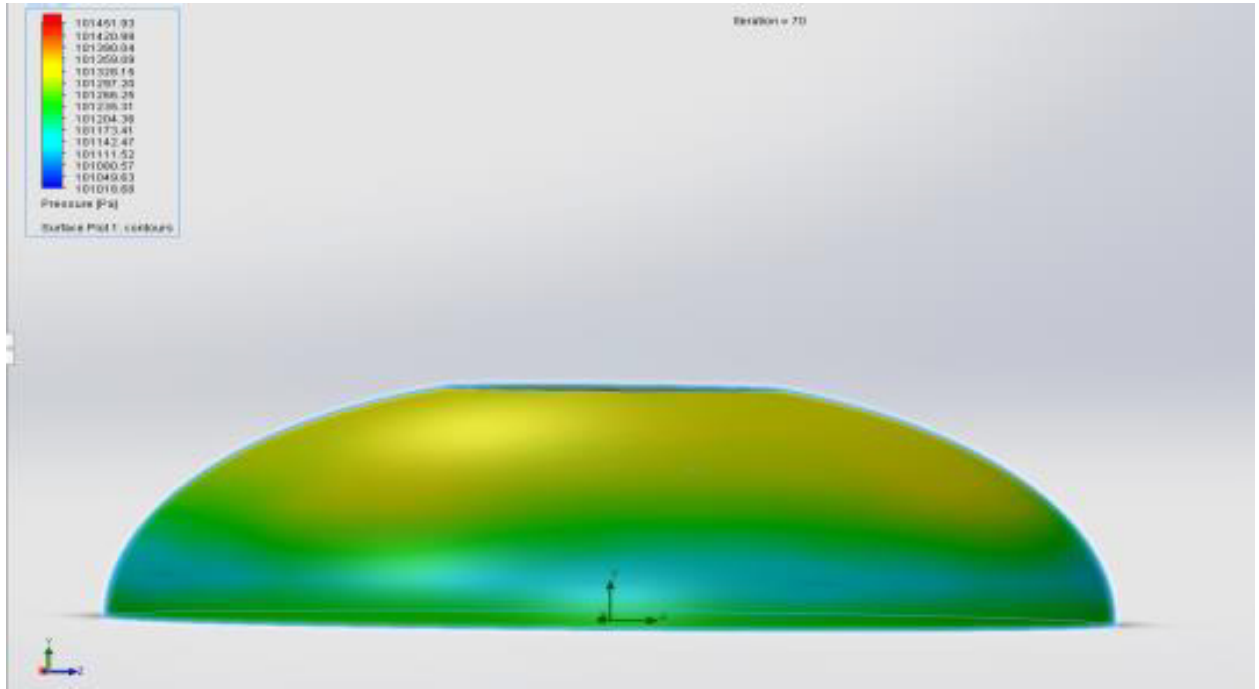


**Figure 40 Pressure contour over the canopy for  $\frac{b}{r_b} = 0.6$**

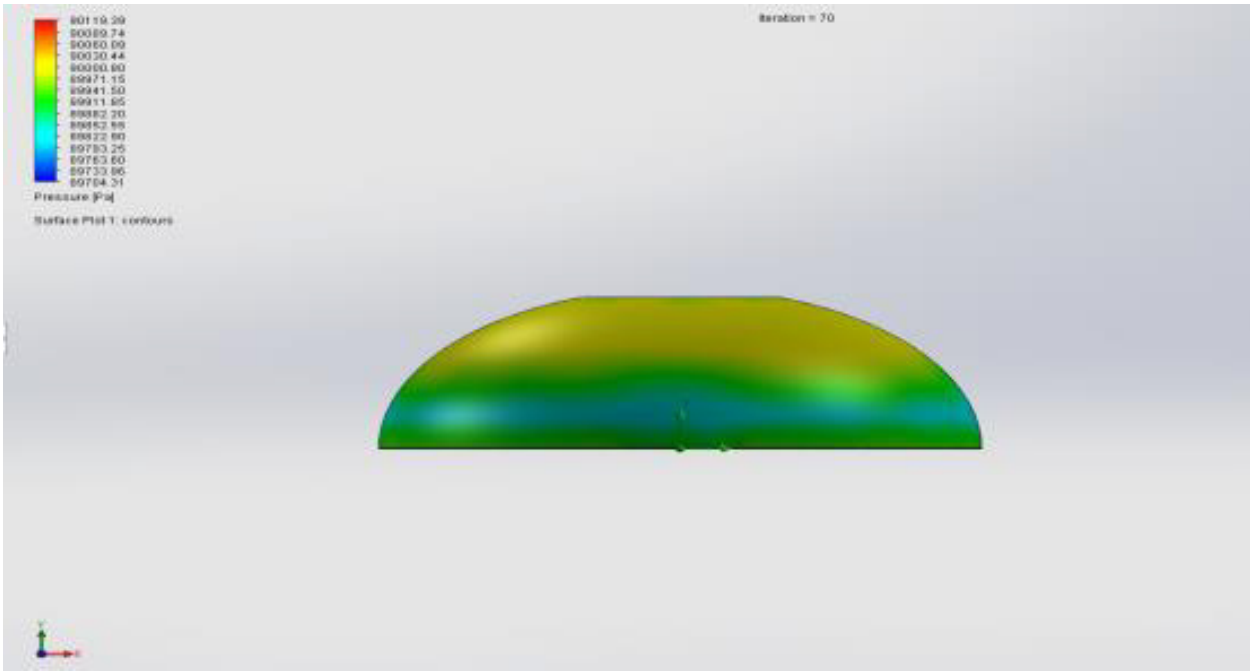


**Figure 41** Pressure contour over the canopy for  $\frac{b}{r_b} = 0.7$

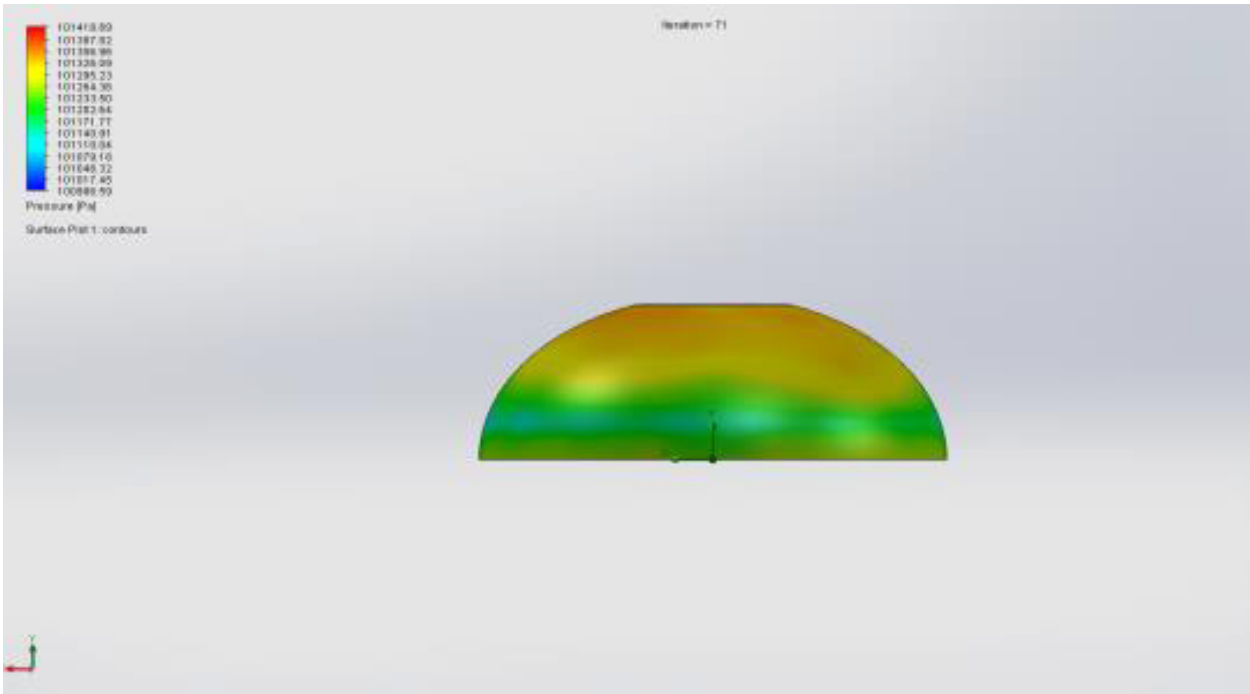


**Figure 42** Pressure contour over the canopy for  $\frac{b}{r_b} = 0.8$

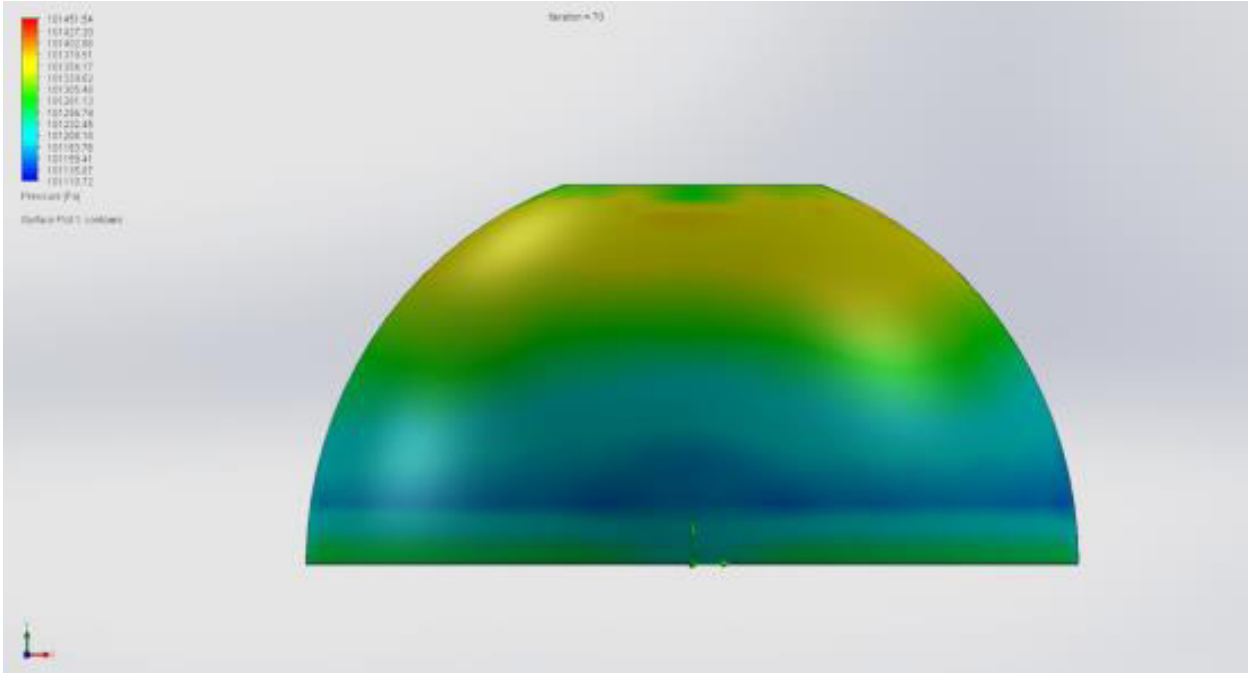


**Figure 43 Pressure contour over the canopy for  $\frac{b}{r_b} = 1$**

It is observed that high-pressure distribution covers more area in parachutes with  $\frac{b}{r_b}$  ratios of 0.6 and 0.7. It is a desirable factor in a canopy so that there is no stress concentration and the material does not fail. After considering these results as well as factors such as the amount of material that will be used and the manufacturability of the pattern, a  $\frac{b}{r_b}$  value of 0.707 was used.

#### 4. Reefing

Reefing was chosen over dual deployment because of the following reasons:

- Reduction of mass and volume as only one parachute is used.
- The deployment sequence is less complicated as a smaller number of components are used.
- Single Parachute deployment results in the rocket being split into only two components from the nose cone rather than having many separations throughout the body.

The canopy opening is about 60% of the skirt diameter in the reefed condition. The drag coefficient for a typical reefed flat circular parachute is dependent on the nominal diameter. Due to less drag force in the reefed condition, the amount of shock force experienced by the rocket is lower, which is essential to prevent failure of the attachment points of the shock cords. The lower drag force also results in a higher descent rate during the initial descent stages, which prevents the rocket from drifting in the presence of crosswinds.

While there are multiple techniques, the critical issue is friction between the reefing line and its attachments to the canopy. With too much friction, full parachute deployment is jeopardised when the reefing line is cut. A metal reefing

line ring is sewn into the canopy's edge, between each pair of suspension lines. Thus, if there are ten suspension lines, the reefing cord would pass through ten rings.

When an increase in drag is needed, the cord is cut, allowing full canopy deployment. The team has designed a dis-reefing system in-house. The setup for this system is as follows: First, the reefing lines are tied through the loops specially designed to restrict the diameter. Next, two Nichrome wires are tied on opposite ends of the parachute to allow redundancy in cutting. Wire leads from the two Nichrome pieces are stretched along the parachute's suspension lines and connected to the appropriate electronics. The Nichrome wires are enclosed in a 3D printed ABS casing that protects the Nichrome from the external environment. When the rocket reaches a height of about 457 m (1500 ft), an electrical charge is sent to the Nichrome wires, heating the element and cutting the reefing lines.

## 5. Materials

### A. Canopy

Ripstop Nylon 42 GSM - Ripstop fabrics are woven fabrics, often made of Nylon, using a unique reinforcing technique that makes them resistant to tearing and ripping. During weaving, (thick) reinforcement threads are interwoven at regular intervals in a crosshatch pattern. The intervals are typically 5 mm – 8 mm (0.20 in – 0.32 in). Thin and lightweight ripstop fabrics have a 3-dimensional structure due to the thicker threads interwoven in thinner cloth. Since our recovery uses a single parachute design, a dis-reefing mechanism is needed, such that when reefed, the parachute behaves like a drogue, and when un-reefed, it becomes the main parachute. This sequence was performed by rigging a cord around the periphery to reduce canopy volume. When an increase in drag is needed, the cord gets cut, allowing full canopy deployment.

### B. Suspension Lines

Ten Nylon (type III) suspension lines - Suspension lines (of length 360 cm) distribute the weight equally. They are tied to a swivel link and are long enough to ensure that the parachute can inflate without encountering any issues.

### C. Quick Link

Connects the suspension lines to the shock cord.

### D. Swivel Link

It prevents the suspension lines from getting entangled by providing rotational freedom.

### E. Shock cord

Made of Aramid, shock chords connect the suspension lines to the fuselage. Their function is to absorb the shock produced when the parachute opens. It prevents any damage to the fuselage as a result of the same. One end of the shock chords connects to the suspension lines with the help of a swivel link, while the other connects to an M10 eye bolt in the Nosecone. The shock chords, as is conventional, are taken to be approximately twice the length of the rocket, which they achieve at a length of 600 cm.

### F. Reefing Cutter

The reefing cutter is an in-house design 3D printed with ABS plastic.

#### G. Reefing Wires

Reefing Wires pass current to the reefing cutters; the wires are 22 AWG insulated copper wires covered in a nylon sleeve.

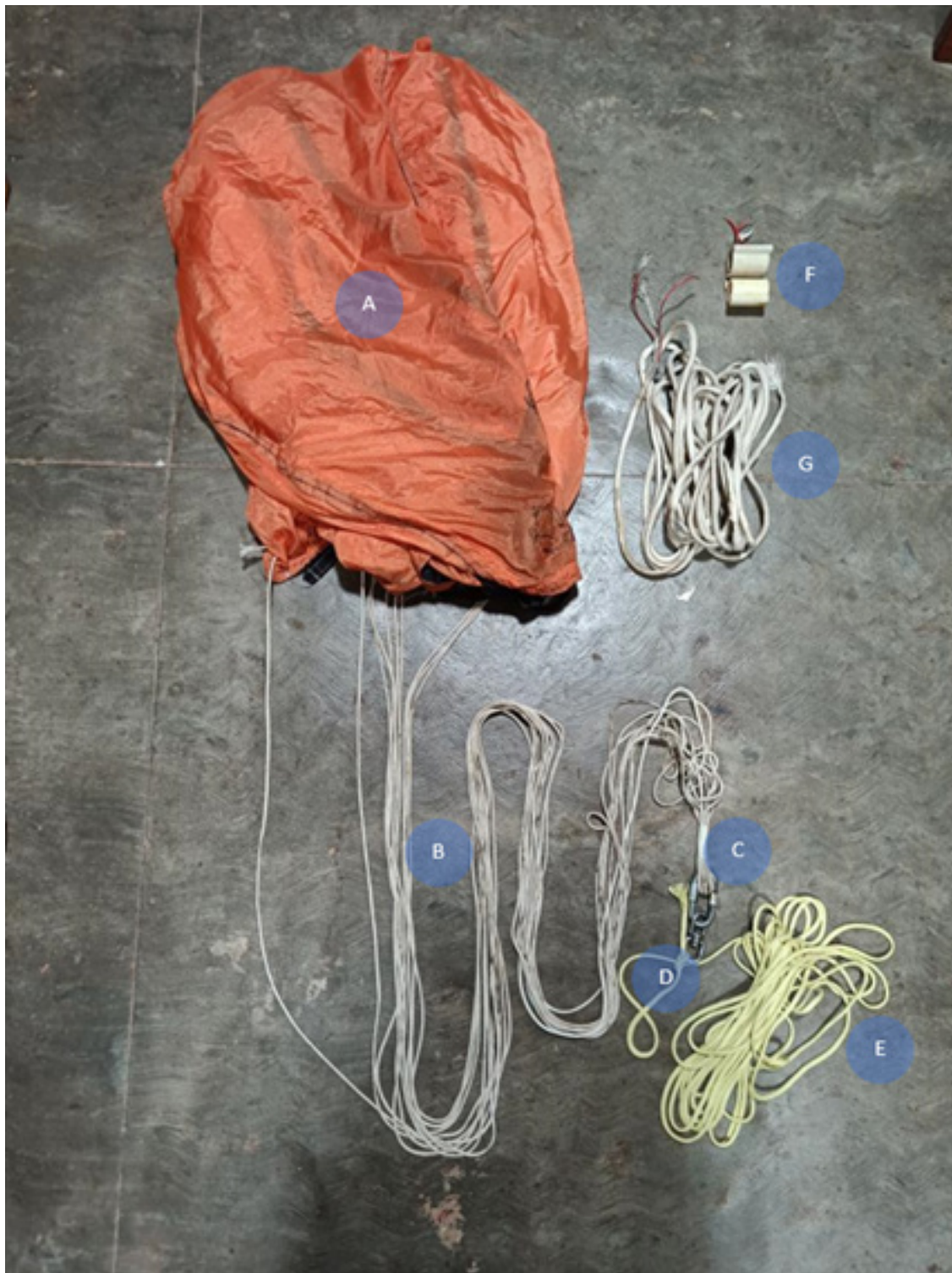


Figure 44 Recovery setup

## D. Avionics

Rayquaza's avionics system handles data logging, telemetry, parachute ejection, GPS tracking, and flight video recording. It consists of the following modules:

- 1) SRAD Flight Computer
- 2) COTS Altimeter
- 3) COTS GPS
- 4) FPV Camera

### 1. SRAD Flight Computer

The Flight Computer is responsible for the following primary purposes:

#### Data Logging

Flight data is instrumental for the team to perform tests and analyse the flight. Data-logging ensures that flight data from the sensors onboard is stored securely in a micro-SD Card.

#### Parachute Deployment

This is the primary function of the flight computer. The rocket uses a reefing mechanism. The flight computer deploys an ejection charge at apogee that partially unfurls the main parachute, followed by complete unfurling when the rocket reaches a safe altitude ( $\leq 457$  m AGL ( $\leq 1500$  ft AGL)).

#### Telemetry

Using an RF module, the flight computer transmits necessary data to the ground station. The transmission happens in the 915 MHz frequency band.

#### GPS

The flight computer collects GPS data to determine the location of the rocket. This data is transmitted to the ground station using radio communication.

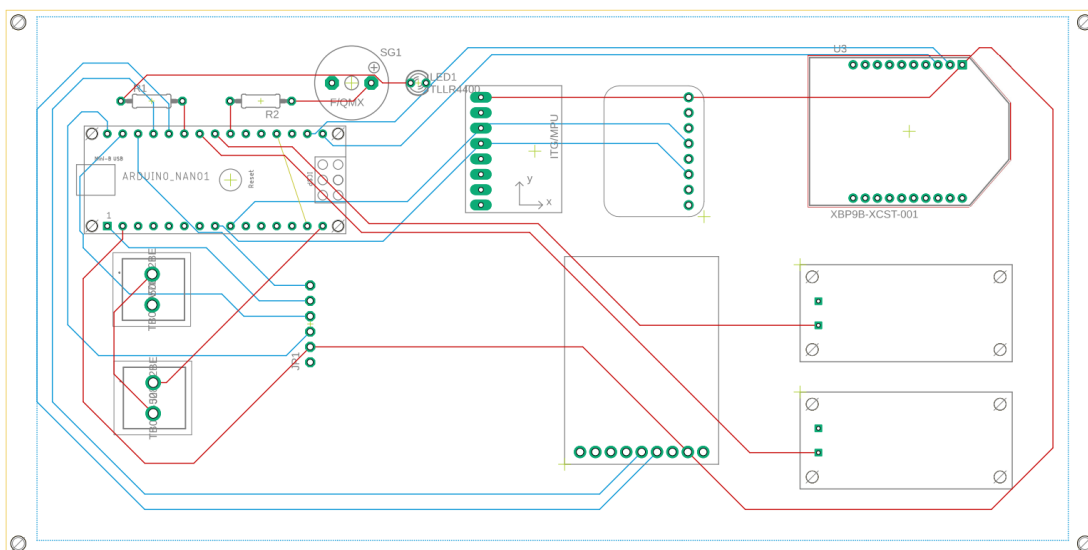


**Figure 45** Flight Computer PCB Design

The SRAD flight computer electronics consists of the following modules:

<b>Arduino Nano</b>	The Arduino Nano uses an ATMega 328P micro controller, has multiple SPI and I2C ports, a small form factor and enough processing power to handle the avionics on-board.
<b>Adafruit Ultimate GPS</b>	The Adafruit Ultimate GPS offers a 10 Hz update rate, consumes very little power, and has an external antenna connector, making it suitable for this rocket.
<b>XBee</b>	The XBee is a 915 MHz long-range RF module with a maximum LoS range of 45 km (28 mi) using antennas. The rocket uses the XBee module for radio communication with the ground station.
<b>BMP388</b>	The BMP388 is the onboard absolute pressure sensor. It has a range of 30 kPa – 125 kPa (4.35 psi – 18.13 psi) with an accuracy of $\pm 8$ Pa ( $\pm 0.0012$ psi) for absolute pressure measurement. It supports I2C and SPI interfacing and has a maximum sampling rate of 200 Hz. This sensor plays an integral part in the apogee detection algorithm.
<b>MPU6050</b>	The MPU6050 is the IMU onboard the rocket. It consists of a 3-axis gyroscope and a 3-axis accelerometer. The rocket's attitude at various flight points is determined using the IMU. It measures accelerations up to $\pm 16$ g, making it suitable for this rocket.
<b>D4184 MOSFET Control Module</b>	This module allows the user to trigger high-powered loads from a low-powered signal using a power MOSFET.

The PCB shown below was designed used to test the functionality of the flight computer.

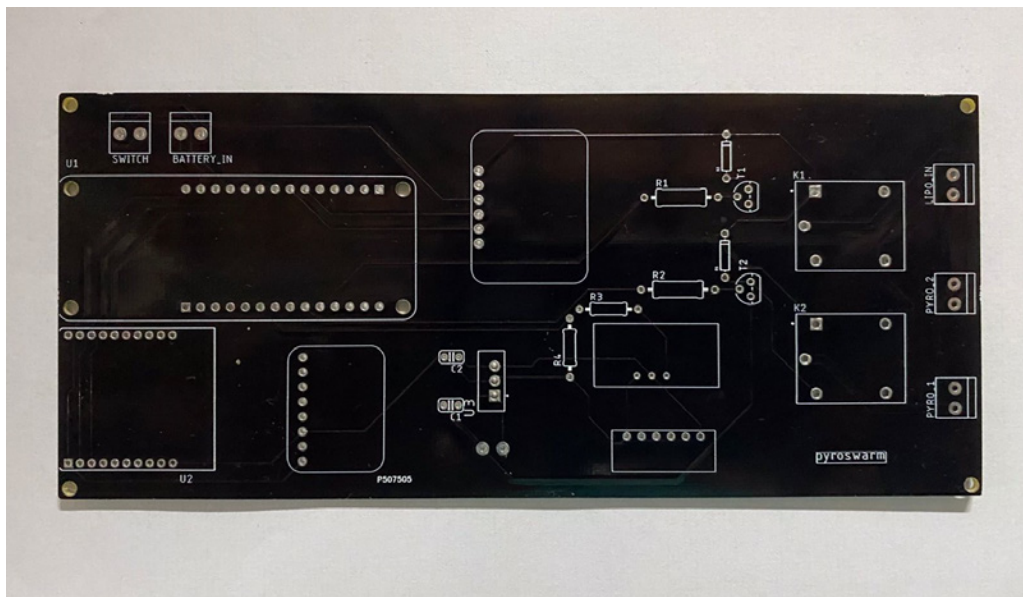


**Figure 46 Test Flight Computer PCB**

## *2. COTS Altimeter*

The RRC3 by MissileWorks is a barometric dual-deploy altimeter capable of recording multiple flights (15 flights with approximately 28 minutes per flight). In addition to this, the RRC3 has an excellent user interface to configure the settings for pre-flight and then analyse the flight with the built-in flight simulator, all of this at a very modest price, making it the best choice for the project.

## *3. COTS GPS*

The Featherweight GPS Tracker is a long-range GPS module capable of transmitting data up to a distance of 300 000 ft using long-range LoRa protocol in the 915 MHz band. The range, combined with ease of use, makes it an excellent choice for the COTS GPS module.

## *4. FPV Camera*

The rocket houses a RunCam Split 3 Lite. This camera has a small form factor and reasonable resolution, making it ideal for the rocket. The camera has a 2 MP resolution and can record 1080p video at 60 FPS. It will be powered by a separate LiPo battery connected to a PDB, since it requires a non-direct power supply.

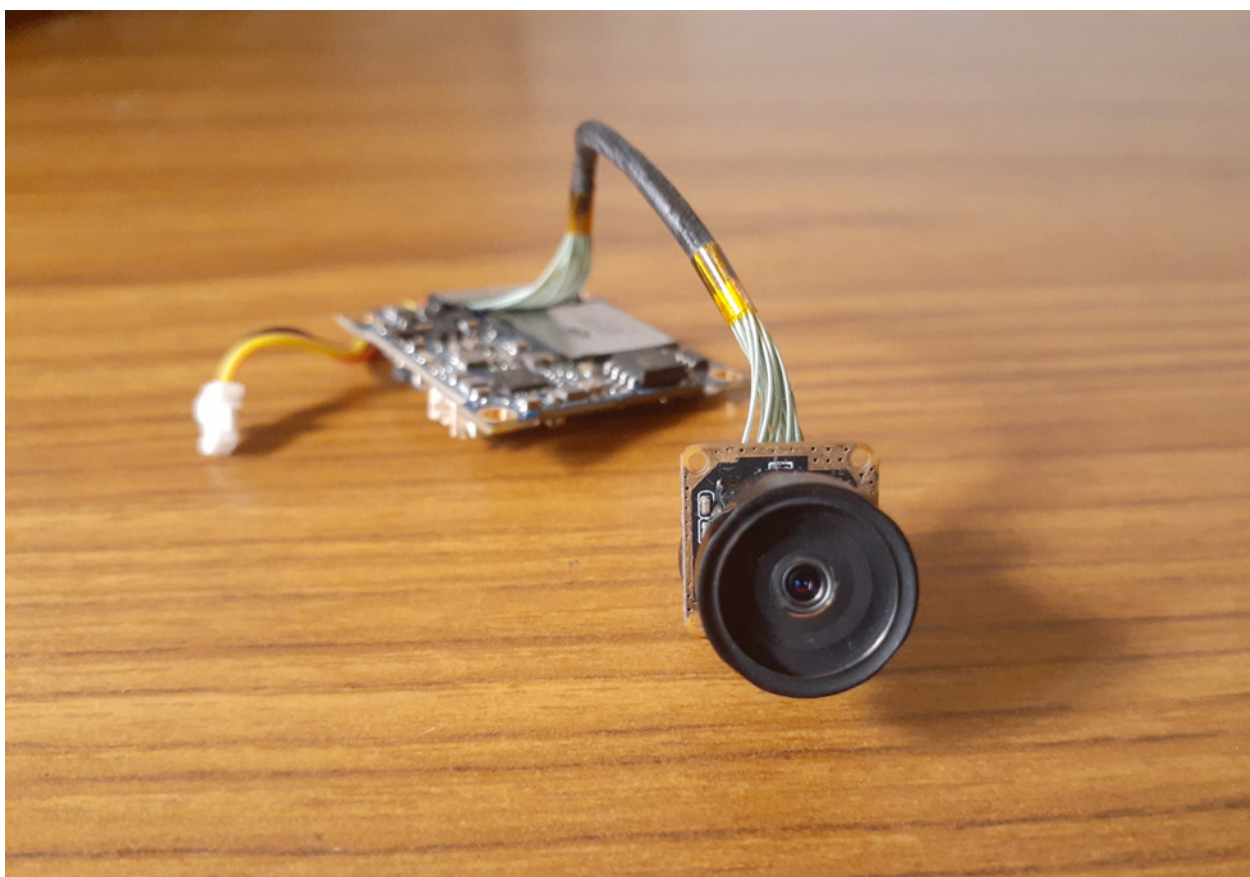


**Figure 47 FPV Camera**

## 5. Plotter

The plotter is a Python-based GUI for live data visualisation of the flight data. The data from the rocket gets represented across various plots to understand the flight conditions better in real-time during flight. All the plots have auto-scaling and also have an option for manual scaling. The start and the stop record buttons save all the values and timestamps to a CSV file. It also features a dummy mode which plots random values and is activated when no ports are available.

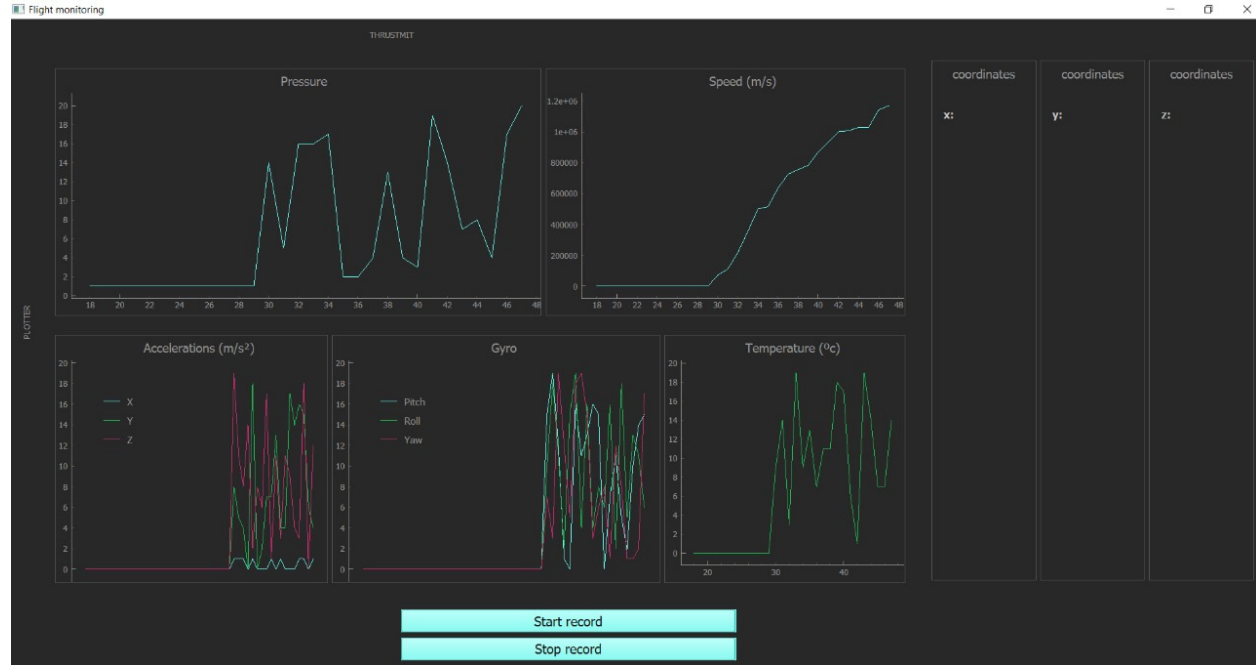


**Figure 48 Plotter**

## 6. Bay Design

The bay's interior consists of a 3D-printed, PLA based 3 stage electronics mount to house the flight computer and other components like the batteries, arming switches and wiring.

The bottom stage of the mount is designed to house both the SRAD flight computer, the Featherweight GPS tracker and the Camera's PCBs; the middle stage of the mount houses all the necessary LiPo batteries and the standard 9 V batteries and the top stage houses the RRC3 Altimeter.

The team chose a 3-stage mount design for this rocket to ensure sufficient space to house and wire all components safely. The middle stage of the mount was designed solely for the batteries to secure them from all kinds of shock loads that the rocket experiences during flight. The mount is attached to the avionics bay stringers using four M5 bolts and is attached to two 15 mm (0.59 in) bulkheads on either end of the mount with three M5 bolts.

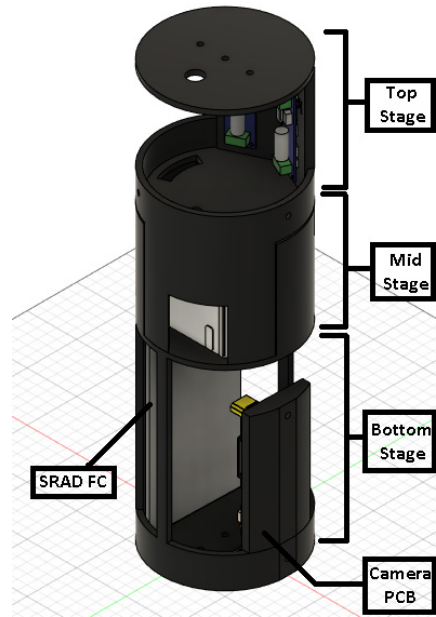


**Figure 49** Avionics mount as seen in Fusion360



**Figure 50** Avionics Mount

The three avionics bay stringers, made of Aluminium 6063, start from a 22 mm (0.87 in) recovery bulkhead, run through the entire avionics section of the mid bay, and end on the upper payload bulkhead of 15 mm (0.59 in) thickness. The stringers have been designed to prevent any excessive loading on the avionics mount and increase the ease of assembly of the recovery, avionics and payload bays at once.

The holes made in the avionics bay body tube, to accomodate for switches, wiring and pressure venting is as follows:

**Table 4 Holes for Switches, Wiring and Venting**

Sr. No.	Purpose	Comments
1.	SRAD Switch	To turn SRAD flight computer on/off
2.	COTS Switch	To turn COTS Altimeter on/off
3.	SRAD Ignition Circuit Switch	To toggle ignition circuit of SRAD flight computer
4.	COTS Ignition Circuit Switch	To toggle ignition circuit of COTS
5.	Vent Holes for RRC3	3 vent holes of equal diameter
6.	Vent Hole for SRAD flight computer	–
7.	Antenna Wiring	Used to wire the SRAD Telemetry, COTS GPS and SRAD GPS Antennas

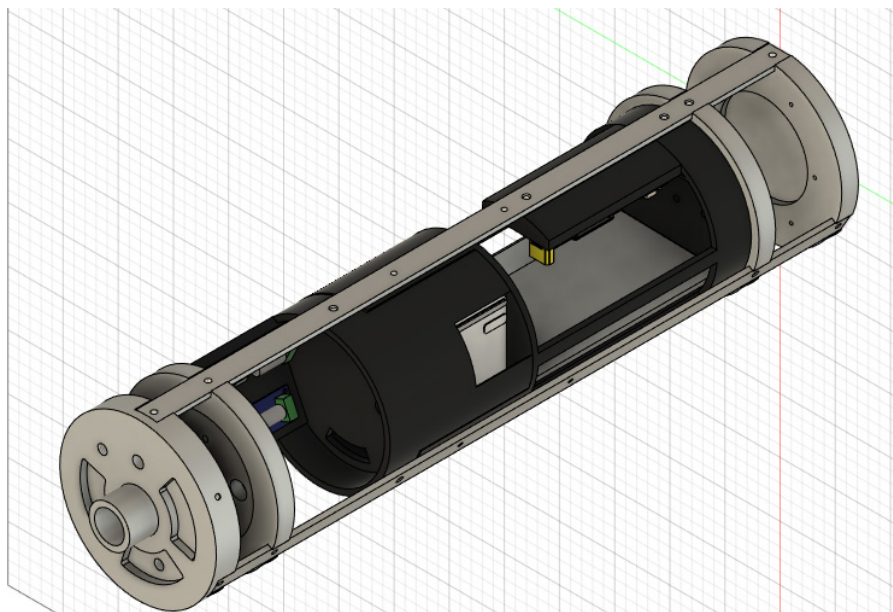


**Figure 51 Section View of the avionics bay (20mm grid with 5 subdivisions for scale)**

## 7. Camera Housing

The rocket's camera housing has been designed to support the FPV camera during the flight. The geometry of this housing was created to minimise drag and hence was designed with a tangent ogive profile. The housing has a cavity behind the ogive profile into which the camera is mounted and secured. The housing is mounted onto the air-frame of the rocket using two M3 bolts, which are secured using a nut on the interior of the rocket. The camera mount is manufactured by 3D printing with the material used as PLA. A protective layer of varnish was applied to the housing to protect it against the thermal loads encountered by the during transonic flight make the surface smooth to minimise drag.

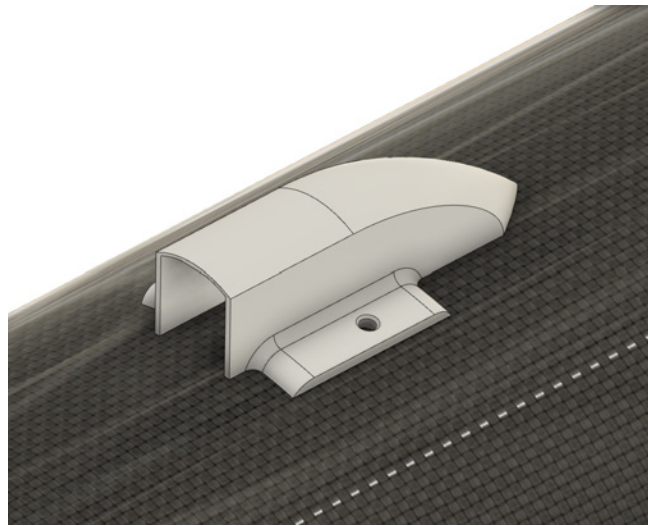


**Figure 52** Camera Housing

## E. Payload - C.A.V.E

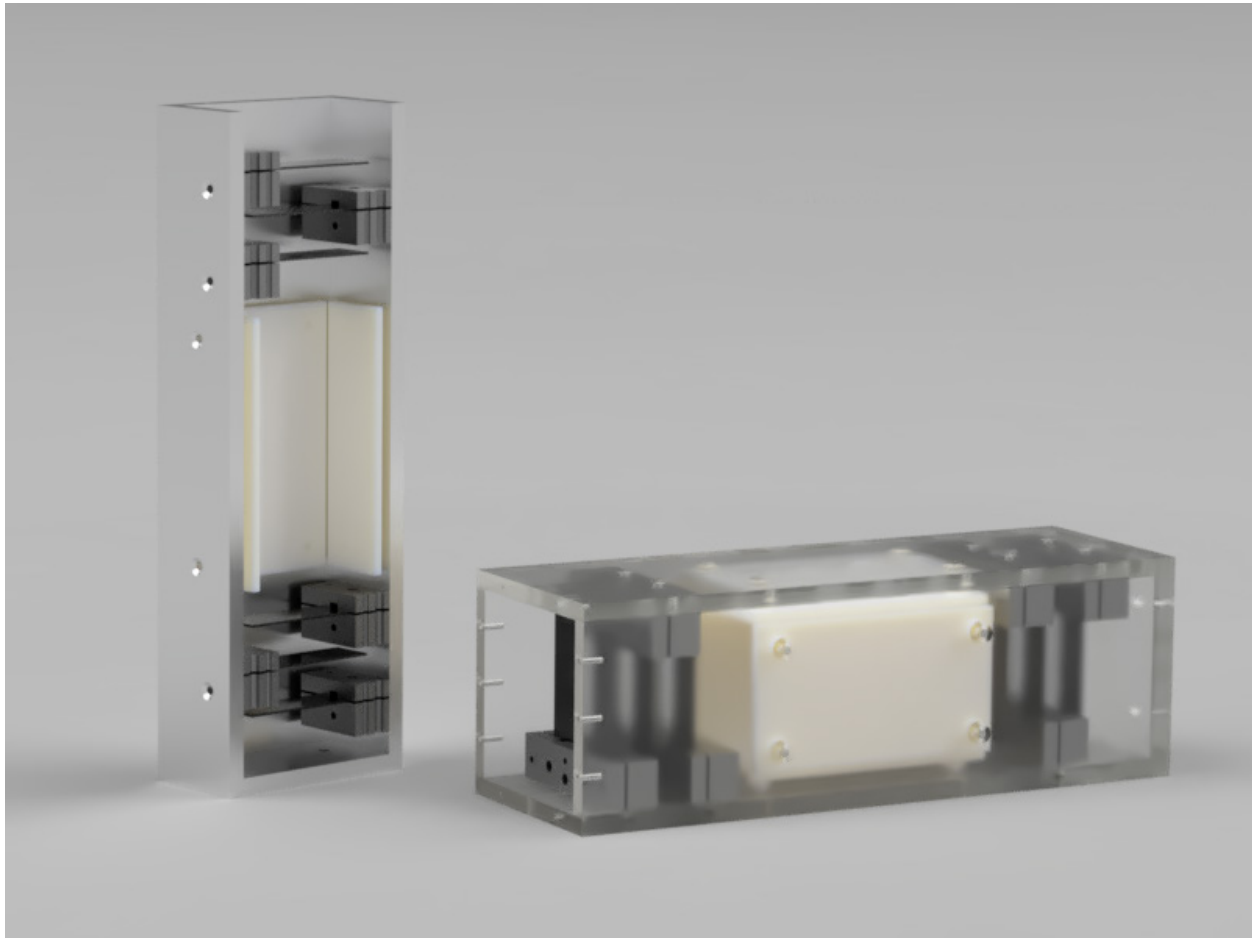


**Figure 53 3U CubeSat Render**

### *1. Introduction*

C.A.V.E (Composite Additive Vibrations Experiment) is the experimental 3U CubeSat payload for Rayquaza. The experiment aims to investigate the acoustic dampening properties of CNT infused CFRP for varying quantities of CNT added to the CFRP. The samples are subjected to the vibrational loads from the motor and the rocket's flight. The results of this experiment will be used to identify the optimal concentration of CNT for maximum dampening properties, which can be of application for manufacturing containers-mounts for launch vehicles housing sensitive equipment.

Vibrations are a mechanical phenomena whereby a system oscillates about a point known as the equilibrium point. In rocketry, these vibrations which are produced by the burning of the solid rocket propellant are known as Thrust Oscillations. These vibrations come in the form of waves and travel throughout the rocket body.

These vibrations may have a damaging effect on the rocket's avionics and hardware. This makes rocket design more challenging since the avionics systems have to be developed such that it can work efficiently in a vibrating environment.

Gathering flight data such as aerodynamic data, pressures, etc is one of the most important missions of any rocket. Vibrations add unwanted noise to the gathered flight data, resulting in false inferences in post flight data analysis. To tackle this problem, there are different Vibration Damping methods. Vibration Damping is the phenomena of absorbing or changing the vibrational energy using suitable materials, essentially reducing the amount of energy which is transmitted through the equipment or structure.

Carbon nanotubes are one of the most efficient materials for vibrational damping because the internal structure of the CNT is such that it absorbs most of the vibrational energy due to internal movement of its molecules.

CNT-reinforced polymers combine the viscoelastic properties of the polymer with the interfacial properties of the CNT, resulting in enhanced vibration damping.

## *2. Methods and Designs*

The top and bottom sections of the payload are identical except for mirrored orientation to facilitate a more balanced mass distribution. Each section has three mounting blocks for the CFRP samples, and each of these blocks holds two samples for a total of twelve samples in the payload.

For the construction of the payload, the outer body is split down the middle along its length resulting in two C channels. This allows easy access to all the components to be placed inside while keeping the assembly process simple. The mounting blocks are steel and serve the additional purpose of holding the two C-channels mentioned above. The mounting blocks have guideways cut into them to allow efficient wire management.

The electronics part of the payload consists of two PCBs:

**Primary Circuit Board** Contains a single microcontroller connected to four piezo transducers and a pressure sensor used for apogee detection. The Primary microcontroller is wired to the GPIO pin of the Secondary Circuit Board microcontrollers for inter-board communication.

**Secondary Circuit Board** Consists of two microcontrollers and four piezo transducers connected to each microcontroller.

In total, there are twelve piezo transducers, one for each sample on either side of the CubeSat.

The system is mounted and powered on the launchpad by toggle switches. Each microcontroller has an independent power source of 3000 mAh, 3.7 V LiPo batteries. Upon powering, each microcontroller starts to log data into the SD card. When the pressure sensor detects apogee on the Primary Circuit Board, the Primary microcontroller sends a stop signal to the Secondary Circuit Board microcontrollers, to stop data logging.

The data obtained is analyzed post-flight to draw conclusion on the optimal composition of CNT infused CFRP needed for maximum damping of vibrations. The circuitry consists of:

- **Arduino MKRZero:** The MKRZero has high-resolution ADC channels and an in-built micro SD card slot, which will be needed to flush large amounts of data. The SAMD21 in the MKRZero also supports Direct Memory

Access, allowing data to be committed to memory and consequently to the SD card, bypassing the processor and increasing data acquisition speed. This performance is required to capture signals of acoustic magnitude and frequency.

- **LDTM-028K Piezo transducer:** Flexible piezo transducer with a baseline sensitivity of  $50 \text{ mV g}^{-1}$ , resonant sensitivity of  $1.4 \text{ V g}^{-1}$ , and resonant frequency of 180 Hz satisfies the required threshold for capturing acoustic vibrations experienced in the rocket.
- **BMP280:** Onboard absolute pressure sensor. Range of 30 kPa – 125 kPa (4.35 psi – 18.13 psi) for absolute pressure measurement. The pressure sensor will be used for apogee detection to provide stopping point for data-sampling.

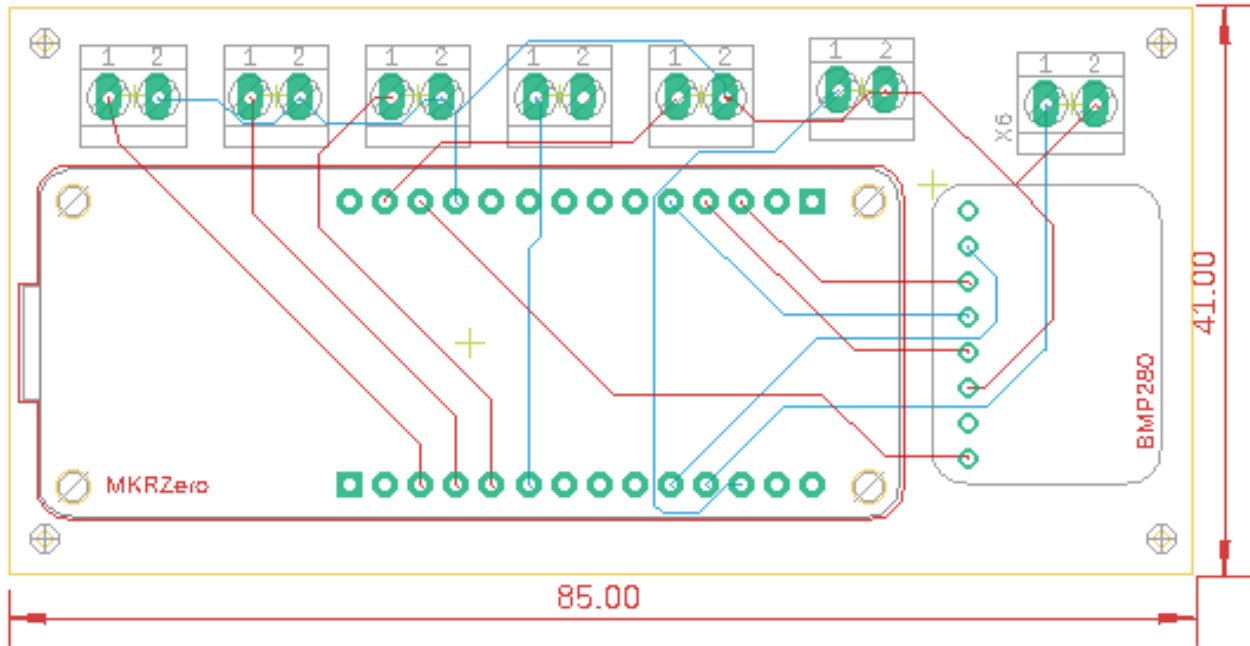


**Figure 54 Primary PCB**

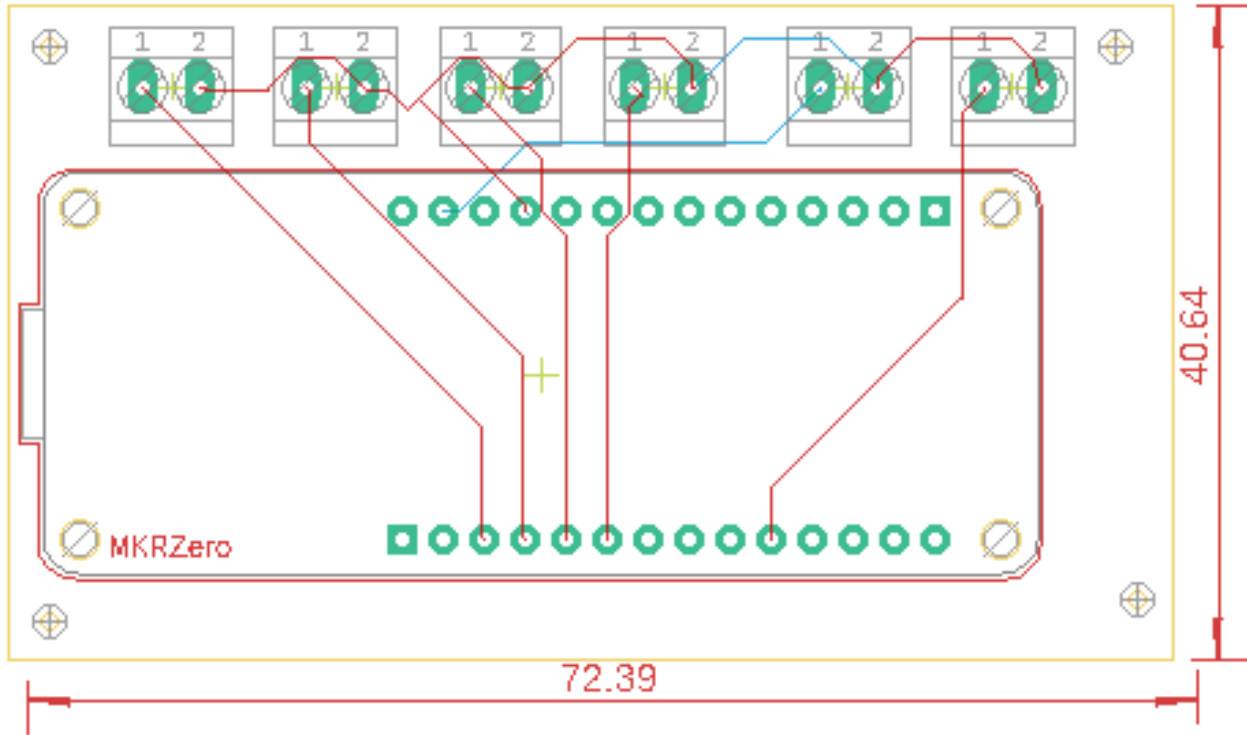


**Figure 55 Secondary PCB**

### 3. Bay Design and Simulations

The interior of the payload bay was designed keeping in mind the mission objectives of the rocket. The payload aims to measure the vibrations caused due to the motor and various other parts of the rocket. The bay was designed in such a way as to enable optimal transmission of motor vibrations to the payload without compromising the bay's structural integrity.

The payload bay consists of the payload CubeSat attached to the lower payload bulkhead of 15 mm (0.59 in) on the lower end using four M6 Bolts. On the upper end it is connect to a 15 mm (0.59 in) bulkhead using six M3 Bolts. The upper bulkhead is connected to three stringers extending from the Avionics Bay using an M5 Bolt each. This was done to reduce the complications involved in assembling and aligning all components within the payload bay. All the internal components were manufactured using Aluminium 6063.

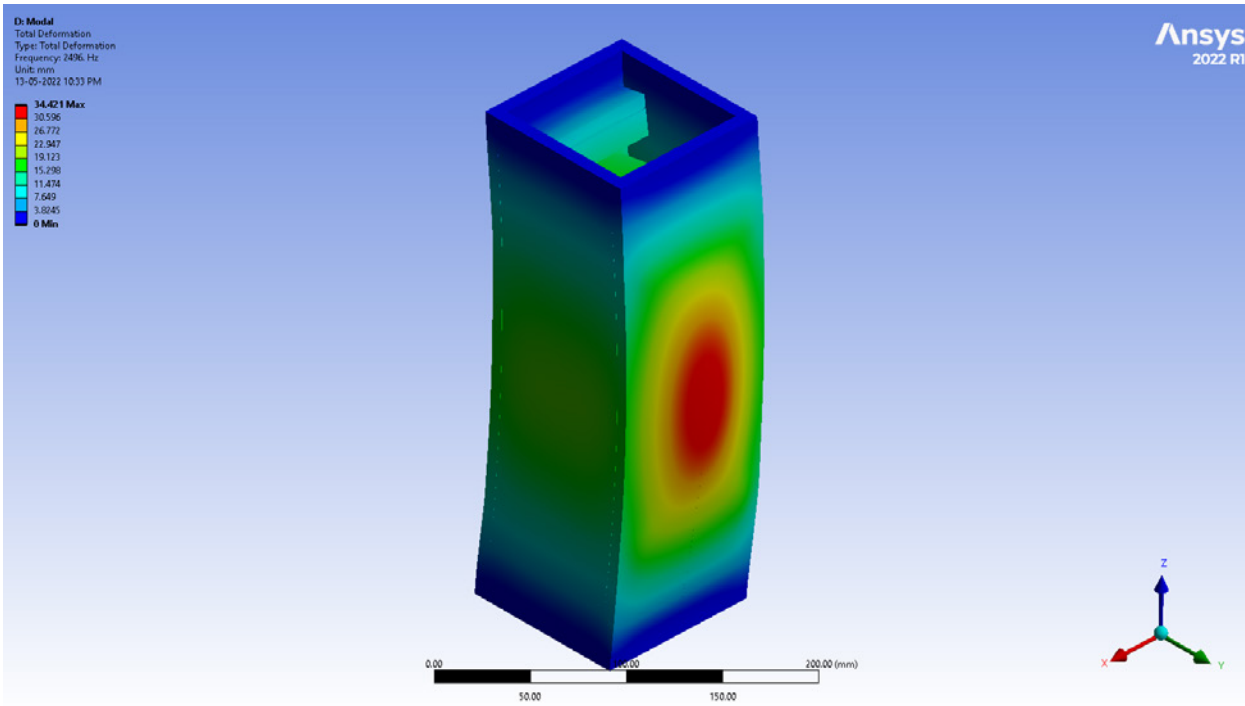


**Figure 56** Modal Displacement of CubeSat - Mode 1

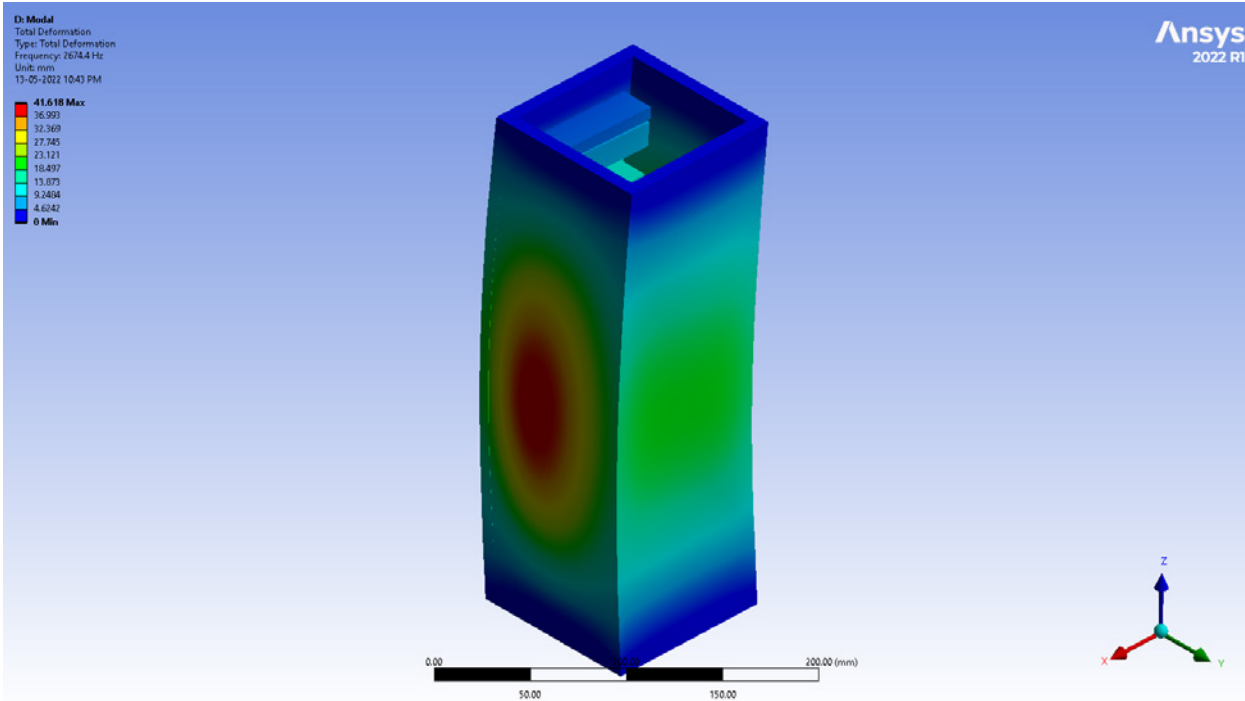


**Figure 57** Modal Displacement of CubeSat - Mode 2

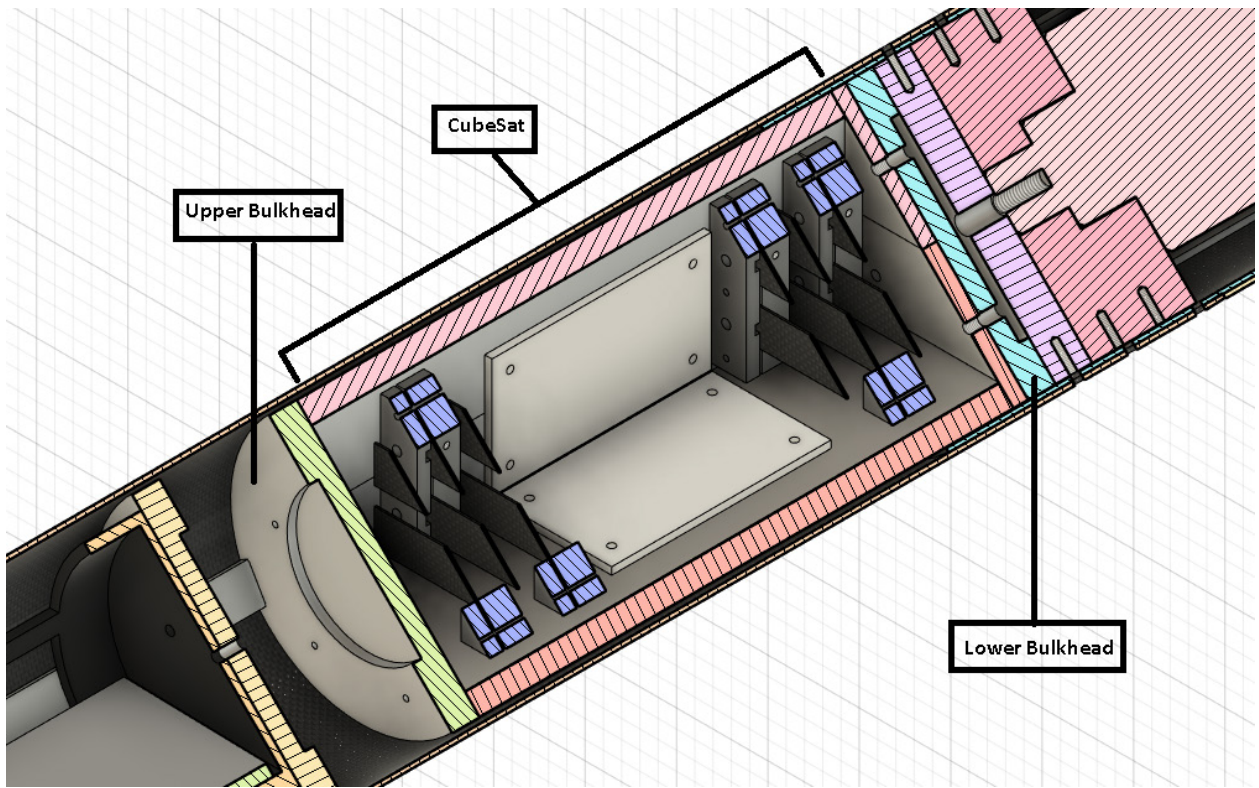


**Figure 58** Section View of the payload bay (50mm grid with 5 subdivisions for scale)

### III. Mission Concept of Operations Overview

- 1) **Assembly:** The launch vehicle is assembled using the checklist. The three bays are fixed together. The continuity of avionics is checked, and all the switches are disarmed. The ejection charge is filled with all the necessary permissions and approval. The motor is assembled and loaded into the vehicle.
- 2) **Pad Preparations:** The launch vehicle is brought to the launch pad with caution and mounted onto the launch rail in a horizontal position. Final inspections are carried out. The rocket is oriented into its launch position. The avionics systems are switched on and telemetry is confirmed with the ground station. Recovery charges are then armed. The igniter squibs are then inserted into the motor, secured and connected once the necessary permissions are given.
- 3) **Pre-launch Preparations:** A continuity test is performed on the ground station electronics before launch, live telemetry is tested and verified. Launch personnel vacate the pad.
- 4) **Ignition:** After the launch Control officer approves the launch, the final countdown shall begin. The launch command is sent at  $T - 0$  s, which initiates motor ignition. Motor ignition is confirmed visually.
- 5) **Lift-off:** Motor is pressurised and begins to produce thrust. The rocket is expected to clear the launch rod at  $T + 0.34$  s.
- 6) **Powered flight:** The rocket goes on its intended path as the motor burns continuously, and the weight of the rocket keeps reducing as the propellant is consumed.
- 7) **Motor burnout:** At approximately  $T + 2.9$  s, the motor completely burns out. The rocket starts coasting.
- 8) **Coasting:** The momentum of the rocket allows it to continue climbing as it decelerates until it reaches the apogee at around  $T + 24.9$  s.
- 9) **Apogee:** Once the rocket hits apogee, the altimeters detect the rise in pressure and fire the ejection charges with the COTS altimeter acting as the primary system and the SRAD Flight Computer acting as the redundant system.
- 10) **Initial descent:** The reefed parachute is ejected out along with the Nosecone, bringing it down to an optimum height without significant horizontal drift.
- 11) **Secondary Descent:** The altimeters track the altitude. Upon reaching a predetermined altitude, the altimeters fire their main charge, enabling the reefing cutter to snip the reefing lines, opening the parachute up and leading to a smooth descent velocity of approximately  $8.4 \text{ m s}^{-1}$  ( $27.5 \text{ ft s}^{-1}$ ).
- 12) **Touchdown and Recovery:** The rocket lands safely, and the ground personnel set out to retrieve it.

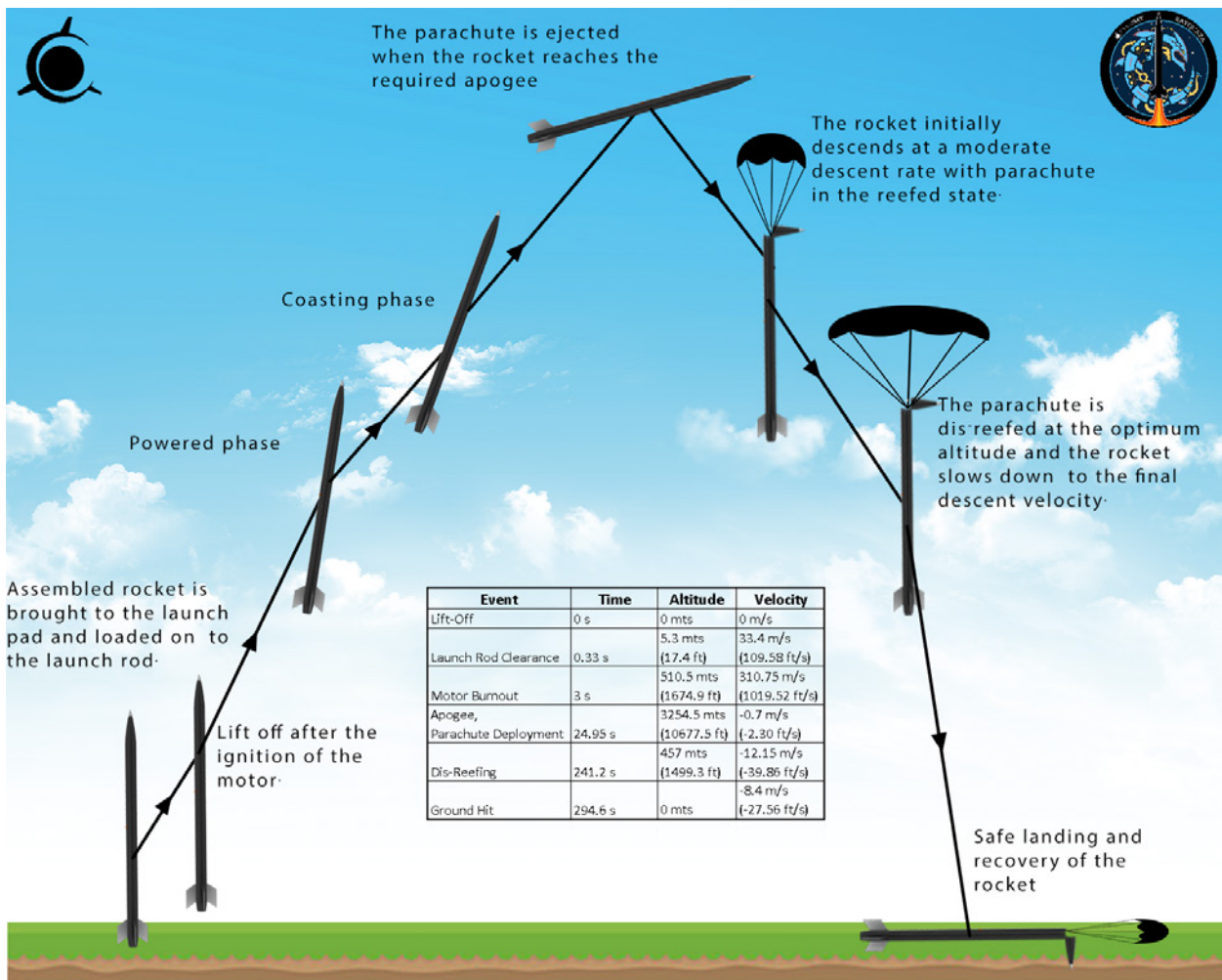


**Figure 59 Mission Concept of Operations Overview**

## **IV. Conclusions and Lessons Learnt**

The design and specifications of the components that are in Rayquaza – thrustMIT’s entry into the Spaceport America Cup 2022 in the 10 000 ft COTS category are outlined in this technical report. The Mission Concept of Operations Overview provides a comprehensive overview of the rocket’s flight while discussing hazards and the nominal system operations.

The rocket’s design was driven by attaining the maximum possible efficiency in both the performance of Rayquaza and its design and manufacturing process due to the transition of the working of the team to a physical setting after spending the duration of the pandemic working remotely.

The team was subjected to various fiscal and logistical restrictions over the year due to the slow rebound of various supply chains and the sharp decline in the availability of sponsorships brought on by the pandemic. These issues made the team change its approach and focus on an efficient, low-cost development model with more components being machined and produced in-house without compromising safety, reliability, and performance. The team used this opportunity to hone its skill in precision manufacturing and will here on channel these newly acquired skills to help it grow.

As a team, over the last year, we have come together in these challenging times to design and analyse the various systems and decode the numerous problems that have arisen throughout the design of our rocket.

Depending on this year’s competition results, the team plans to move on to the SRAD motor category and aim to reach the target apogee of 10 000 ft at the 2023 Spaceport America Cup.

## Acknowledgements

We would like to thank thrustMIT's faculty advisor Dr. Srinivas G, Assistant Professor - Senior Scale at Manipal Institute of Technology, for his endless support and guidance throughout Rayquaza's design and development process. We would like to thank our college Manipal Institute of Technology, and by extension, our university, Manipal Academy of Higher Education, for graciously providing us with their support and facilities.

The team would like to acknowledge the valuable inputs and recommendations in the design of the rocket by our various mentors and advisors in Manipal Institute of Technology; Dr. Yogananda Jeppu, Dr. Suhas Nayak, Dr. Padmaraj N. H., Mr. Ganesh Nayak, Mr. Nagaraj, Prof. Jonathan Monteiro, Prof. Dilifa Jossley Noronha and Mr. Shrinivas Somayaji. We would also like to extend our heartfelt gratitude to the Department of Aeronautical and Automobile Engineering, the Department of Mechanical and Industrial Engineering and the Department of Electronics and Communication Engineering for their constant support and assistance.

We would also like to express our gratitude towards our mentor Mr. Bob Schoner, who is serving as our flyer of record and has guided us in optimising the design to ensure a safe and reliable flight.

We are truly grateful for this opportunity to learn and grow, which has been made possible by ESRA, Spaceport, SDL, and all other organisations and individuals involved in conducting this competition and providing us with this wonderful platform.

We want to thank and express our gratitude to all our sponsors and their representatives, without whom this project could not have been completed: STAR Lab, Dassault Systèmes SolidWorks, ANSYS, and Babaji Shivram. Their patronage is deeply appreciated.

Finally, we would like to thank our families and friends whose support has encouraged us at every step.

## References

- [1] Lamar, J., and Frink, N., "Aerodynamic Features of Designed Strake-Wing Configurations," *Journal of Aircraft*, Vol. 19, 1981.  
<https://doi.org/10.2514/3.57444>.
- [2] Barrett, D. H., "SP-8051 - Solid Rocket Motor Igniters," Tech. rep., National Aeronautics and Space Administration, 1971.
- [3] Newlands, R., Heywood, M., and Lee, A., "Rocket Vehicle Loads and Airframe Design," Tech. rep., Aspire Space, 2011.
- [4] Hoult, C. P., "Sounding Rocket Structural Design Loads," Tech. rep., Rocket Science and Technology, 2014.
- [5] ANSYS Inc., *Mechanical User's Guide Release 2022 R1*, 2022.
- [6] ANSYS Inc., *Explicit Dynamics Analysis Guide Release 2022 R1*, 2022.
- [7] ANSYS Inc., *Ansys Composite Pre-Post Guide Release 2022 R1*, 2022.
- [8] ANSYS Inc., *Fluent Theory Guide Release 2022 R1*, 2022.
- [9] Anderson, J. D., *Introduction to Flight*, McGraw Hill, 1978.
- [10] Anderson, J. D., *Fundamentals of Aerodynamics*, McGraw Hill, 2010.
- [11] Anderson, J. D., *Modern Compressible Flow: With Historical Perspective*, McGraw Hill, 1982.
- [12] Knacke, T. W., *Parachute Recovery Systems: Design Manual*, Para Publishing, 1992.
- [13] *OpenRocket Technical Documentation*, 2013.
- [14] Arduino, "Arduino Nano," , 2022. URL <https://docs.arduino.cc/hardware/nano>.
- [15] Bosch, "BMP388 Pressure Sensor," , -. URL <https://www.bosch-sensortec.com/products/environmental-sensors/pressure-sensors/bmp388/>.
- [16] TDK, "MPU6050 IMU," , -. URL <https://invensense.tdk.com/products/motion-tracking/6-axis/mpu-6050/>.
- [17] Adafruit, "Adafruit Ultimate GPS Breakout v3," , -. URL <https://www.adafruit.com/product/746>.
- [18] Digi, "XBee-PRO 900HP," , -. URL <https://www.digi.com/products/embedded-systems/digi-xbee/rf-modules/sub-1-ghz-rf-modules/xbee-pro-900hp>.
- [19] MissileWorks, "RRC3 "Sport" Altimeter," , -. URL <https://www.apogeerockets.com/Electronics-Payloads/Altimeters/RRC3-Sport-Altimeter>.
- [20] Featherweight, "Featherweight GPS Tracker," , -. URL <https://www.featherweightaltimeters.com/featherweight-gps-tracker.html>.
- [21] RunCam, "RunCam Split 3 Lite," , -. URL [https://www.runcam.com/download/split-3-series/RC\\_Split\\_3\\_series\\_Manual\\_EN.pdf](https://www.runcam.com/download/split-3-series/RC_Split_3_series_Manual_EN.pdf).
- [22] Arduino, "Arduino MKR Zero," , 2021. URL <https://store.arduino.cc/usa/arduino-mkrzero>.
- [23] Bosch, "BMP280 Pressure Sensor," , -. URL <https://www.bosch-sensortec.com/products/environmental-sensors/pressure-sensors/bmp280>.

sensors/bmp280/.

- [24] Sparkfun, “Piezoelectric Bending Transducer,” , -. URL <https://www.sparkfun.com/products/9196>.
- [25] Mallick, P. K., *Fiber-Reinforced Composites: Materials, Manufacturing, and Design*, CRC Press, 2007.
- [26] “BhorForce PC200 Datasheet,” , May 2018. URL <https://bhor.com/wp-content/uploads/2018/05/BhorForce-PC200.pdf>.
- [27] “Huntsman Araldite LY5052/Aradur 5052,” , Nov 2012. URL [https://samaro.fr/pdf/FT/Araldite\\_FT\\_LY\\_5052\\_Aradur\\_5052\\_EN.pdf](https://samaro.fr/pdf/FT/Araldite_FT_LY_5052_Aradur_5052_EN.pdf).
- [28] “Multi-Walled Carbon Nanotubes,” , Jul 2020. URL <https://nanocliff.com/product/multi-walled-carbon-nanotubes/>.
- [29] Nayak, S. Y., Shenoy, S., Sultan, M. T. H., Kini, C. R., Seth, A., Prabhu, S., and Safri, S. N. A., “Effect of CNT-Based Resin Modification on the Mechanical Properties of Polymer Composites,” *Frontiers in Materials*, Vol. 7, 2021, p. 609010.
- [30] E756-05, “Standard Test Method for Measuring Vibration-Damping Properties of Materials,” *American Society of Testing and Materials*, 2017.
- [31] Barra, G., Guadagno, L., Vertuccio, L., Simonet, B., Santos, B., Zarrelli, M., Arena, M., and Viscardi, M., “Different methods of dispersing carbon nanotubes in epoxy resin and initial evaluation of the obtained nanocomposite as a matrix of carbon fiber reinforced laminate in terms of vibroacoustic performance and flammability,” *Materials (Basel)*, Vol. 12, No. 18, 2019, p. 2998.

## A. Appendix: System Weights, Measures, and Performance Data

**Table 5 Rocket Information**

Parameter	Value	Optional Comments
Total Length	108.86 in (2765 mm)	
Airframe Outer Diameter	5.91 in (150 mm)	
Airframe Inner Diameter	5.75 in (146 mm)	
Rocket Dry Mass without Motor	47.62 lb (21.60 kg)	
Empty Motor Case Mass	8.06 lb (3.66 kg)	
Propellant Mass	9.81 lb (4.45 kg)	
Rocket Wet Mass	65.54 lb (29.73 kg)	Including Payload Mass
Payload Mass	9.33 lb (4.23 kg)	
Number of Stages	1	
Nosecone Length	21.65 in (550 mm)	Including Nosecone Extension
Number of Fins	4	
Fin Semi-Span	5.51 in (140 mm)	
Fin Thickness	0.12 in (3 mm)	
Fin Flutter Velocity	$1297 \text{ ft s}^{-1}$ ( $395.32 \text{ m s}^{-1}$ )	
Center of Pressure at Lift-off	77.5 in (1968 mm)	Measured from Nose tip
Center of Gravity at Lift-off	67.79 in (1722 mm)	Measured from Nose tip
Static Margin at Lift-off	1.6	

**Table 6 Propulsion Information**

Parameter	Value	Optional Comments
Cluster	No	
Type	Solid	
COTS, SRAD, or Combination?	COTS	
Manufacturer	Cesaroni Technology	
Manufacturer Designation	9994M3400-P	
Total Length	27.64 in (702.00 mm)	
Casing Diameter	3.86 in (98.00 mm)	
Empty Motor Case Mass	8.06 lb (3.66 kg)	
Propellant Mass	9.82 lb (4.45 kg)	
Motor Wet Mass	17.88 lb (8.11 kg)	
Letter Classification	M	
Total Impulse of All Motors	2246.8 lb s (9994.5 N s)	
Specific Impulse	228.92 s	
Average Thrust	769.1 lbf (3421.1 N)	
Maximum Thrust	895.4 lbf (3983.0 N)	
Motor Burn Time	2.92 s	

**Table 7 Predicted Flight Data**

Parameter	Value	Optional Comments
Launch Rail	ESRA Provided	
Launch Rail Length	17 ft (5182 mm)	
Thrust-to-Weight Ratio at Launch Rail	11.97:1	
Launch Rail Departure Velocity	$109.9 \text{ ft s}^{-1}$ ( $33.5 \text{ m s}^{-1}$ )	
Minimum Static Margin During Boost	1.6	
Maximum Acceleration	$414.69 \text{ ft s}^{-2}$ ( $126.4 \text{ m s}^{-2}$ )	
Maximum Velocity	$1042.32 \text{ ft s}^{-1}$ ( $317.7 \text{ m s}^{-1}$ )	
Target Apogee	10 000 ft (3048 m)	
Predicted Apogee	11 628.38 ft (3544.33 m)	
Time till Apogee	24.9 s	Measured from motor ignition

**Table 8 Recovery Information**

Parameter	Value	Optional Comments
COTS Altimeter	MissileWorks RRC3	
Redundant Altimeter	SRAD	
Drogue Deployment Charge - Primary	0.11 oz (3 g)	4F Black Powder
Drogue Deployment Charge - Backup	0.14 oz (4 g)	4F Black Powder
Main Deployment Charge - Primary	–	Reefing Cutter
Main Deployment Charge - Backup	–	Reefing Cutter
Drogue Deployment Altitude	11 628.38 ft (3544.33 m)	Reefed parachute
Drogue Descent Velocity	$39.86 \text{ ft s}^{-1}$ ( $12.15 \text{ m s}^{-1}$ )	Reefed parachute
Main Deployment Altitude	1500 ft (457.2 m)	Dis-reefed parachute
Main Deployment Descent Velocity	$27.56 \text{ ft s}^{-1}$ ( $8.4 \text{ m s}^{-1}$ )	Dis-reefed parachute
Ground hit Velocity	$27.56 \text{ ft s}^{-1}$ ( $8.4 \text{ m s}^{-1}$ )	
Time till Ground hit	221 s	Measured from motor ignition

## B. Appendix: Project Test Reports

### A. Recovery System Testing

The recovery subsystems team has been working on developing effective recovery systems over the past years. We have designed the parachute canopy, apogee detection system and are developing a redundant reefing mechanism. Various tests have been performed to ensure the recovery system's accuracy and reliability:

- 1) **Inflation test:** The parachute was taken to a location with high wind speed and checked if the parachute, completely inflates. This was done to ensure that the canopy can handle the forces during inflation.
- 2) **Reefing cutter test:** The reefing cutters were rigorously tested to ensure the dis-reefing of the parachute after reaching the main descent altitude.
- 3) **Reefing test:** The reefing test was again done on a windy location where the reefed parachute, along with the reefing cutters inside it, was inflated, and then reefing lines were cut using the reefing cutters opening the whole parachute.
- 4) **GPS testing:** The SRAD GPS was plugged into the Arduino, where the latitude and longitude readings were acquired from the GPS and compared with the actual coordinates.
- 5) **Apogee detection for parachute ejection:** The SRAD altimeter uses barometric values to detect apogee. The algorithm had been tested and verified in a wind tunnel and a vacuum pump.
- 6) **Ejection mechanism test:** The ejection test is done at ground level to ensure the proper functioning of the piston-cylinder arrangement and making sure the amount of charge used successfully separates the nose cone from the recovery bay and ejects out the parachute.

Link for recovery testing videos:

<https://drive.google.com/drive/folders/1wgcv91PXTqvYTgJBsgKVMmxLnLRiYrx0>



Figure 60 The reefing cutter test



**Figure 61** The parachute fully expanding after reefing lines are cut



**Figure 62** The vacuum pump used to test the apogee detection algorithm.



**Figure 63 Ejection mechanism test**

## B. Composite Shear Testing

A composite shear test was conducted to test the ability of the body tubes and couplers to resist bearing failure due to the bolts. A hole was made in the body tube, and gradually increasing weights were suspended from the hole with the help of a Nylon rope. Weights ranging from 4.5 kg – 10.16 kg (9.92 lb – 22.70 lb) were used for the test. The test concluded that the CFRP body tubes would successfully resist bearing failure in flight and are safe for launch.



**Figure 64** Weight of the Objects used for Shear Testing in kg



**Figure 65** Weights suspended with a Nylon Rope from the Body Tube

### **C. SRAD Propulsion System Testing**

**THIS PAGE INTENTIONALLY LEFT BLANK**

**D. SRAD Pressure Vessel Testing**

**THIS PAGE INTENTIONALLY LEFT BLANK**

## **E. Payload Recovery System Testing**

**THIS PAGE INTENTIONALLY LEFT BLANK**

## C. Appendix: Hazard Analysis

**Table 9 Hazard Analysis Matrix**

Hazard	Possible Causes	Risk of Mishap and Rationale	Mitigation Approach	Risk of Injury after Mitigation
Burns, respiratory problems due to propellant grain ignition	Inadvertent ignition of propellant in confined spaces	Low, commercially manufactured propellant grain	Safe storage and handling as per manufacturer guidelines in open spaces	Very Low
Skin irritation due to contact with igniter	Improper handling of the igniter resulting in direct contact with ignition charge	Very Low, the igniter is packed in a suitable container	Igniter stored in a cool, dry place and within its packaging until loading into the motor, igniter handled by essential personal	Very Low
Burns to due inadvertent ignition of ejection charge	Improper handling, ignition sources nearby during handling	Medium	Storing in a cool, dry place and handling with adequate fire-proof safety equipment away from any ignition sources	Low
Skin irritation due to motor adhesive being absorbed by the skin	Exposure to adhesive without safety gear	Medium, improper handling of adhesives during assembly, packaging failure during handling	Wearing proper safety gear (gloves, masks and goggles as per OSHA and manufacturer guidelines), safety briefing before the start of assembly	Low
Eye irritation due to motor adhesive coming in contact with the eyes				
Burns, injury due to ignition of LiPo battery	Improper handling of the battery.	Low	LiPo transported in special LiPo safe bags and stored in cool, dry places.	Very Low

<b>Hazard</b>	<b>Possible Causes</b>	<b>Risk of Mishap and Rationale</b>	<b>Mitigation Approach</b>	<b>Risk of Injury after Mitigation</b>
Skin irritation and rashes	Allergic reactions to composite dust	Medium	The dust (if any) should be removed with the vacuum cleaner and disposed of properly. Gloves and other safety equipment should be worn.	Low
	Cuts		Gloves and other safety equipment should be worn while handling composites. Sharp edges on unprocessed parts should be sanded down.	

## D. Appendix: Risk Assessment

**Table 10 Risk Analysis Matrix**

Risk	Possible Causes	Risk of Mishap and Rationale	Mitigation Approach	Risk of Injury after Mitigation
Explosion of solid-propellant rocket motor during launch with blast or flying debris causing injury - CATO	Cracks in propellant grain Debonding of propellant from wall Gaps between individual propellant segments and between the last segment and the nozzle Chunk of propellant breaking off and plugging the nozzle Motor fails during launch due to manufacturer errors	Low; certified COTS motor and propellant	Visually inspect grain for visible cracks and imperfections before assembly Proper cleaning and preparation of the case liner as per manufacturer instructions Ensure all fits are as per manufacturer specifications Inspect motor case for damage during final assembly of the motor before launch Motor only used if in proper visual condition on delivery, only essential personnel in the launch crew, crew to vacate to a safe distance behind an adequate barrier before launch	Very Low
Deployment charge ignition on the launch rail	The COTS altimeter/relay on the SRAD Flight Computer might misfire.	Medium	The device shall be armed immediately before the vacation of the launch area by essential personal. The SRAD Flight Computer is encoded to fire deployment charges only after lift-off is detected.	Low
Deployment charge ignition before the intended apogee during flight	Inadvertent command sent by SRAD flight computer	Medium	the SRAD flight computer is inhibited from sending the command during boost phase and is programmed to send the command if the pressure values rise for 3 consecutive samples	Low

Risk	Possible Causes	Risk of Mishap and Rationale	Mitigation Approach	Risk of Injury after Mitigation
Motor ignition due to inadvertent firing of the igniter before launch signal	Misfire of triggering circuit at the receiver end of the ignition system.	Low; COTS Ignition system	The igniter is connected to the motor right before the launch pad is cleared and the firing lines are ensured to be powered down before the connection is made	Very Low
Motor ignition during assembly/transport	The propellant is to be stable up to 75 °C (167 °F) and drop tested for impact stability from a height of 12 m (39.37 ft) as per UN test series 3(c) and 4(b) by the manufacturer	Low	The igniter will be loaded into the motor once the rocket is on the launch rail and fully ready for flight will all electronics armed only. Motor shall be stored and assembled as per manufacturer guidelines. Assembly of the motor will only be done by essential personnel in the presence of TRA L3 certified personnel.	Very Low
Rocket deviates from nominal flight path, comes in contact with personnel at high speed	The stability might waver due to poor manufacturing of the fins, inadequate anchoring of the launch rod to the ground, failure of rail buttons during launch	Medium; fins have been made using suitable grade materials	The fins have to be checked for any defects/damage before the launch; the rail buttons must be tightly secured and placed into a sturdy launch rod	Low
Recovery system fails to deploy, rocket or payload comes in contact with personnel (ballistic descent trajectory)	Clumsy packing and storing of parachute, charge required was not sufficient; electrical connections may have faltered, detection of apogee by altimeter was not proper	Low; testing of deployment mechanism has been taken place to ensure a smooth recovery	Make sure the parachute has been folded using the proper technique, cautiously weigh the amount of charge being used, check to see if the signals are passed through the connections or not	Low

Risk	Possible Causes	Risk of Mishap and Rationale	Mitigation Approach	Risk of Injury after Mitigation
Main (disreefed) parachute is deployed at apogee	Accidental firing of main charge by the Altimeters, faulty connections while assembling the rocket	Low	The altimeters are configured to fire the main charge only after they've passed a certain altitude during the descent phase. Wiring is verified before launch	Very Low
Reefing failure causing main parachute not to deploy	Reefing cutter failure, poor electrical connections, sensor failure, battery failure	Medium	LiPo batteries used in the rocket are handled with all necessary precautions and care before and during flight. Wiring connections are tested before flight to fix any loose connections. Sensors are tested on ground multiple times to ensure they work properly during the flight, redundant systems are placed in the rocket to account for sensor, battery or reefing failure	Low
Recovery system partially deploys, the rocket or payload comes in contact with personnel	The packed parachute might have tangled suspension lines or shock cords; faulty shear pins have been attached	Medium; suspension line may tangle during deployment	When packing the parachute, the suspension lines and shock cords must be placed carefully, so they do not tangle up while deploying	Low
Rocket does not ignite when the command is given ("hang fire") but does ignite when the team approaches to troubleshoot	Ignitor partial failure	Low	Utilise two igniters for launch and observe the rocket for a few minutes to either allow non-visible combustion to reach a steady-state (thereby resulting in an instantaneous $TWR > 1$ ) or to "cool off" any combustion remanents	Very Low
Rocket falls from launch rail during pre-launch preparations, causing injury	Improper handling of the rocket	Low	Handling of the only by essential personnel who are capable in performing pre-launch operations	Very Low

Risk	Possible Causes	Risk of Mishap and Rationale	Mitigation Approach	Risk of Injury after Mitigation
Nosecone splits into two halves in-flight	Improper attachment of two halves during layup process	Low	The Nosecone must be inspected for any weak point before assembly; The nose tip and Nosecone bulkhead must be attached securely	Low
Bolt holes in the body tubes and couplers undergo bearing failure in-flight	Insufficient stress concentration clearances given while drilling holes	Low	Adequate clearances must be given while drilling bolt holes in all components; reinforcements must be provided in case a proper clearance can't be provided	Low
Fins shear during flight	Failure of the fin attachment welds or failure of the stringers	Medium	The fins are seam welded using TIG welding to the stringers which are securely fastened to the body tube, centring ring and thrust plate; A specially designed jig is used to ensure positional accuracy of the fins during the welding process.	Low

## **E. Appendix: Assembly, Pre-flight and Launch Checklists**

### **A. Assembly Checklist**

- Assemble the Avionics setup containing the avionics modules, including the flight computer, altimeter, FPV camera, GPS module, antennas and arming switches.
- Ensure all switches are in the disarmed position, then connect the batteries to the leads.
- Assemble all components except the ejection charge onto the recovery bulkhead.
- Assemble the central stringer structure leading from the recovery bulkhead to the upper payload bulkhead.
- Since the payload cannot be removed from the rocket after assembly, the payload is submitted for inspection before assembly. Ensure payload is powered down.
- Complete the payload set up by attaching the payload onto the upper payload bulkhead.
- Insert the payload and avionics into the mid bay, align the bolt holes on the coupler and body tube with the stringer holes and fasten.
- Attach lower payload bulkhead.
- Check for the connectivity of Nichrome wire with a multimeter. Cross check if system is fully powered down and disarmed.
- Fill up the Recovery piston with the required quantity of ejection charge.
- The piston is connected to the recovery bulkhead using a Nylon rope and placed on a recovery cylinder with a ejection charge charge.
- Align the recovery fuselage. Fix these with M5 bolts to the recovery bulkhead.
- Apply sealant on the sides of the recovery bulkhead to prevent leakages.
- Connect the Nosecone and recovery bulkhead by tying a shock chord to the eyebolts on the Nosecone bulkhead and recovery bulkhead, and insert the folded parachute with all the reefing components attached.
- Connect the Nosecone setup to the recovery bay using four #2-56 Nylon shear pins.
- Assemble the internal motor bay setup consisting of the centring ring, stringers, the damper and the thrust plate.
- Place the setup inside the fuselage and place the coupler on top. Connect all parts using M5 bolts.
- Insert the COTS motor from the bottom of the motor bay. Connect the motor to the damper and thrust plate using a 3/8"-16 UNC bolt.
- Attach lower launch rail button.
- Place all other bays on top of the motor bay and connect using M5 bolts.

## **B. Pre-Launch Checklist**

- Check and ensure that all avionics switches are in the dis-armed position.
- Perform a visual check to ensure the integrity of the rocket body and have the flight safety review.
- Submit vehicle for the launch safety inspection.
- Fill in and submit the flight card to the Launch Control Officer.
- At the appointed time, transport the rocket to the launch pad accompanied by required personnel only.
- Ensure launch pad and surrounding area are clear of all combustible material.
- Slide the rocket onto the launch rail.
- Perform a final visual inspection of the rocket to check for any damage during transportation.
- Raise the rocket and the rail to launch orientation.
- After obtaining all necessary clearances, enable the Altimeter and Flight Computer's power supplies and payload's power supply.
- Listen for an audible beep to confirm a successful power up.
- Power on the camera.
- Communicate with ground station to verify successful telemetry link.
- Arm the recovery mechanism.
- Listen for an audible beep to confirm successful arming.
- Acquire permission from Range Manager to insert the igniter.
- Insert the igniter into the motor, leaving the leads unconnected.
- Cross check if the firing line is not "hot".
- Confirm non-essential personnel have evacuated the launch pad area.
- Authorised personnel shall connect the igniter to the firing line and check for continuity.

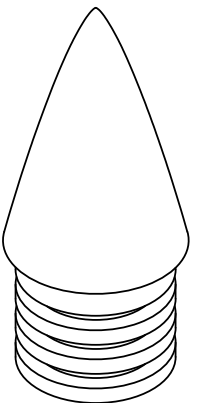
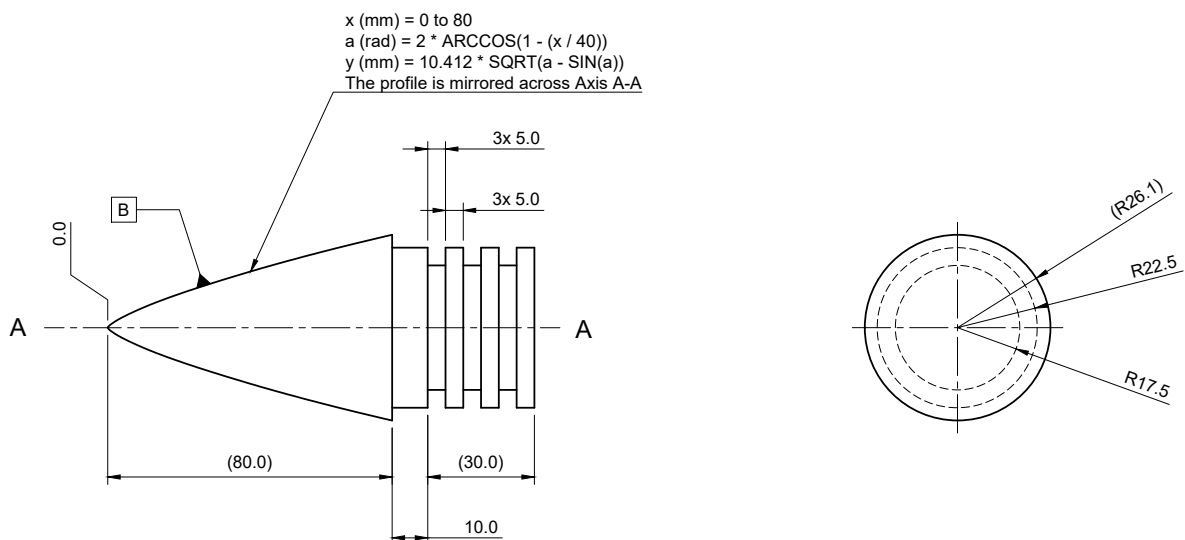
### C. Launch Checklist

- Wait for the Launch Control Officer's readiness criteria to be satisfied.
- An RF module is connected to the computer at the base station, and telemetry is tested and verified.
- Check whether the packet loss and latency of telemetry is within acceptable criteria.
- Cross check launch commit criteria.
- Cross check that any previously launched rockets in the salvo have not created a safety hazard.
- Upon receiving the appropriate instructions from the Launch Control Officer, arm the launch controller and verify continuity.
- Enter the launch command as per the final countdown process.
- Verify successful motor ignition visually.
- Safe the launch control unit after the flight successfully initiates and exceeded the scope of a scrubbed launch or a hangfire.

## **F. Appendix: Engineering Drawings**

**THIS PAGE INTENTIONALLY LEFT BLANK.**  
**APPENDIX F BEGINS ON THE FOLLOWING PAGE.**

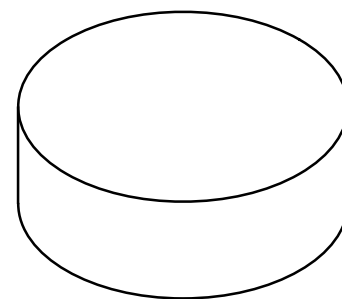
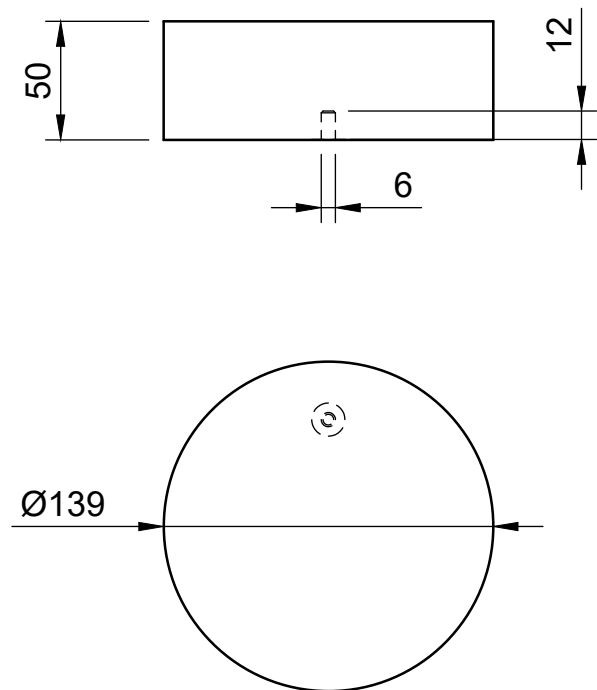
	1	2	3	4	5	6	7	8	9	10	11	12
	Datum B Profile Points											
	Point No.	X-Coordinate	Y-Coordinate									
A	1	0.00	0.00									
	2	0.20	0.38									
	3	0.60	0.87									
	4	1.10	1.36									
	5	1.60	1.80									
	6	2.40	2.44									
	7	3.60	3.30									
B	8	5.00	4.21									
	9	7.50	5.68									
	10	10.30	7.16									
	11	14.00	8.95									
	12	18.50	10.92									
	13	23.50	12.92									
	14	28.90	14.89									
C	15	34.90	16.90									
	16	41.50	18.89									
	17	48.90	20.89									
	18	57.40	22.87									
	19	68.00	24.84									
	20	80.00	26.10									



All Linear Dimensions are in mm.  
Linear Tolerances are  $\pm 0.1$  mm unless specified.  
Angular Tolerances are  $\pm 1^\circ$  unless specified.

Dept. Aerodynamics	Technical reference Prajwal Jayaraman	Created by Aryaman Srivastav 04-04-2022	Approved by Advait Bongu 11-04-2022
Document type Part Drawing	Document status Released		
Title RAYQ-NC-NSE-TIP	DWG No.		
Rev. 2	Date of issue 12-04-2022	Sheet 1/1	

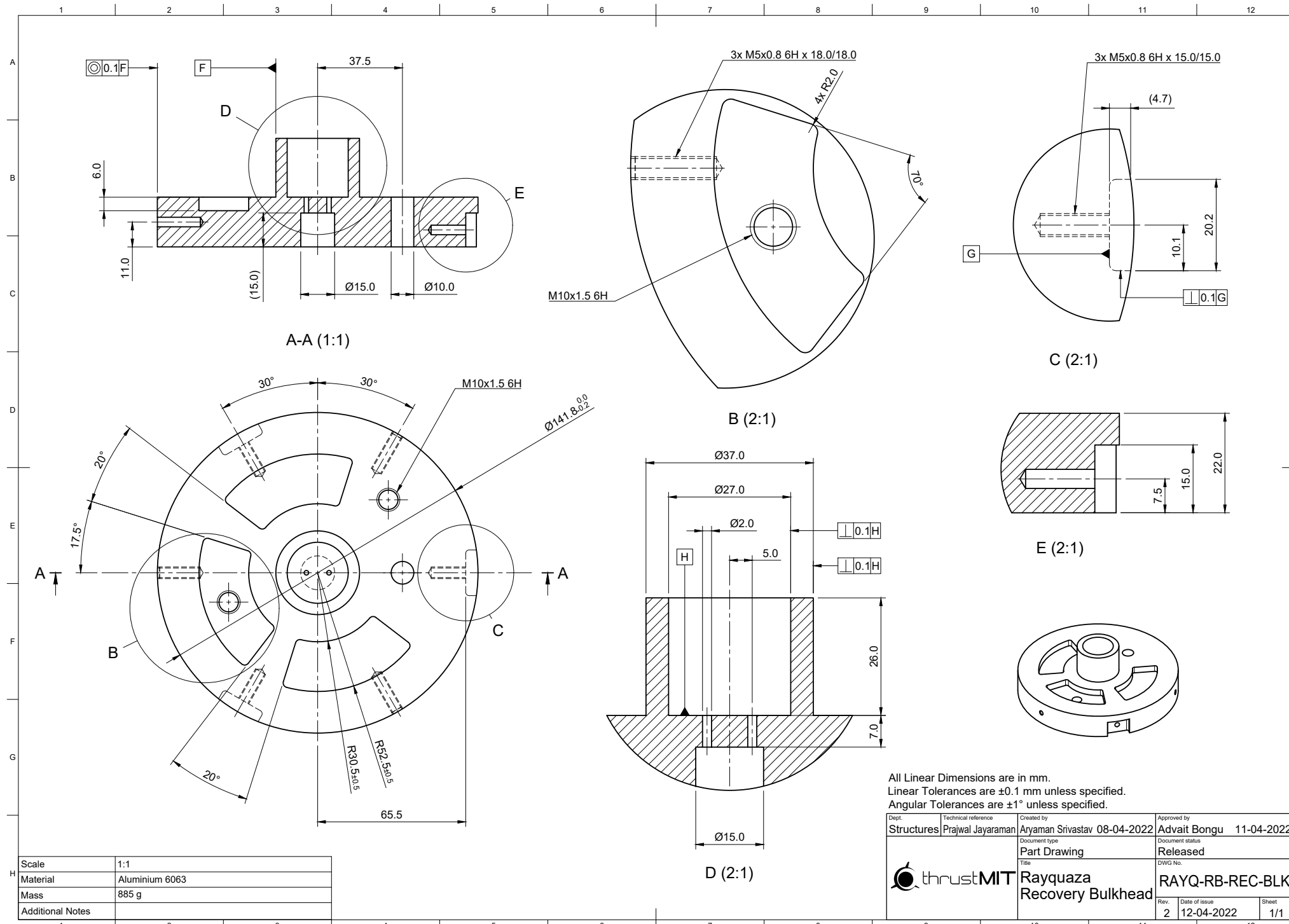
Scale	1:1
Material	Aluminium 6063
Mass	335 g
Additional Notes	



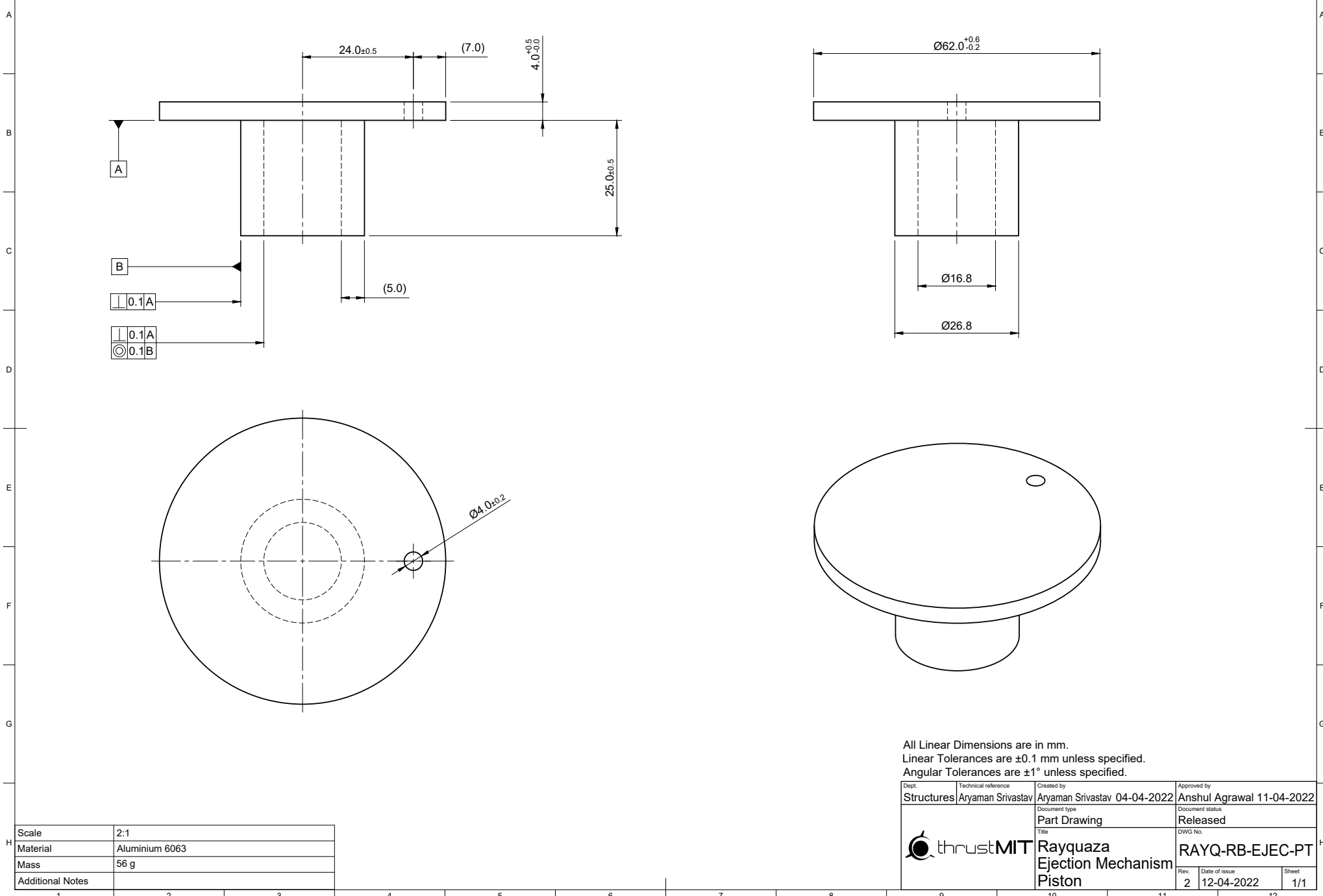
Dept. Structures	Technical reference Prajwal Jayaraman	Created by Aastha Bhatnagar 10-05-2022	Approved by
		Document type Part Drawing	Document status Released
		Title Rayquaza NC.Bulkhead	DWG No. RAYQ-NC-BLK
		Rev. 1	Date of issue 11-05-2022
			Sheet 1/1



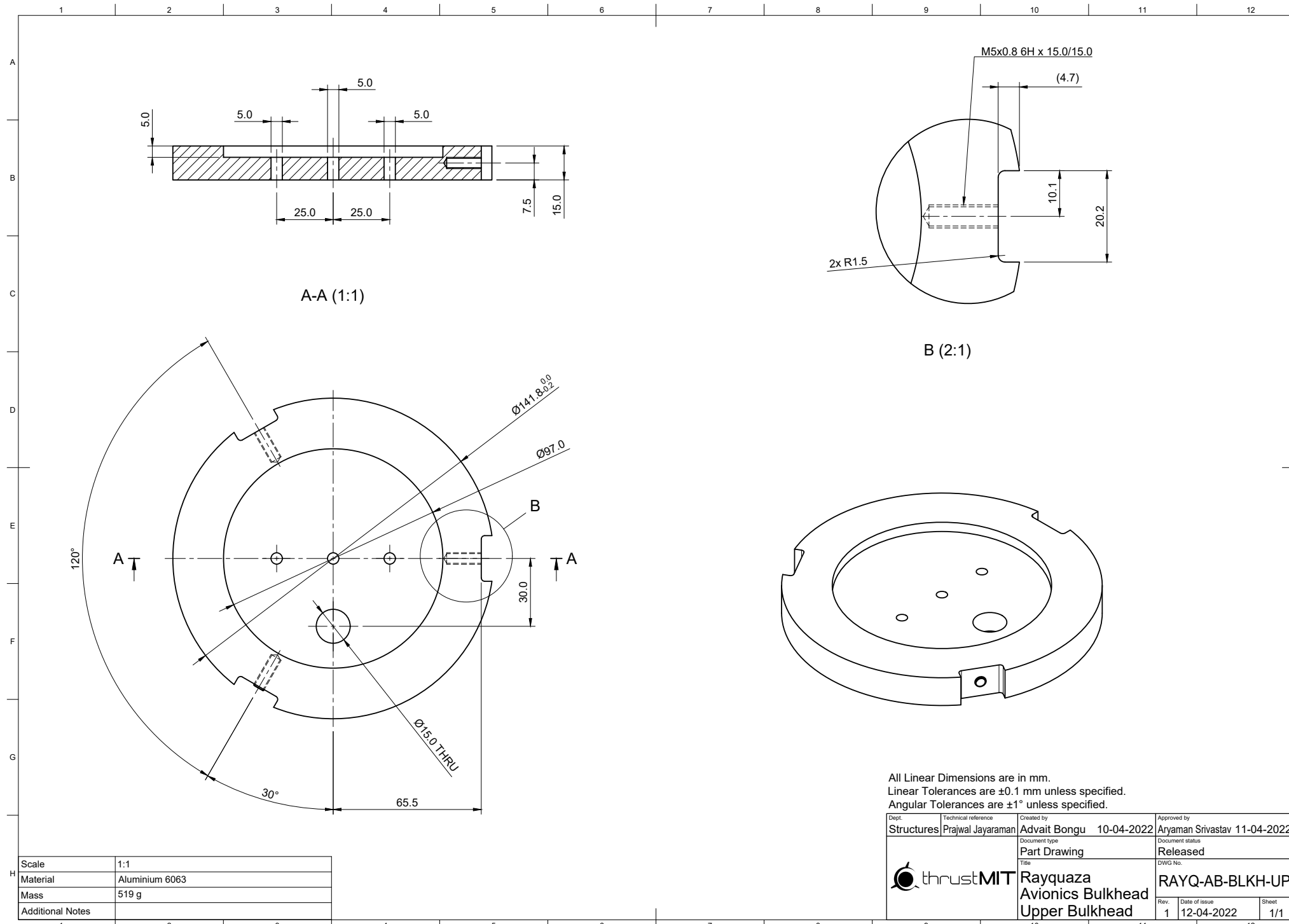
thrustMIT



1 2 3 4 5 6 7 8 9 10 11 12



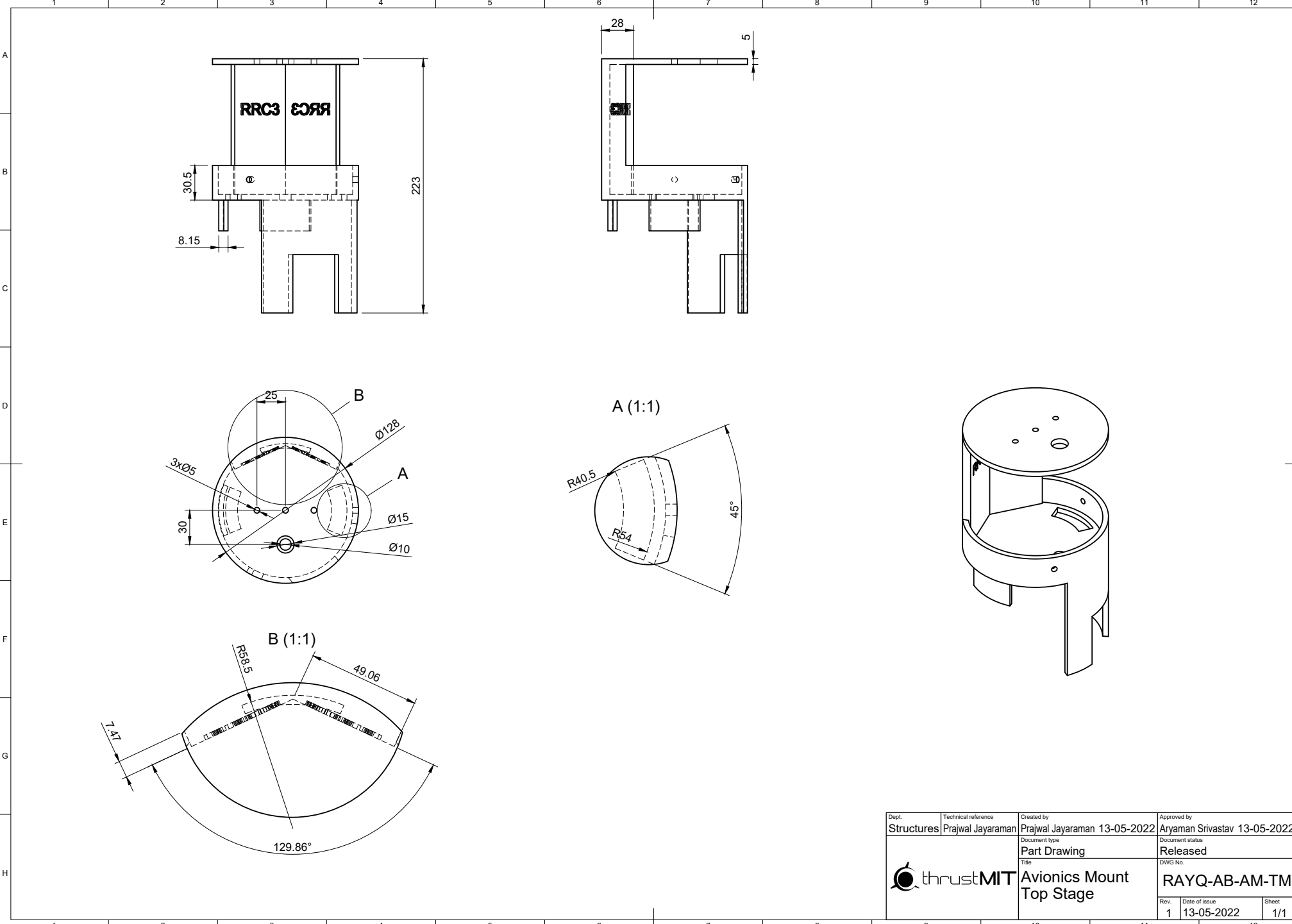
Rayquaza  
Ejection Mechanism  
Piston



All Linear Dimensions are in mm.  
Linear Tolerances are  $\pm 0.1$  mm unless specified.  
Angular Tolerances are  $\pm 1^\circ$  unless specified.

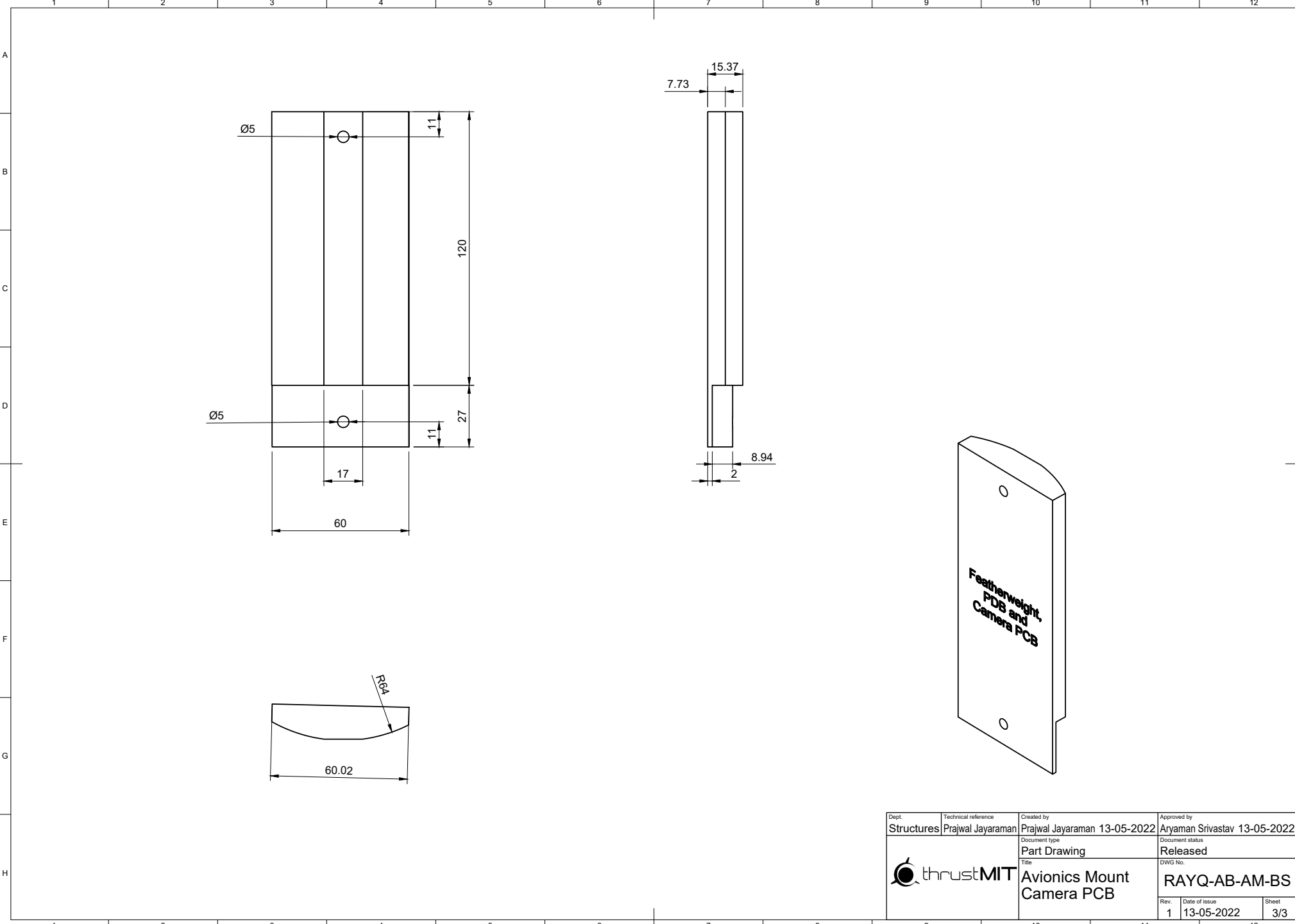
Dept.	Technical reference	Created by	Approved by
Structures	Prajwal Jayaraman	Adwait Bongu 10-04-2022	Aryaman Srivastav 11-04-2022
		Document status	
		Part Drawing	Released
		Title	DWG No.
		RAYQ-AB-BLKU-UP	
		Rev.	Date of issue
		1	12-04-2022
		Sheet	1/1





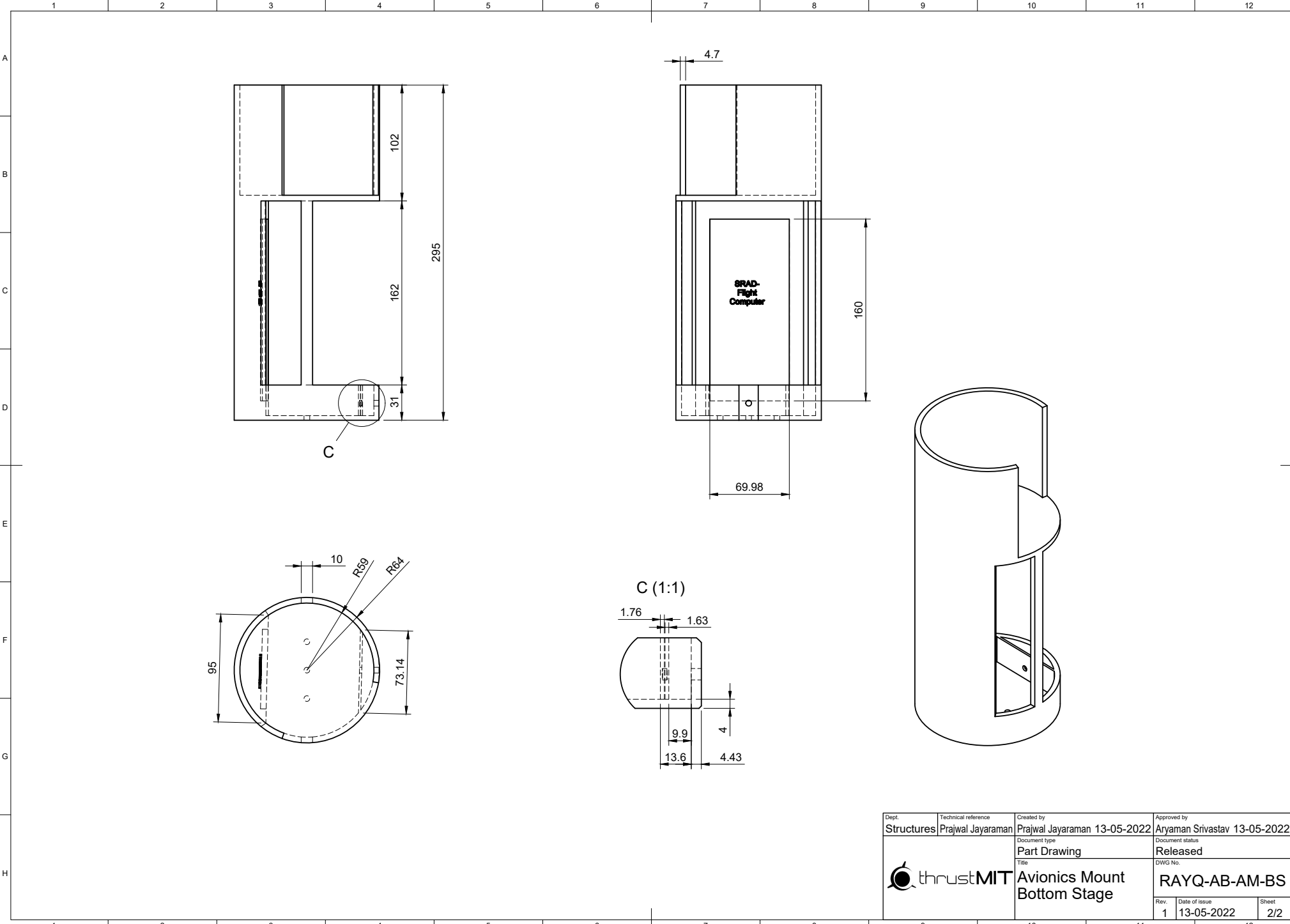
Dept. Structures	Technical reference Prajwal Jayaraman	Created by Prajwal Jayaraman 13-05-2022	Approved by Aryaman Srivastav 13-05-2022
	Document type Part Drawing	Document status Released	
	Title Avionics Mount Top Stage	DWG No.	RAYQ-AB-AM-TM
Rev. 1	Date of issue 13-05-2022	Sheet 1/1	



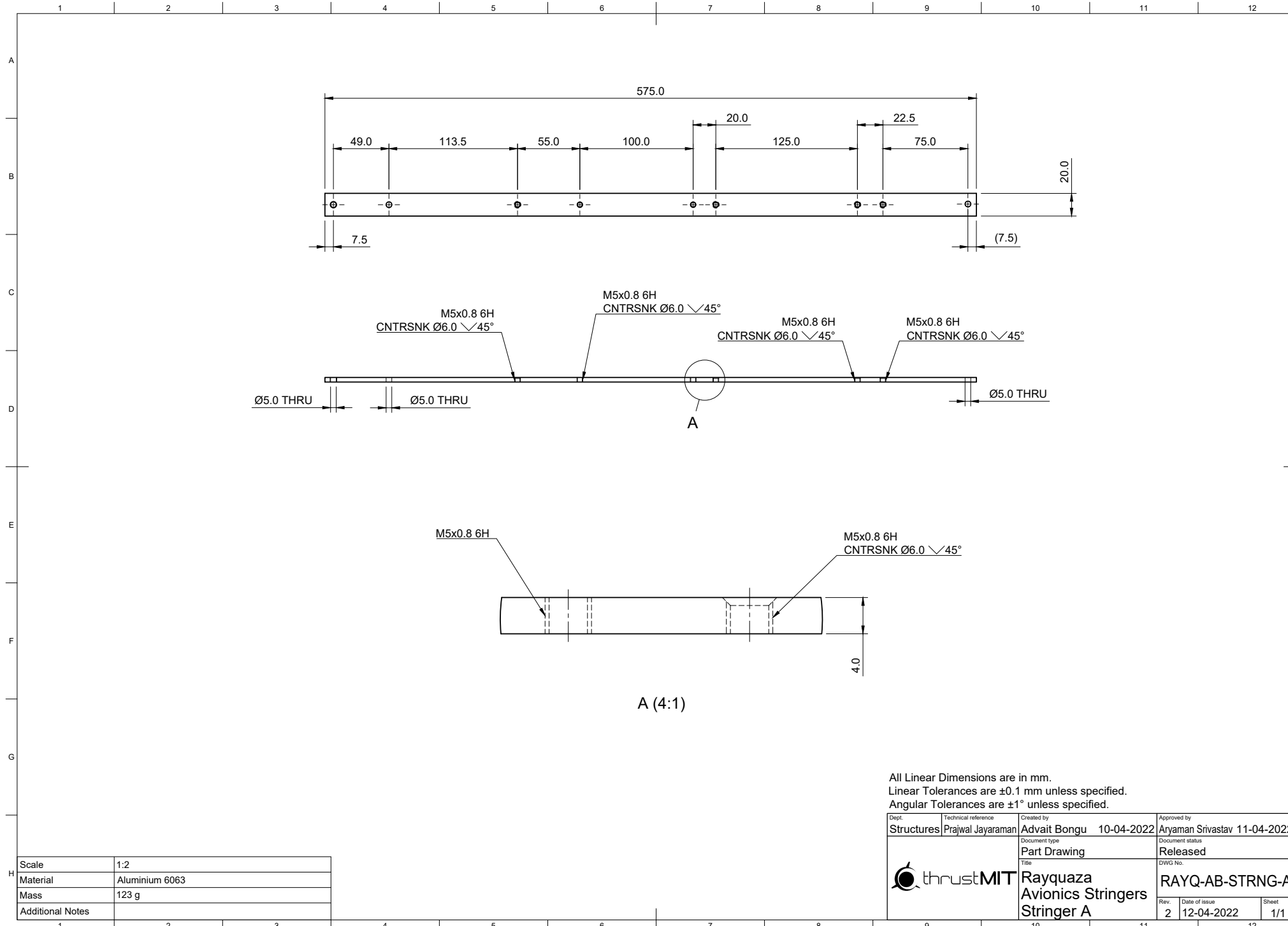


Dept. Structures	Technical reference Prajwal Jayaraman	Created by Prajwal Jayaraman 13-05-2022	Approved by Aryaman Srivastav 13-05-2022
	Document type Part Drawing	Document status Released	
	Title Avionics Mount Camera PCB	DWG No. RAYQ-AB-AM-BS	
	Rev. 1	Date of issue 13-05-2022	Sheet 3/3





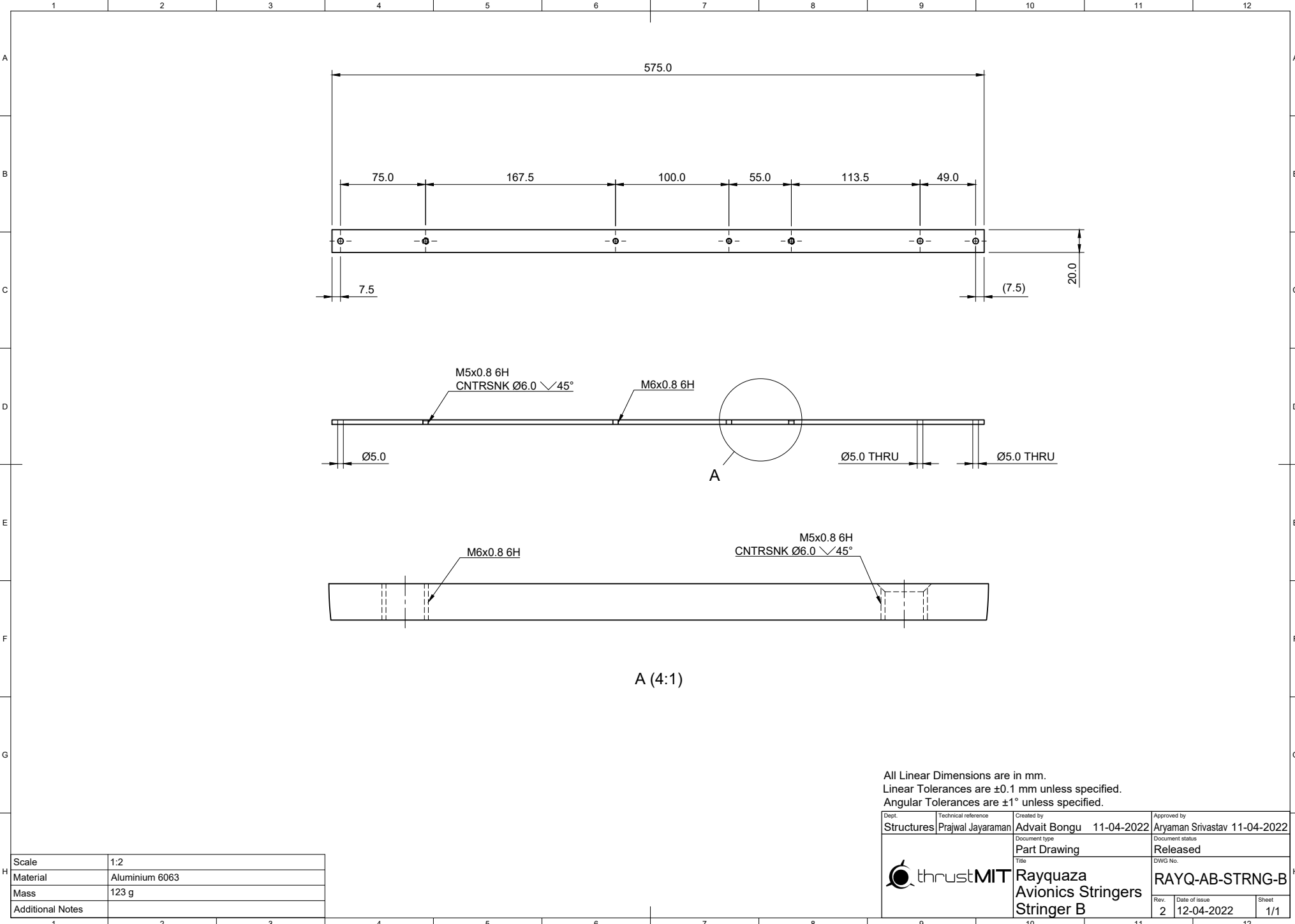
Dept. Structures	Technical reference Prajwal Jayaraman	Created by Prajwal Jayaraman 13-05-2022	Approved by Aryaman Srivastav 13-05-2022
	Document type Part Drawing	Document status Released	
	Title Avionics Mount Bottom Stage	DWG No.	
	Rev. 1 Date of issue 13-05-2022	Sheet 2/2	

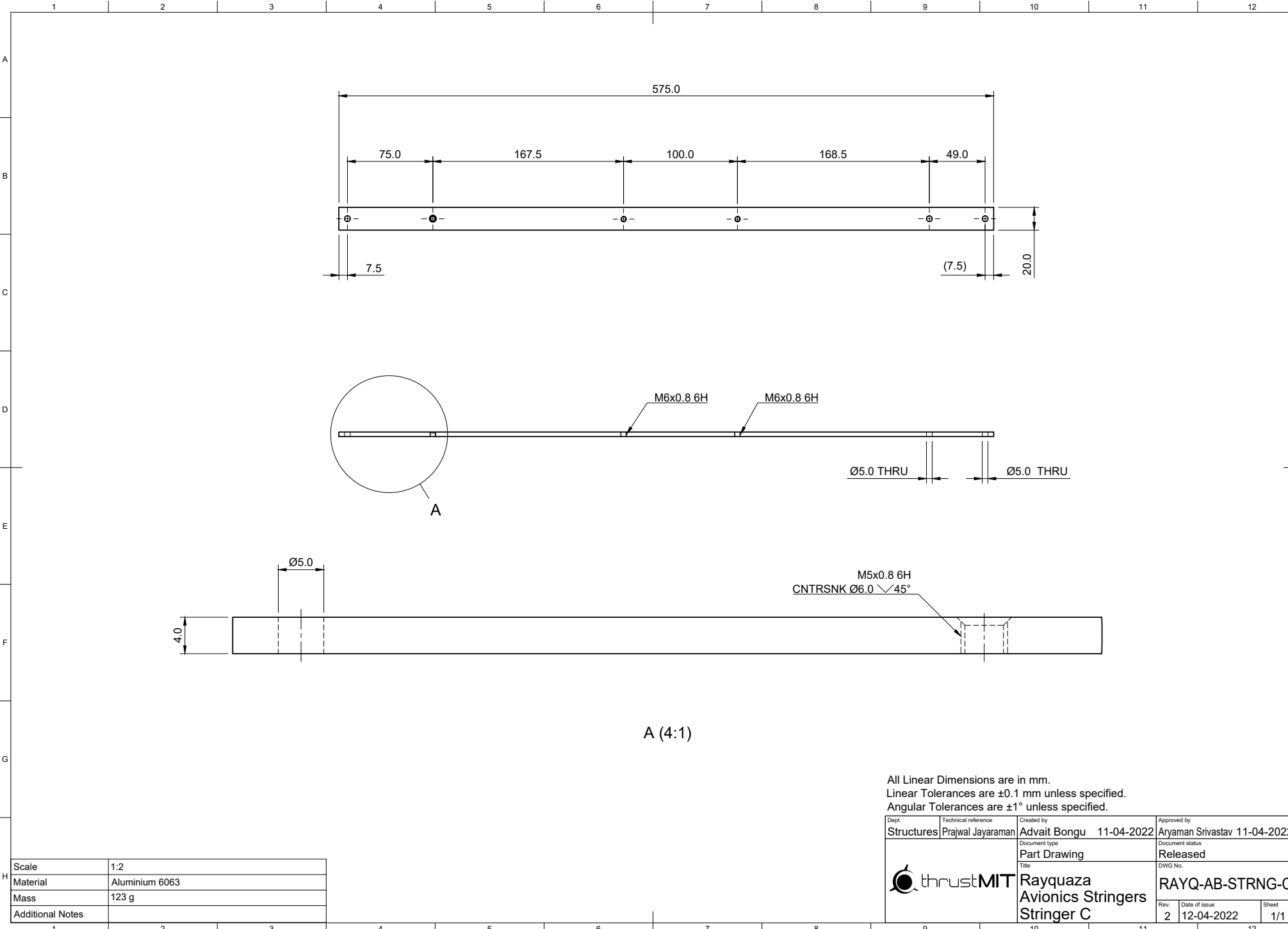


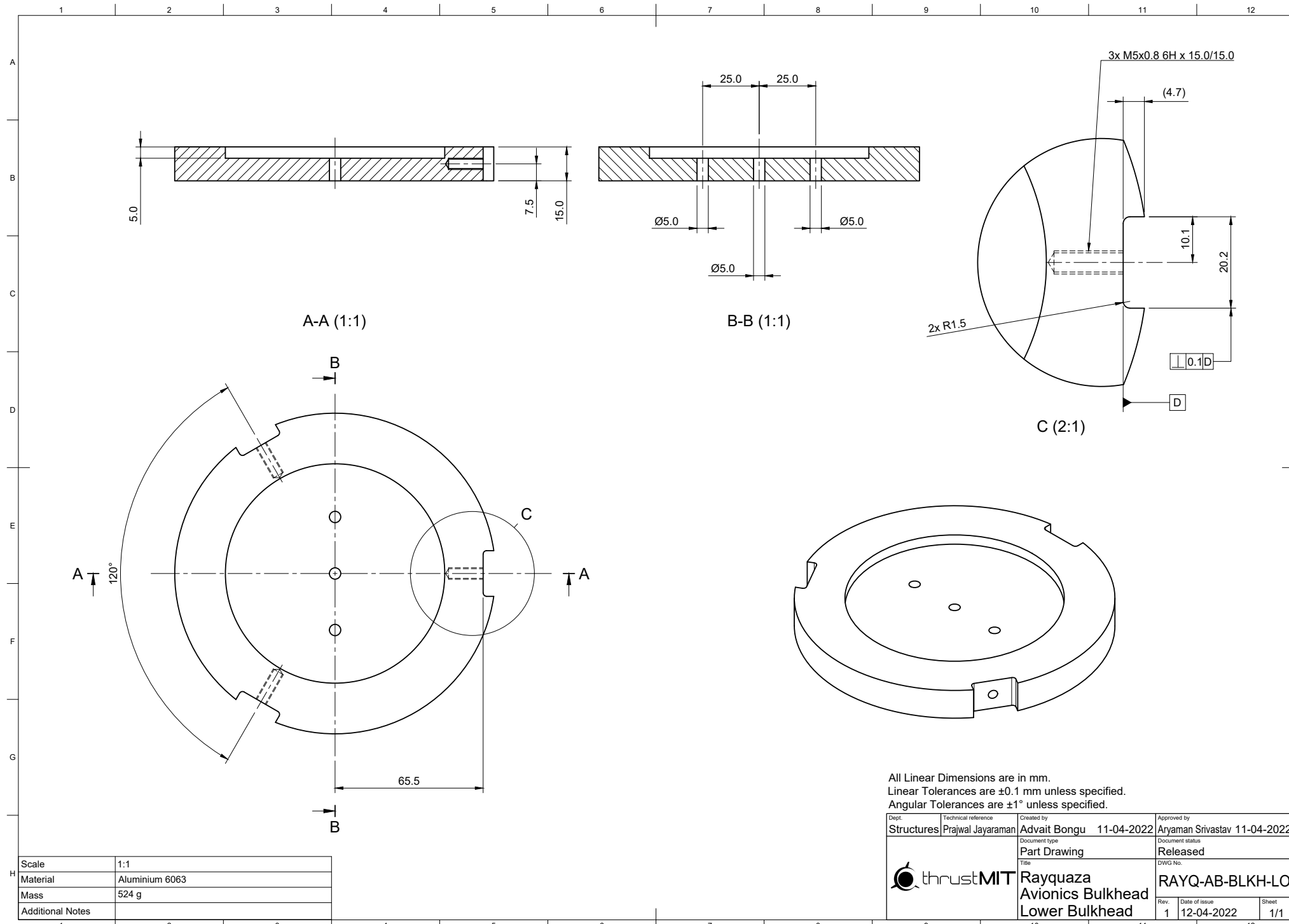
Dept.	Technical reference	Created by	Approved by
Structures	Prajwal Jayaraman	Adwait Bongu 10-04-2022	Aryaman Srivastav 11-04-2022
		Document type	Document status
		Part Drawing	Released
		Title	DWG No.
		RAYQ-AB-STRNG-A	
		Rev.	Date of issue
		2	12-04-2022
		Sheet	1/1

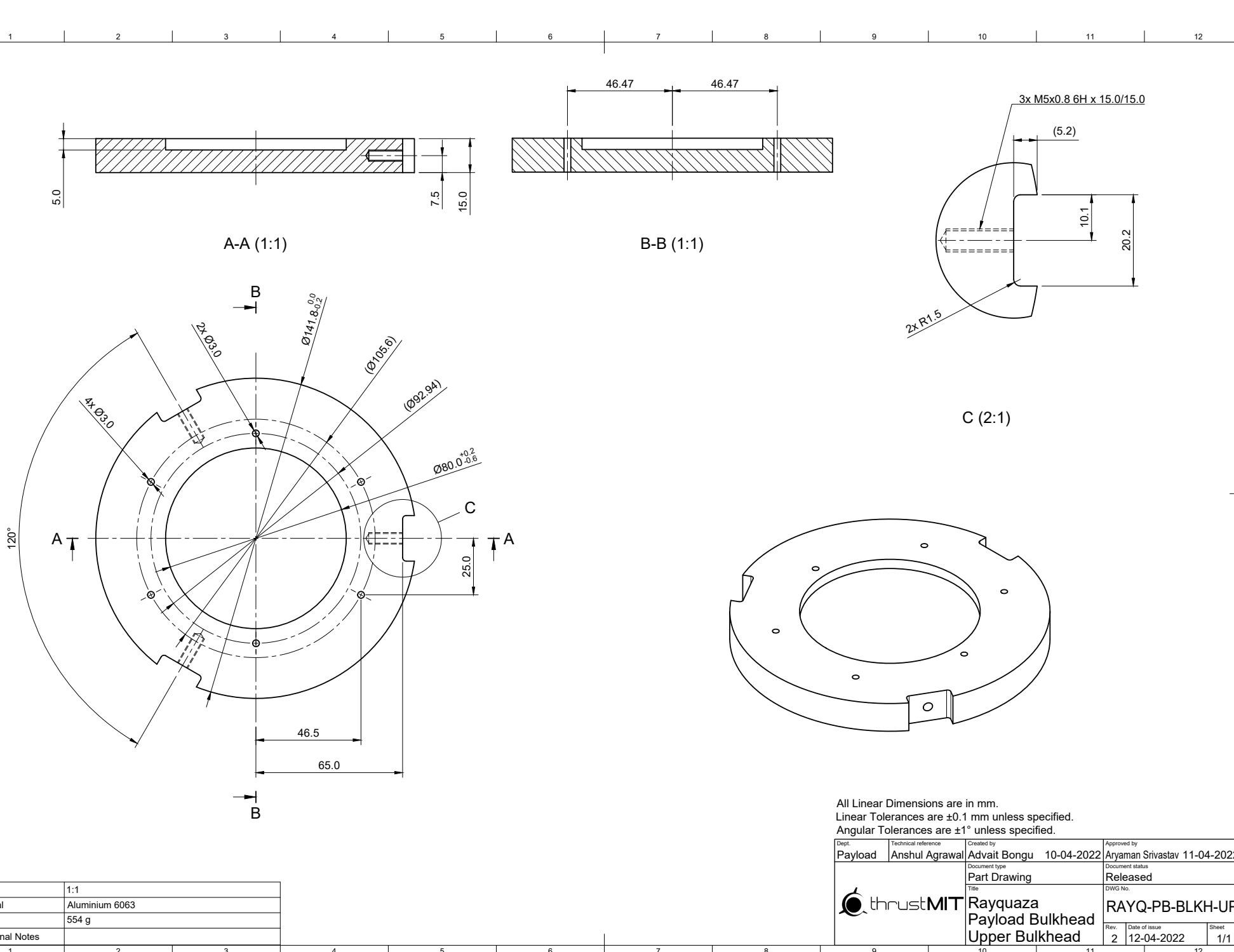


Rayquaza  
Avionics Stringers  
Stringer A



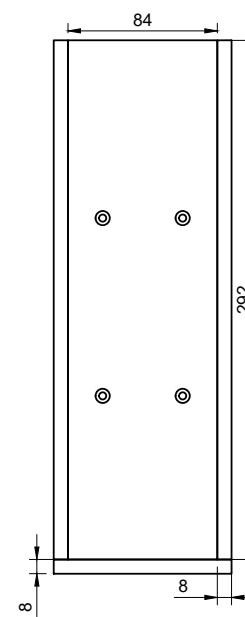
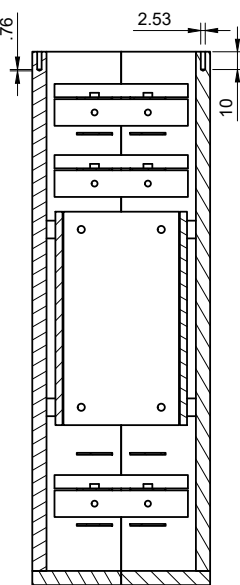
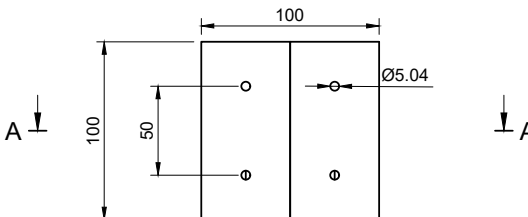
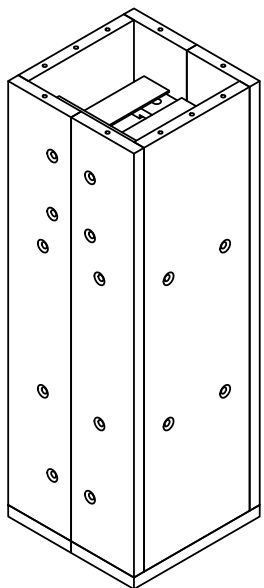
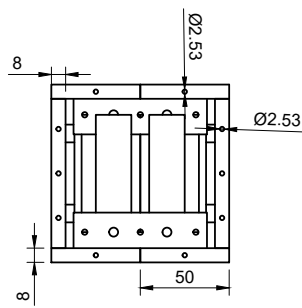
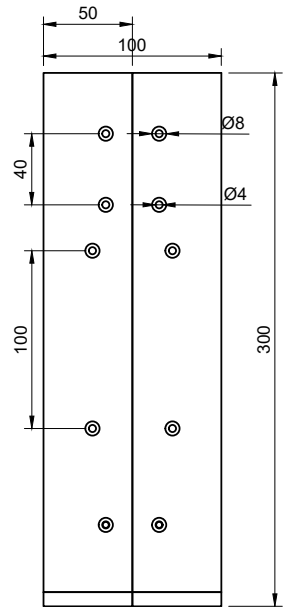






All Linear Dimensions are in mm.  
Linear Tolerances are  $\pm 0.1$  mm unless specified.  
Angular Tolerances are  $\pm 1^\circ$  unless specified.

Angular Tolerances are ±1 unless specified.					
Dept.	Technical reference	Created by	Approved by		
Payload	Anshul Agrawal	Advait Bongu	10-04-2022	Aryaman Srivastav	11-04-2022
		Document type	Document status		
		Part Drawing	Released		
		Title	DWG No.		
 thrustMIT		Rayquaza	RAYQ-PB-BLKH-UP		
		Payload Bulkhead			
		Upper Bulkhead			
			Rev.	Date of issue	Sheet
			2	12-04-2022	1/1



A-A (1:2)

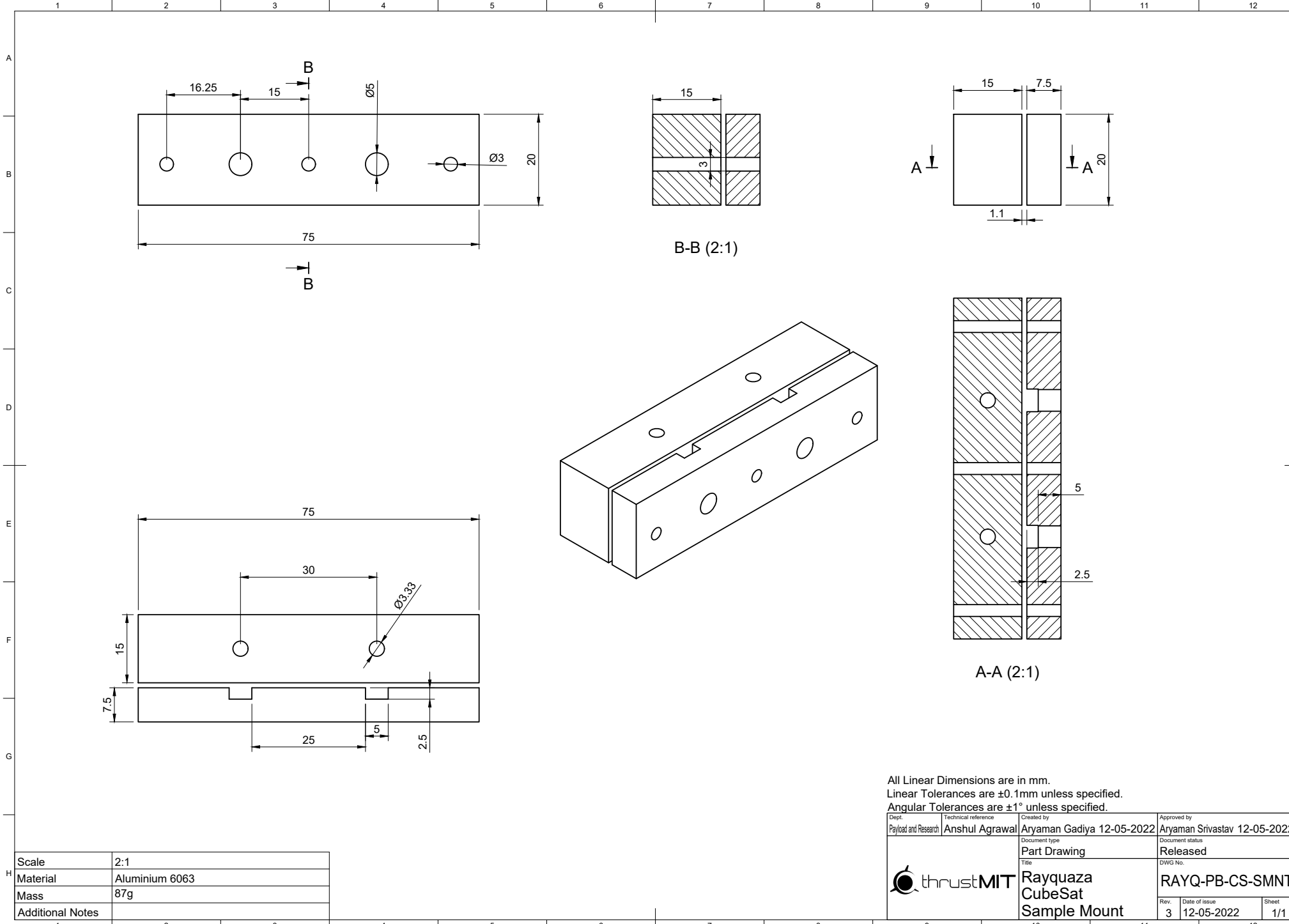
All Linear Dimensions are in mm.  
Linear Tolerances are  $\pm 0.1$ mm unless specified.  
Angular Tolerances are  $\pm 1^\circ$  unless specified.

Angular Tolerances are 2° unless specified.			
Dept. payload and Research	Technical reference Anshul Agrawal	Created by Aryaman Gadiya 12-05-2022	Approved by Aryaman Srivastav 12-05-2022
		Document type Part Drawing	Document status Released
		Title Rayquaza CubeSat	DWG No. RAYQ-PB-CUB-SAT
		Rev. 3	Date of issue 12-05-2022
			Sheet 1/1



 thrustMIT Title  
Rayquaza  
CubeSat

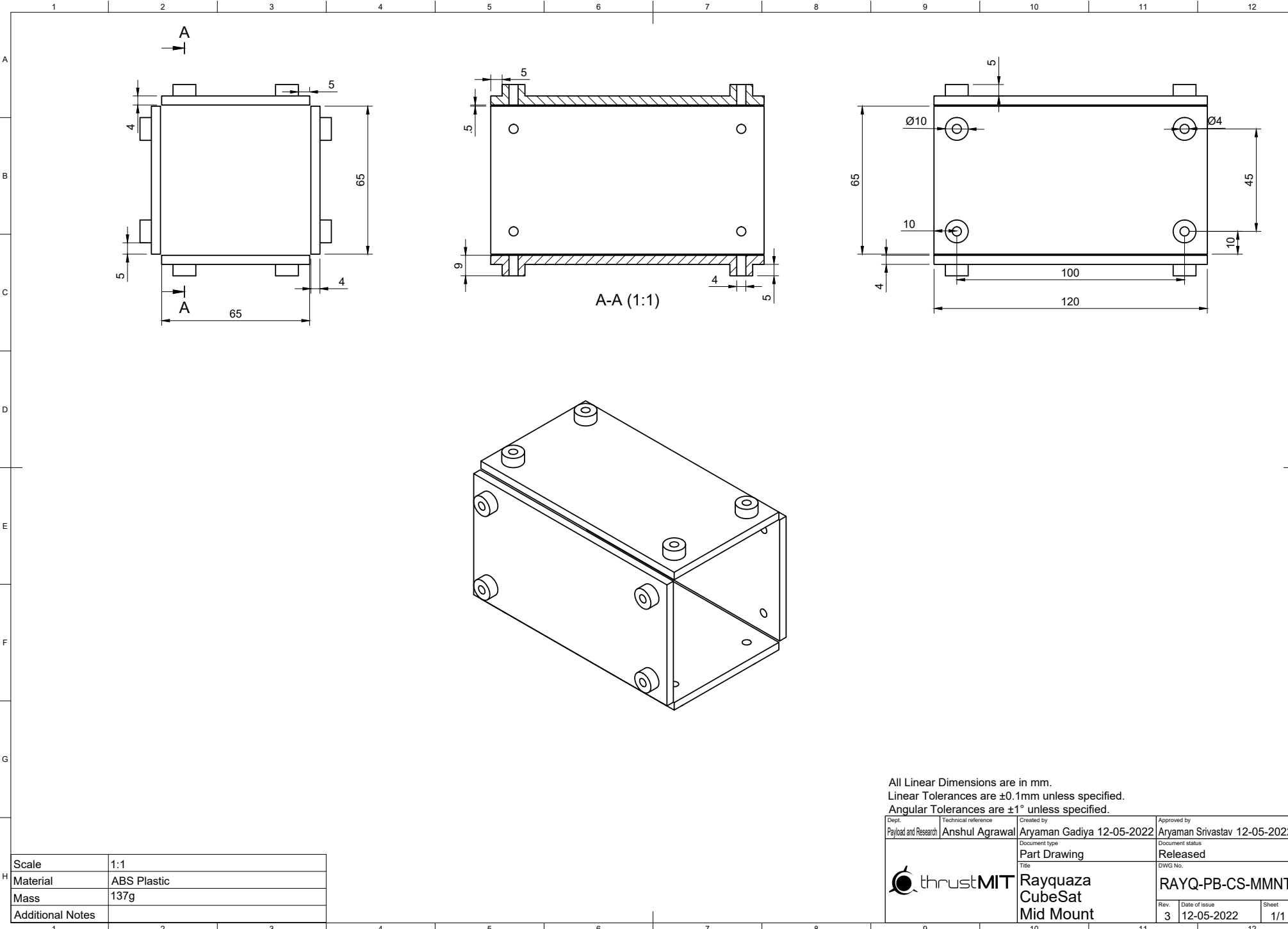
Scale	1:2
Material	Aluminium 6063
Mass	2524.876g
Additional Notes	



All Linear Dimensions are in mm.  
Linear Tolerances are  $\pm 0.1$ mm unless specified.  
Angular Tolerances are  $\pm 1^\circ$  unless specified.

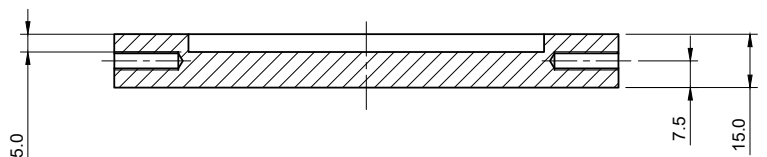
Angular tolerances are ± 1 unless specified.	
Dept.	Technical reference
Payload and Research	Anshul Agrawal
	Created by Aryaman Gadiya 12-05-2022
	Approved by Aryanam Srivastav 12-05-2022
	Document type Part Drawing
	Document status Released
	Title DWG No.
 thrustMIT	Rayquaza CubeSat Sample Mount
	RAYQ-PB-CS-SMNT
	Rev. Date of issue Sheet
	3 12-05-2022 1/1





1 2 3 4 5 6 7 8 9 10 11 12

A



B

C

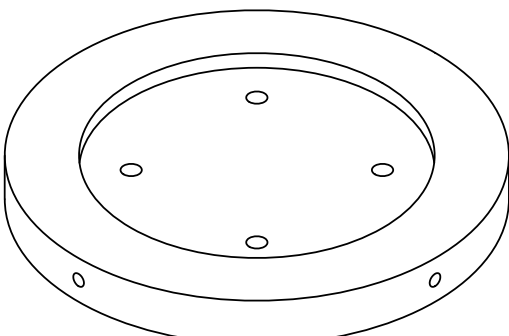
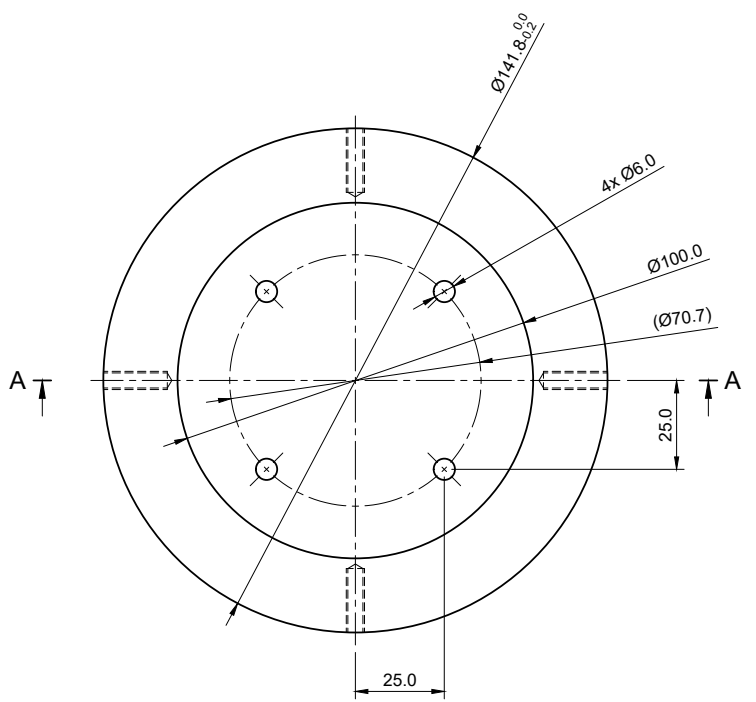
D

E

F

G

A-A (1:1)

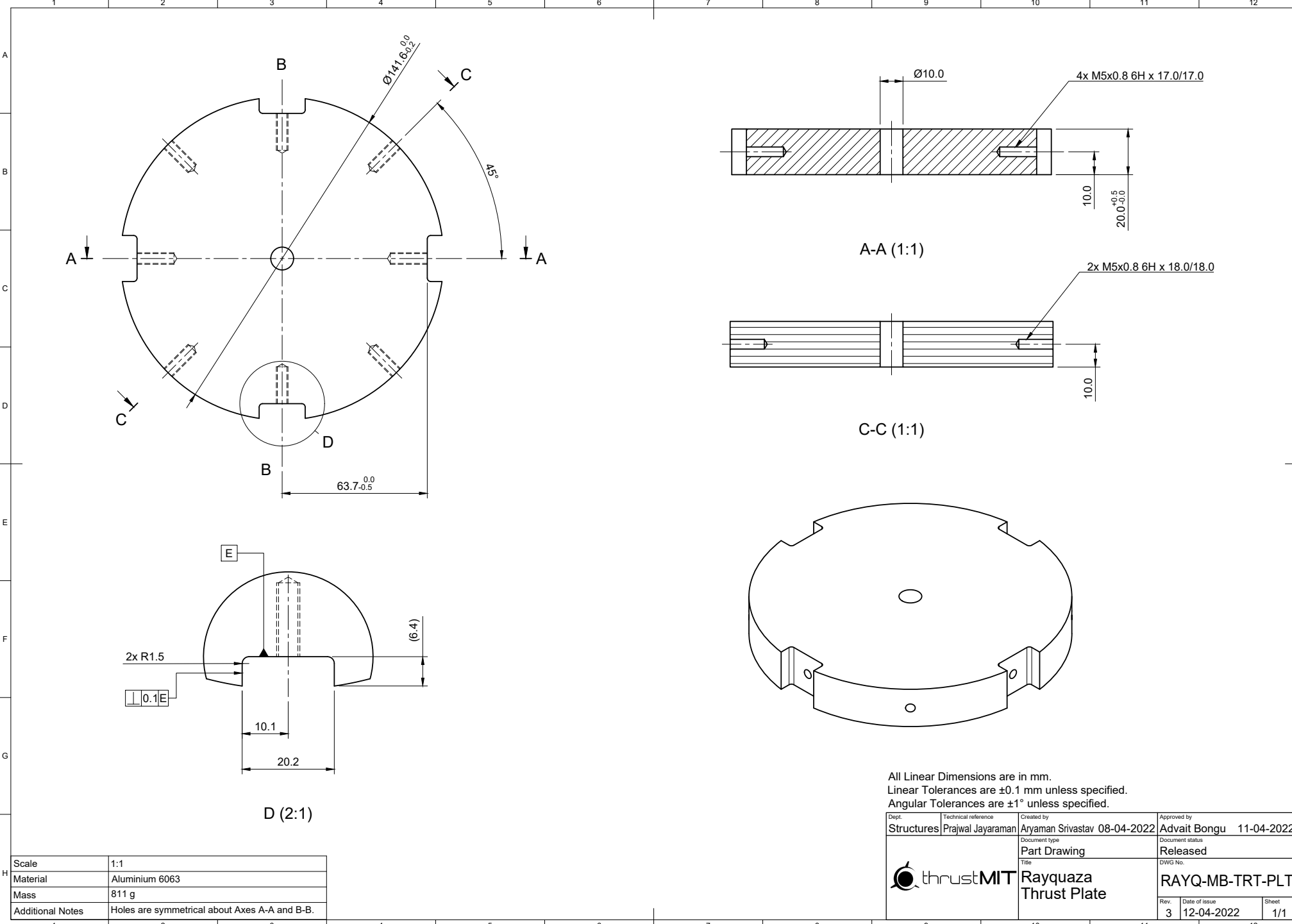


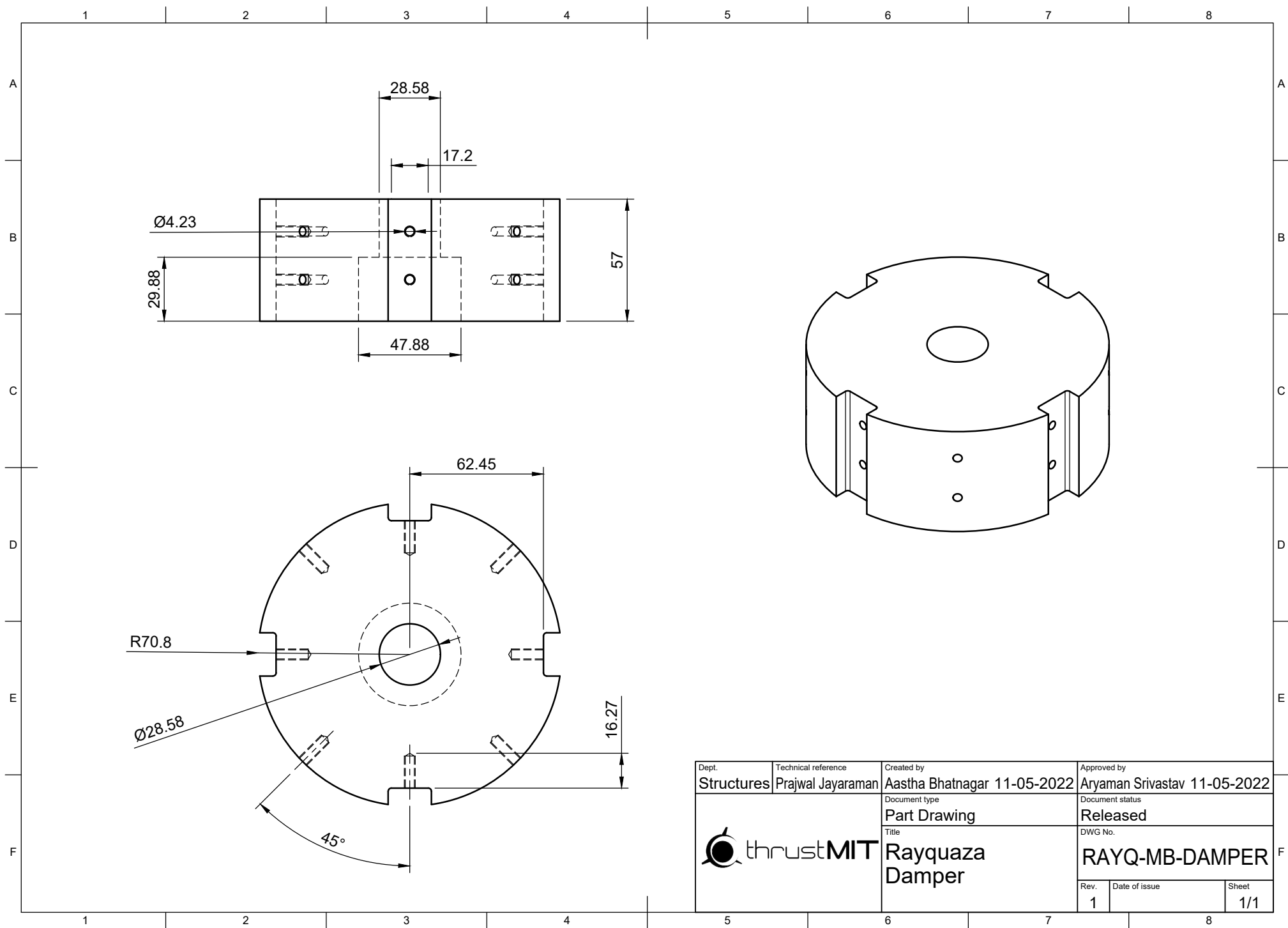
All Linear Dimensions are in mm.  
Linear Tolerances are  $\pm 0.1$  mm unless specified.  
Angular Tolerances are  $\pm 1^\circ$  unless specified.

Scale	1:1
Material	Aluminium 6063
Mass	528 g
Additional Notes	

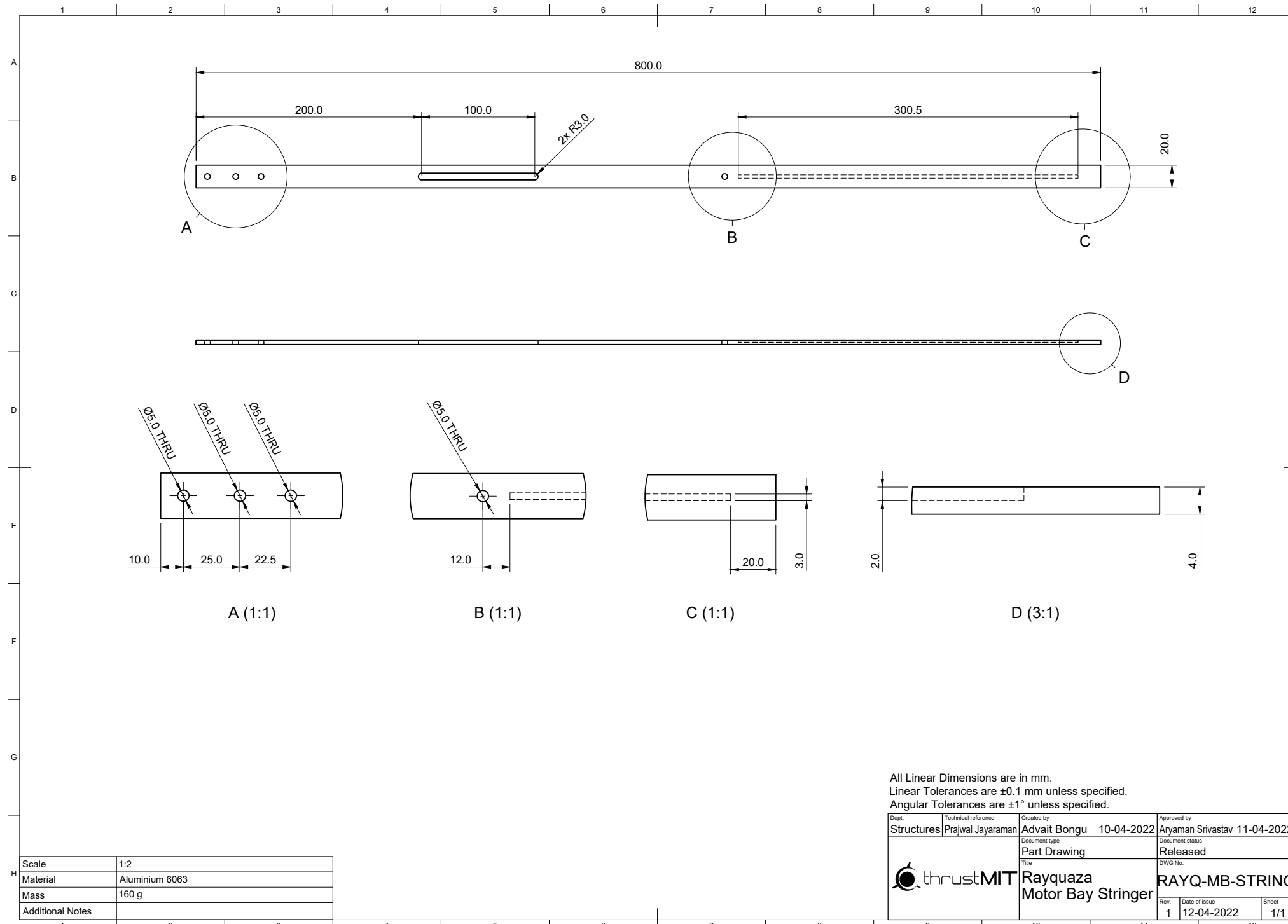
Dept.	Technical reference	Created by	Approved by
Payload	Anshul Agrawal	Aryaman Srivastav 12-04-2022	Anshul Agrawal 12-04-2022
Document type	Part Drawing	Document status	Released
Title	Rayquaza	DWG No.	RAYQ-PB-BLK-H-LO
Rev.	Date of issue	Sheet	1/1
2	12-04-2022		

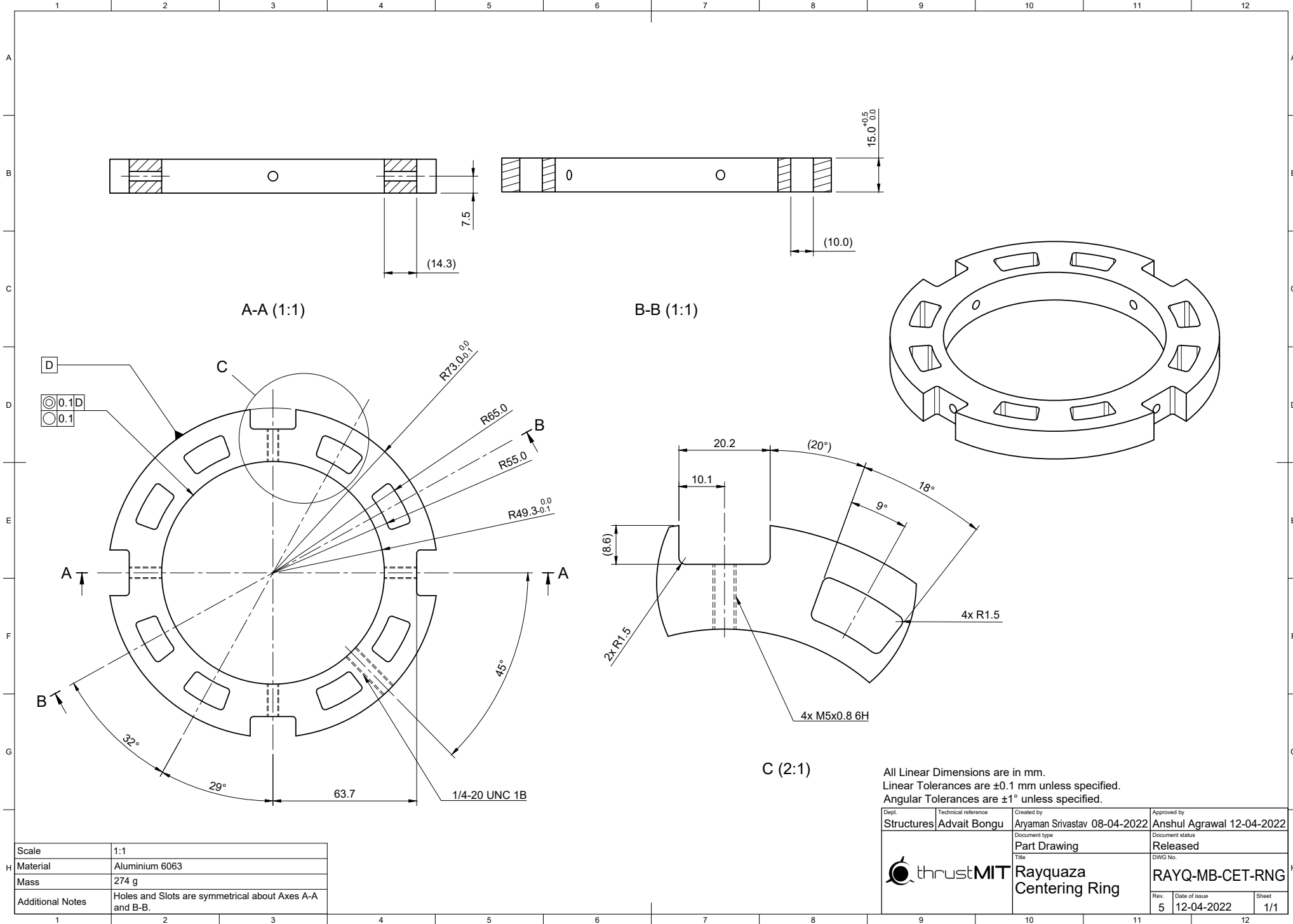






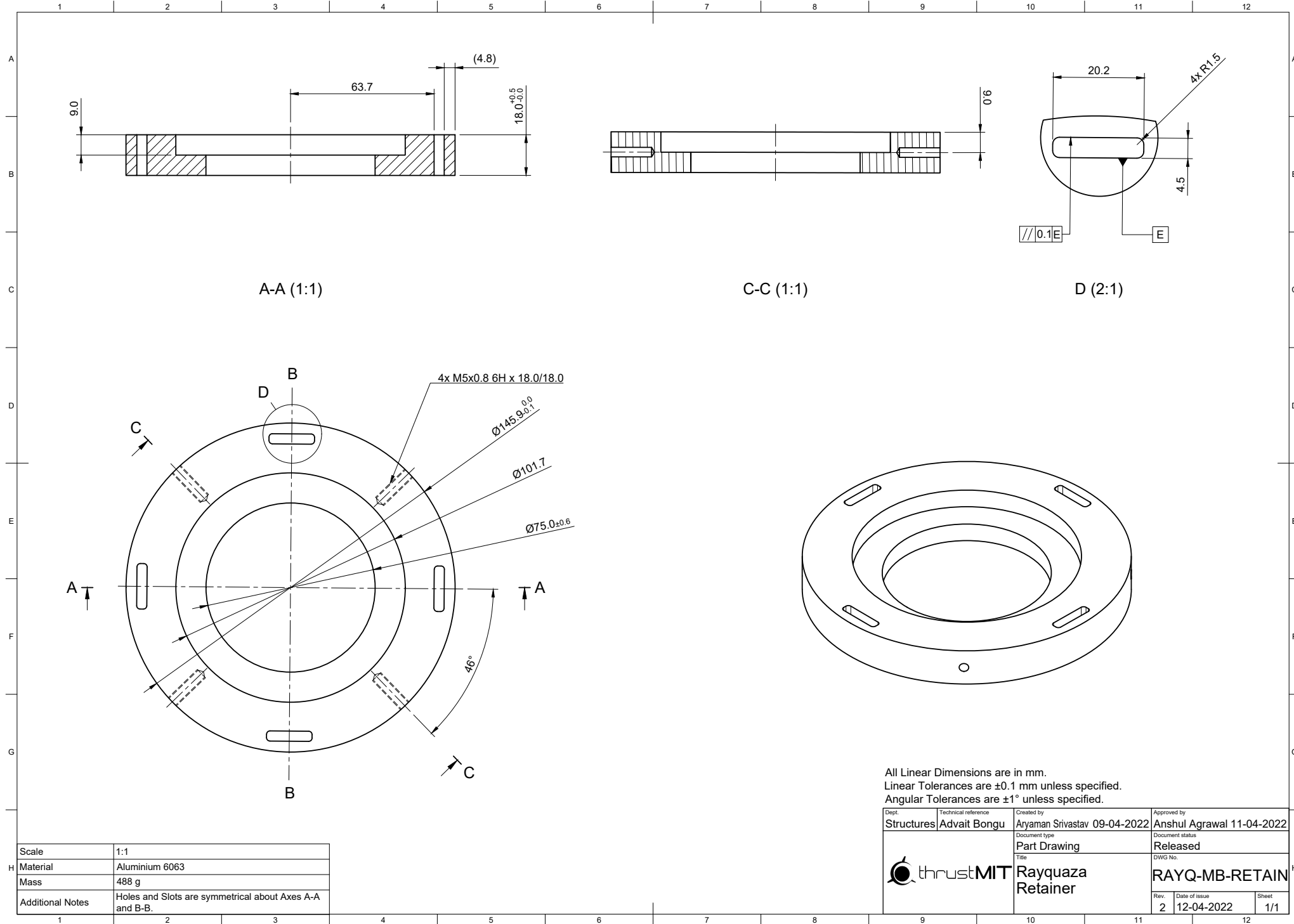
Dept. Structures	Technical reference Prajwal Jayaraman	Created by Aastha Bhatnagar 11-05-2022	Approved by Aryaman Srivastav 11-05-2022
	Document type Part Drawing	Document status Released	DWG No.
	Title Rayquaza Damper		
Rev. 1	Date of issue	Sheet 1/1	

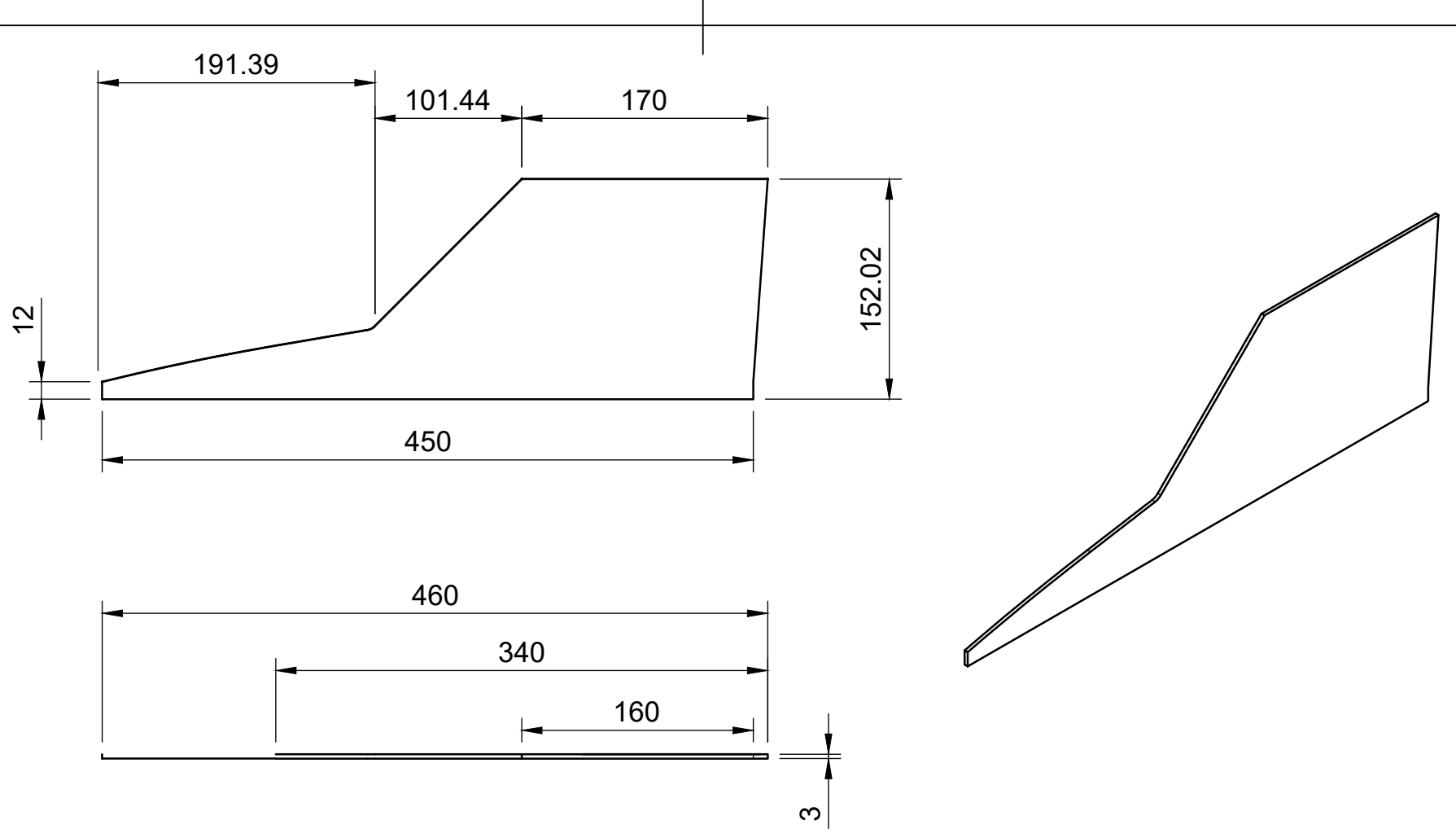




All Linear Dimensions are in mm.  
Linear Tolerances are  $\pm 0.1$  mm unless specified.  
Angular Tolerances are  $\pm 1^\circ$  unless specified.

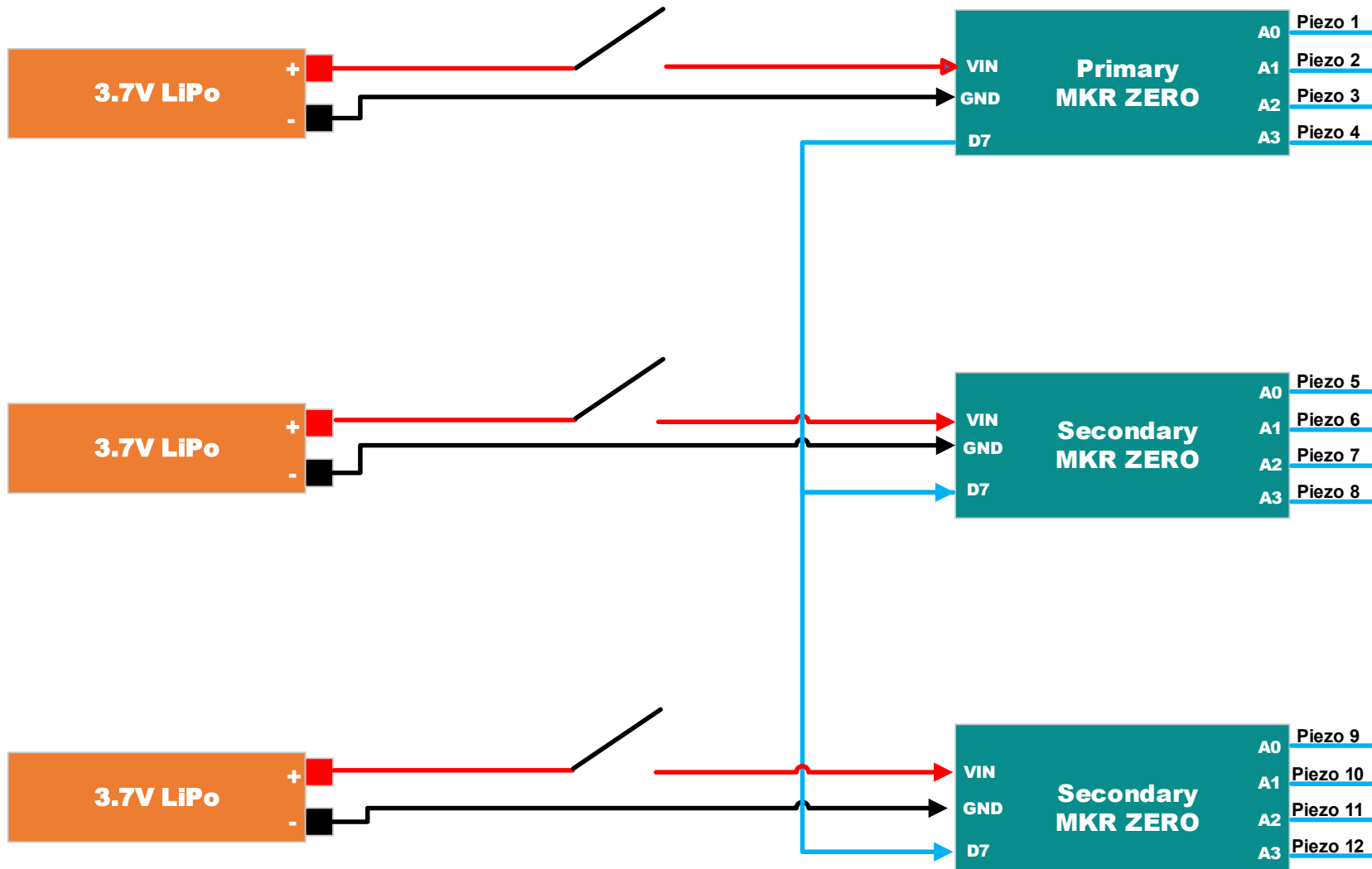
Dept.	Technical reference	Created by	Approved by
Structures	Advait Bongu	Aryaman Srivastav 08-04-2022	Anshul Agrawal 12-04-2022
	Document type	Document status	
	Part Drawing	Released	
	Title	DWG No.	
 thrustMIT	Rayquaza Centering Ring	RAYQ-MB-CET-RNG	
	Rev.	Date of issue	Sheet
	5	12-04-2022	1/1





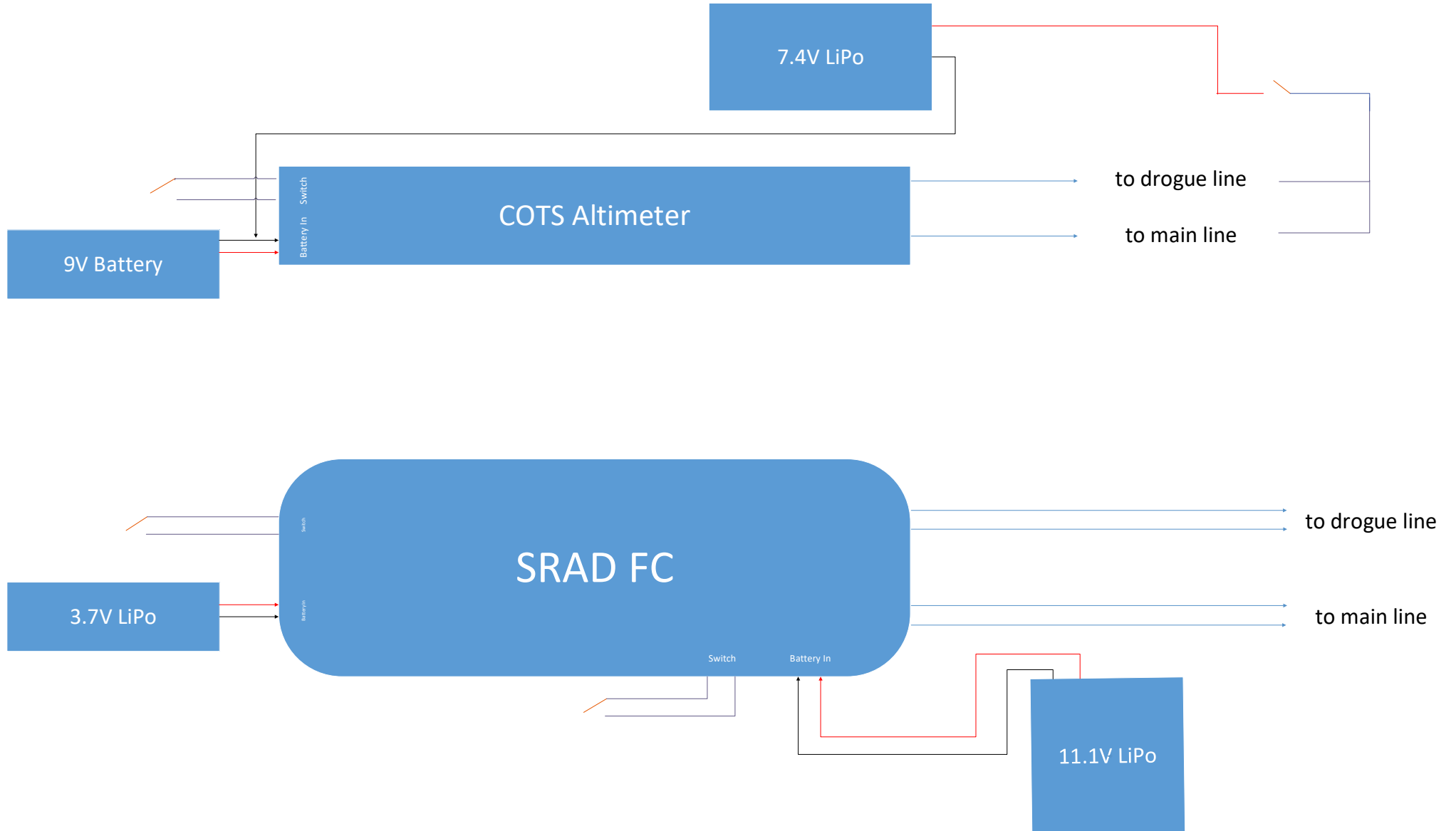
Dept. Structures	Technical reference Prajwal Jayaraman	Created by Aastha Bhatnagar 10-05-2022	Approved by Aryaman Srivastav 10-05-2022
		Document type Part Drawing	Document status Released
Title <b>Rayquaza Fins</b>		DWG No.  <b>RAYQ-FINS</b>	
Rev. 1	Date of issue 10-05-2022	Sheet 1/1	

## Payload Wiring Diagram



**PINS**  
D7 - Stop Data Logging  
A0 .. A3 - Analog Pins

# Avionics Wiring Diagram



## **G. Appendix: Team Members**

### **A. Faculty Advisor**

**Dr. Srinivas G.** Assistant Professor - Senior Scale, Department of Aeronautical & Automobile Engineering, Manipal Institute of Technology, Manipal Academy of Higher Education

### **B. Team Mentors**

**Bob Schoner** TRA L3, Flyer of Record; Assistant Manager - Advanced Engineering Design Lab, Virginia Tech

**Dr. Yogananda Jeppu** Adjunct Faculty, Department of Instrumentation & Control Engineering, Manipal Institute of Technology, Manipal Academy of Higher Education

### **C. Project Leads**

**Aneesh Salian** Team Leader, Aerodynamics Head; B.Tech Aeronautical Engineering, Batch of 2023

**Samanway Chakraborty** Team Manager; B.Tech Aeronautical Engineering, Batch of 2023

**Siddharth Sudhakar** Avionics Head, Computation Head; B.Tech Electronics & Communication Engineering, Batch of 2023

**Aryaman Srivastav** Mechanical Head, Propulsions Head; B.Tech Mechanical Engineering, Batch of 2023

**Vignesh R.** Controls Head; B.Tech Electronics & Instrumentation Engineering, Batch of 2023

**Prajwal Jayaraman** Structures Head; B.Tech Aeronautical Engineering, Batch of 2023

**Prishita Rathore** Payload and Research Head - Avionics; B.Tech Electronics & Communication Engineering, Batch of 2023

**Anshul Agrawal** Payload and Research Head - Mechanical; B.Tech Mechanical Engineering, Batch of 2023

**Prakhar Swarnakar** Management Head; B.Tech Electronics & Communication Engineering, Batch of 2023

### **D. Aerodynamics Team**

**Abhyudaya Singh** B.Tech Aeronautical Engineering, Batch of 2023

**Ashwinraj Renuka** B.Tech Aeronautical Engineering, Batch of 2024

**Kadar Azad** B.Tech Aeronautical Engineering, Batch of 2024

**Tanvi Agrawal** B.Tech Mechanical Engineering, Batch of 2024

#### **E. Avionics Team**

<b>Aditya Vamsi Kumbhari</b>	B.Tech Electronics & Communication Engineering, Batch of 2023
<b>Anway Das</b>	B.Tech Electrical & Electronics Engineering, Batch of 2024
<b>Darpan Theng</b>	B.Tech Aeronautical Engineering, Batch of 2024
<b>Ronan D'souza</b>	B.Tech Data Science Engineering, Batch of 2024
<b>Vainavi Samant</b>	B.Tech Computers & Communication Engineering, Batch of 2024

#### **F. Structures Team**

<b>Khushal Agarwal</b>	B.Tech Mechanical Engineering, Batch of 2023
<b>Nathan Karl Tauro</b>	B.Tech Mechatronics, Batch of 2023
<b>Aastha Bhatnagar</b>	B.Tech Aeronautical Engineering, Batch of 2024
<b>Aryaman Gadiya</b>	B.Tech Aeronautical Engineering, Batch of 2024
<b>Gaurang Alonè</b>	B.Tech Mechanical Engineering, Batch of 2024

#### **G. Propulsions Team**

<b>Advait Bongu</b>	B.Tech Mechanical Engineering, Batch of 2023
<b>Chinmay Raje</b>	B.Tech Aeronautical Engineering, Batch of 2024
<b>Gangarapu Jayadeep</b>	B.Tech Mechanical Engineering, Batch of 2024
<b>Sharada Belagavi</b>	B.Tech Aeronautical Engineering, Batch of 2024
<b>Raeid Mukadam</b>	B.Tech Mechanical Engineering, Batch of 2024

#### **H. Payload Team**

<b>Utkarsh Anand</b>	B.Tech Electrical & Electronics Engineering, Batch of 2024
<b>Vanshita</b>	B.Tech Computers & Communication Engineering, Batch of 2024
<b>Diya Parekh</b>	B.Tech Mechatronics, Batch of 2024
<b>Thakur Pranav Singh</b>	B.Tech Mechanical Engineering, Batch of 2024

#### **I. Management Team**

<b>Jeslyn Biju</b>	B.Tech Mechanical Engineering, Batch of 2023
<b>Kesari Srinidhi</b>	B.Tech Aeronautical Engineering, Batch of 2024
<b>Arjun Chhabra</b>	B.Tech Aeronautical Engineering, Batch of 2024

## H. Appendix: SRAD Six Degree of Freedom Simulator

thrustMIT has developed a six-degrees of freedom trajectory simulator which is built on MATLAB. The simulator is used to accurately simulate a rocket's trajectory and find its apogee using aerodynamic coefficients and data obtained from computational fluid dynamics and the rocket's model is simulated using data obtained from the CAD design. It takes the rocket's initial launch angle, mean wind speed, and turbulent intensity as the inputs. Other data related to the rocket such as thrust, rocket dimensions, aerodynamic coefficients are computed and stored into a lookup table database. The Von Kármán wind turbulence model is used to generate random wind gusts during the flight. The disturbing and correcting forces are calculated in the wind and stability axis system respectively. The net forces and moments are calculated in the inertial axis system which is used to solve the six degrees of freedom equations. For better accuracy, these equations are solved using a fourth-order Runge-Kutta method.

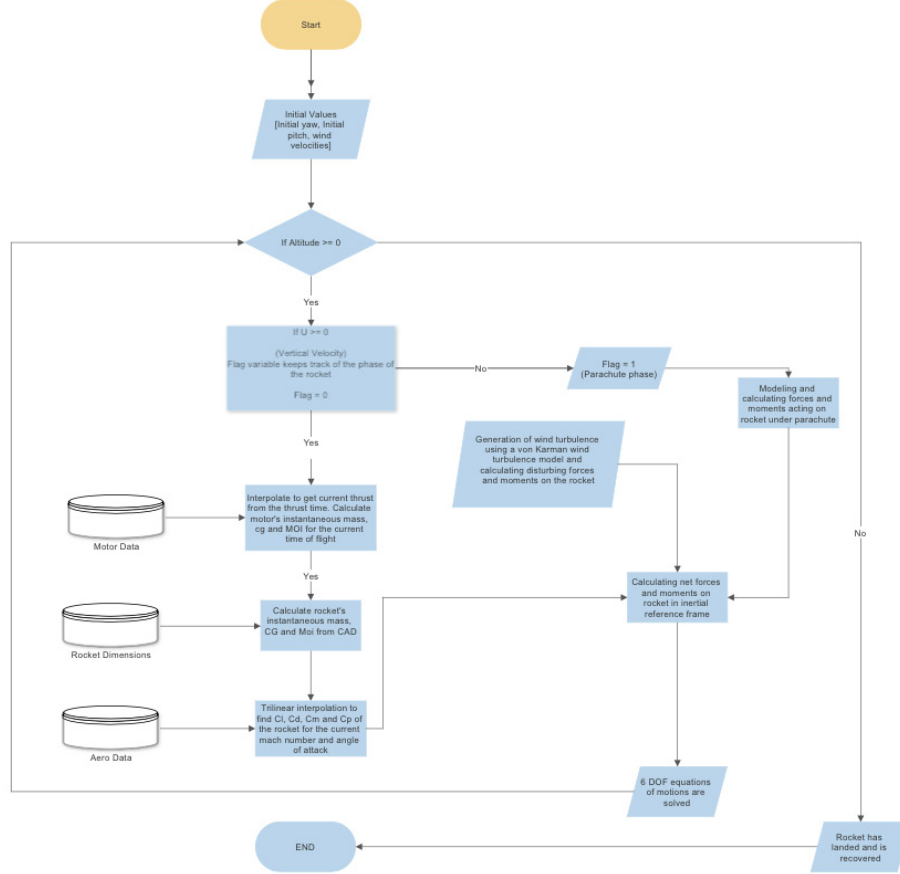


**Figure 66 Simulator Algorithm**

This code has been numerically validated and tested against RASAero II software by using aerodynamic data obtained from RASAero II to create a uniform benchmark, then running the same model on both platforms and comparing the results. A number of different rocket designs were used in the validation study and the results showed an acceptable error margin of less than 5 %, giving us enough confidence to use it for our main rocket.

## I. Appendix: SRAD Plotter

The team has designed and developed a Python-based GUI plotter to plot the data transmitted by the flight computer in real-time. Some features of the plotter are:

- 1) The plotter supports the plotting of a live data stream from a serial port or a text file.
- 2) According to the requirements, two modes for plotting are supported - dummy mode (activated when the serial port is absent) and real-time mode (activated when actual flight data is incoming).
- 3) When using the serial port as an input, file creation and storing of received data is done with available options on the plotter given, which provides you with the facility to start and stop data storing in a CSV file.
- 4) Dynamically changing the maximum number of data points visible in a graph at any time is supported.
- 5) Scrolling through the graph is allowed to study the graph at any given timestamp.
- 6) Options like top padding and bottom padding are present to control the range over which data can be viewed.
- 7) The plotter employs Cyclic Redundancy Check, an error checking method used to verify the integrity of data so that erroneous data is detected.
- 8) The plotter allows the usage of multiple serial connections simultaneously, allowing the use of incoming and outgoing connections simultaneously.



**Figure 67 Plotter UI**

## J. Appendix: C.A.V.E Post Flight Processor

The team has developed an in-house Python-based GUI processor to plot the data logged by the piezo transducers to the SD Card post-recovery. This processor enables data analysis immediately after flight. It is used for checking of corrupted data without overloading the base station system. Its features include-

- 1) Filters and data pre-processing techniques to remove unwanted noise in the dataset with the help of popular Python libraries such as Numpy and Pandas.
- 2) Filtered ADC serial data conversion to voltage data.
- 3) Fast Fourier Transforms to analyse which frequency bands are most dominant in the vibrations generated by the rocket during its flight.
- 4) Data plotting where each piezo transducer has a separate plot

Comparison of plots of data received from different piezo transducers are used to identify the ideal concentration of Carbon Nano Tube sample for maximum dampening. This tool is meant to facilitate the fast and accurate post processing to decide the next step in the quantification of the dampening properties of CNT infused CFRP.

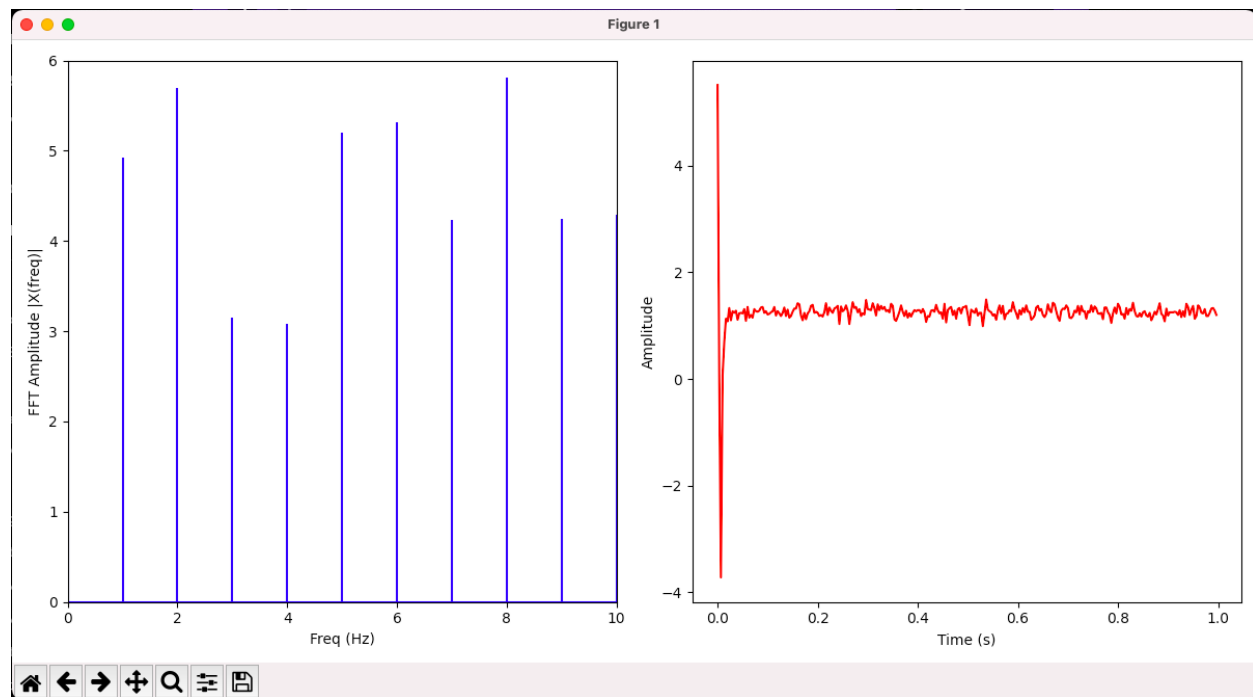


**Figure 68 Post Flight Processor UI**

## K. Appendix: MATLAB Code for Gore

```
1 clc
2 clear all
3 close all
4 % constructed diameter
5 D = 360;
6 % ellipse
7 a = D / 2;
8 b = a * 0.707;
9 = 648.273/4;
10 % no of panels
11 n = 10
12 % panel angle
13 fi = (2 * pi) / n;
14 th = linspace(pi / 2, 0, 100);
15 r_sec = a * cos(th);
16 y = 0.5 * fi * r_sec;
17 d = l - b * ellipticE(atan(a / b * tan(th)), 1 - (a / b) ^ 2);
18 plot(d, y);
19 hold on;
20 plot(d, -y);
```